

DISS. ETH Nr. 14767

**Iron sulfides in Baldeggersee during the last 8000 years:
Formation processes, chemical speciation and
mineralogical constraints from EXAFS spectroscopy**

ABHANDLUNG
zur Erlangung des Titels eines
DOKTORS DER NATURWISSENSCHAFTEN
der
EIDGENÖSSISCHEN TECHNISCHEN HOCHSCHULE ZÜRICH

vorgelegt von
MARKUS BOTT
dipl. chem. ETH Zürich
geboren am 11. Dezember 1968
in Richterswil (ZH)

Angenommen auf Antrag von
Prof. Dr. B. Wehrli, Referent
Prof. Dr. A. Manceau, Korreferent
Prof. Dr. L. Sigg, Korreferentin

2002

Die vorliegende Arbeit ist besonders

meinen Eltern *Beatrice und Georges Bott,*
meiner Frau *Regula Bott-Flury,*
und meinen Kindern *Priska Martina, Judith Johanna und Manuel Romeo*
gewidmet.

Schwefel der Weisen

Das höchste Ziel der Alchimisten war die Erzeugung des „Schwefels der Weisen“. Er hat gleich zwei Eigenschaften: Bei der Zugabe einer kleinen Menge dieses „Steins“ wird ein strömendes unedles Metall in Gold verwandelt. Zudem hat es lebenserhaltende Wirkung. Wer den Schwefel der Weisen herstellen konnte, durfte sich Adept nennen. Das Rezept ist aber auf keinen Fall einfach (auch nicht mit einer Waage von Mettler-Toledo). Wichtige Elemente sind Schwefel, Merkur und Salz [1]. Diese sind gleichzeitig drei Prinzipien der Natur [2].

Name	Symbol	Bedeutung
Schwefel	♁	männliche Aktivität, schöpferische Energie, Verlangen
Merkur (Quecksilber)	♃	Flüssigkeit, Erkenntnisvermögen, Kraft der Übertragung
Salz	⊖	Träger dieser beiden Energien, formend und auf diese einwirkend, das inaktive Prinzip der Natur, weiblich

„Den drei Daseinsebenen oder Welten entsprechend ist die geheime Wissenschaft von den Buchstaben eine dreifache. Im höchsten Sinne ist sie die Erkenntnis der Ur-Prinzipien, im mittleren Sinne ist sie die Kenntnis der Kosmogenie, das Wissen vom Entstehen der wahrnehmbaren Welt, und im unteren Sinne ist sie die Kenntnis der Eigenschaften der aus Buchstaben gebildeten Wörter und Namen, sowie der Zahlen. In den Buchstaben eines Namens verrät sich die Natur jedes geschaffenen Wesens, daher vermag die Kenntnis eines Namens über das betreffende Wesen eine gewisse Macht zu verleihen. Die Anwendung der arabischen Geheimwissenschaft von den Buchstaben ist der untere Grad dieser esoterischen Kenntnis. Der höchste Grad, der nur von wenigen erklommen wird, verleiht die Macht, auf allen drei Daseinsebenen wirken zu können. Wer diese Erkenntnistiefe erreichte, der kennt das große Magisterium, das Meisterwerk der Alchimie, den Stein der Weisen oder den „roten Schwefel der Weisen“ [1]

Die Adepten erwähnen stets die Farben, die im Werk während der Bereitung sichtbar werden. Drei Farben sind die hauptsächlichsten, schwarz, weiß, rot. Die zuerst erscheinende Farbe ist die Schwärze, es ist „der Rabe, der in der Nacht ohne Flügel fliegt“. Die zweite ist die weiße Farbe, in die allmählich die schwarze übergeht, sie heißt der Schwan, die weiße Taube, das weiße kristallinische Salz oder die weiße Rose, und die dritte Hauptfarbe ist dann die rote, die aus der weißen entsteht, die rote Rose, der himmlische Rubin. „Tödt den Raben, daß eine Taube gebohren werde, und hernach ein Phoenix, mache aus dem Schwarzen das Weiße und das Rothe, so wirst du glücklich seyn.“ [1]

Eisen ♂ wurde Mars zugeordnet. Mars ist ein lebhafter Gott gleich Jupiter, und als Gott des Krieges bekannt. Sein erstes Sinnbild war das in die Erde gestoßene Schwert und die Lanze, die aber nicht allein Kriegswaffen bedeuten, sondern mehr noch Pflug und Egge, die den Schoß der Erde öffnen und ihn der Befruchtung zugänglich machen. Mars war die dynamische Energie: „Mars beeinflusst Gallenblase, Nieren, männliche Zeugungsorgane, Muskeln, Sehnen und linkes Ohr. Mineralien sind Eisen, roter Jaspis, Amethyst, Hyacynth, Onix.“ [2]

Besuchte Internetseiten zum Thema (5. Februar 2002):

[1] <http://www.deurer-consulting.de/relax/lektion2.htm>

[2] <http://www.allgaeu-web.de/imbolc/Downloads/Max%20Retschlag%20-%20Die%20Alchimie.pdf>

Dank

Meinem Doktorvater Bernhard Wehrli möchte ich meinen grössten Dank aussprechen. Er hat mir das Projekt nicht nur ermöglicht, er hat mich auch stark unterstützt. Besten Dank für die Zeit, die Du für die zahlreichen Gespräche aufgewendet hast. Besten Dank auch für die mir zur Verfügung gestellten Literatur. Du warst mir nicht nur fachlich eine grosse Hilfe, Du hast auch ein grosses Verständnis für meine familiäre Situation entgegengebracht. Zudem schätzte ich Deine unkomplizierte Art. Du hast den „Titel“ Doktorvater in jeder Hinsicht verdient. Ich bedanke mich auch bei Lorenzo Spadini von der Universität Grenoble. Die Tage und Nächte im Synchrotron und vor dem Computer werde ich nicht vergessen. Es hat Spass gemacht, mit Dir zu EXAFSen. Immer wieder konnte ich von Deiner EXAFS-Erfahrung profitieren. Besten Dank auch für die Unterkunft in St. Martin d'Uriage. Uns verbindet wohl nicht nur diese Arbeit, wir werden Freunde bleiben. Das bestätigen die Ferien mit meiner Familie in Grenoble und Deine Besuche in der Schweiz. Ich möchte mich auch bei meinem Korreferenten Alain Manceau von der Universität Grenoble bedanken. Dank Dir habe ich immer wieder Messzeit in Orsay erhalten. Ich konnte vor allem von Deiner langjährigen Messerfahrung im Synchrotron profitieren. Mit der Unterstützung von Lorenzo habe ich zwar bei der Auswertung nicht viel mit Dir zu tun gehabt. Trotzdem hast Du uns bei der Interpretation von EXAFS-Spektren geholfen. Vielen Dank auch für das Angebot des Postdocs, welches ich dann aber vorwiegend aus familiären Gründen nicht angenommen habe. Mein Dank gilt auch meiner Korreferentin Laura Sigg (EAWAG). Deine Erfahrung in der Speziierung hat mir vor allem bei den Leachingversuchen weitere Ideen gegeben, die ich dann verwirklicht habe. Ein grosser Dank gilt auch Mike Sturm. Dir verdanke ich die Probenahme des Langkernes auf dem Baldeggersee. Mit Deiner Unterstützung ist es uns gelungen, 6 Langkerne in 4 Tagen zu ziehen. Trotz der grossen Last auf dem Schiff haben wir immer das Ufer erreicht und alle Kerne sind heil im Labor angekommen. Auch Alois Zwysig (EAWAG) möchte ich für die Hilfe auf dem Baldeggersee danken. Zudem hast Du mir beim Beprobieren, Trocknen und Fotografieren der Kerne geholfen. Die dazu notwendigen Hilfsmittel hast Du mir grosszügig zur Verfügung gestellt. Toni Mares von der EAWAG verdanke ich die Totalschwefel-Analysen. Er hat die vorbereiteten Proben gemessen und mir die Rohdaten geliefert. Martin Mengis (EAWAG) hat mich

Dank

sehr oft bei den Probenahmen begleitet. Vielen Dank für die dafür aufgewendete Zeit. Von Dir erhielt ich am Anfang meiner Arbeit viele Tips auf dem Feld. Ich bedanke mich auch bei Gerald Joedicke. Du hast bei mir die Diplomarbeit gemacht und AVS und CRS gemessen. Besten Dank für diese Daten, die ich in dieser Arbeit verwendet habe. Mein Dank gilt auch Anja Sinke. Anja hat mit mir während 2 intensiven Tagen die „most probable number“-Experimente gemacht. Ohne Dich hätte ich ohne Erfahrung grosse Schwierigkeiten mit dem sterilen Arbeiten gehabt. Sandra Steingruber danke ich für die Daten Ihrer Diplomarbeit an der EAWAG. Mit Hilfe der Resultate der „in situ Hybridisierung“ konnte ich die Prozesse an der Sediment-Wasser-Grenzschicht besser verstehen. Vielen Dank auch an Christian Dinkel (EAWAG). Als Praktiker hat er mich gelegentlich auf den See begleitet und er konnte mir immer wieder in praktischen Dingen helfen. Das gilt auch für den von Dir zur Verfügung gestellten Platz in Deinem Elektroniklabor. Tobias Schaller danke ich für die Messungen von totalem Eisen am freeze core (EAWAG). Auch Du hast mir auf dem See geholfen. Ich bedanke mich auch bei Gabriela Friedel. Beim Lesen Deiner Diss. habe ich erste Kontakte mit dem EXAFS knüpfen können. Jane Teranes (ETH) hat mir vor allem bei der Beschaffung von digitalen Klimadaten geholfen. So konnte ich viele Stunden „digitalisieren“ sparen. Erwin Grieder und Ruth Stierli (EAWAG) verdanke ich für die Bestimmung der Trockengewichtsdaten. Besten Dank Euch beiden auch für die Mitbenützung des Analysenlabors. Vor allem bei AAS-Messungen konnte ich auf Eure Erfahrung zurückgreifen. Ich bedanke mich auch bei der Schweizerischen Meteorologischen Anstalt. Ihre Temperatur- und Niederschlags-Daten habe ich zum Teil für diese Arbeit verwendet. Herr Schweingruber vom WSL verdanke ich die Dendrochronologie-Daten. Last but not least bedanke ich mich bei Regula Müller (EAWAG). Wir haben während gut 3 Jahren den gleichen Raum geteilt. Rotierende Magnetfelder sind fast so schön wie Riesenmohrenköpfe. Ich bedanke mich auch bei meiner Frau und meinen Kindern. Neben der Arbeit haben sie mich immer daran erinnert, dass es nicht nur ein Leben im Labor gibt. Meinen lieben Eltern verdanke ich nicht nur mein Leben. Sie haben mir auch meine Ausbildung ermöglicht.

Zusammenfassung

Die vorliegende Arbeit hatte zum Ziel, die Eisen- und Sulfidprofile in den Sedimenten des Baldeggersees zu interpretieren. Klimatische Faktoren beeinflussen die Tiefenwasserwassermischung und damit die Redoxverhältnisse im See. In dieser Studie wurde die Hypothese geprüft, dass klimatische Schwankungen die Eisensulfidkonzentration im Sediment beeinflussen. Dazu wurde die Spezierung von Fe und S mit einer Kombination von chemischen und spektroskopischen Methoden analysiert. Mit einer Prozessstudie wurden Transport und Transformation von Fe und S im Sediment quantifiziert. Die Resultate dieser Studie an Kurzkernen wurden dann in einer Langkernstudie angewandt, um die Schwankungen in der FeS Sedimentation über mehrere Tausend Jahre zu interpretieren. Diese paleolimnologische Studie hatte zum Ziel, die Oszillationen in der Ablagerung von Varven zu analysieren und mit neuen Ergebnissen zu Klimaschwankungen im Nordatlantik zu verknüpfen.

Die Sedimentkerne stammen von der tiefsten Stelle im Baldeggersee (65 m), wo datierte Kerne (^{14}C und Varvenzählungen) zur Korrelation zur Verfügung standen. Die maximale Konzentration von sulfatreduzierenden Bakterien wurde an der Sedimentoberfläche und in 5 cm Tiefe gefunden. Aus Porenwassergradienten wurde eine aktuelle, mittlere Diffusionsrate von $0.45 \text{ mmol m}^{-2} \text{ d}^{-1}$ ermittelt. Daraus liess sich eine Sulfidkonzentration von $150 \text{ } \mu\text{mol g}^{-1}$ abschätzen. Der Wert stimmt relativ gut mit dem gemessenen Mittelwert von $190 \text{ } \mu\text{mol g}^{-1}$ überein. Etwa 70% des Schwefels waren als FeS und nur ca 5% als FeS_2 gebunden. Pyrit und Eisenmonosulfid waren negativ korreliert. Pyritmaxima und FeS Minima konnten mit Mischungs- und Oxidationsereignissen in Verbindung gebracht werden, welche bei tiefen Jahresmitteltemperaturen auftreten. Die totale Eisenkonzentration lag im Mittel bei $300 \text{ } \mu\text{mol g}^{-1}$ und übertraf den totalen Schwefelgehalt deutlich. Die eisenreichen Sedimente agierten deshalb als effiziente Senke für reduzierten Schwefel. Im Gegensatz zur deutlichen Mobilität von Fe(II) im Porenwasser war kein gelöstes Sulfid nachweisbar. Die Eisenreduktion im Sediment erfolgte über zwei Reaktionswege. Einerseits wurden aktive eisenreduzierende Bakterien an der Sedimentoberfläche und 2 cm im Sediment gefunden. Andererseits reagierten die Produkte der Sulfatreduktion auf chemischem Weg mit Eisenoxiden im Sediment.

Zusammenfassung

Mit Extraktionsexperimenten wurde FeS als dominantes Mineral gefunden, Pyrit und Vivianit trugen nur unbedeutend zum totalen Eisengehalt bei.

Aus EXAFS Spektren wurde Sauerstoff als wichtigster nächster Nachbar der gebundenen Eisenionen ermittelt. Die spektroskopischen Daten wiesen auf zwei dominierende Eisenphasen hin. Eine davon war im tieferen Sediment die wichtigste Komponente. Der beste Fit für diese unbekannte Phase wurde mit einer festen Lösung von Fe(II) und Fe(III) in einer Calcitphase erzielt. Die zweite Phase wurde als amorphes Eisensulfid mit tetraedrischer Fe(II) Koordination ähnlich wie in Mackinawit identifiziert. In diesem Fall stimmten spektroskopische und chemische Analysen sehr gut überein.

Eisensulfide wurden auch in einem 8 m langen Sedimentkern gemessen. Die Konzentration schwankte zwischen "nicht nachweisbar" und etwa $60 \mu\text{mol g}^{-1}$. Verschiedene Segmente mit FeS Maxima wurden identifiziert und korrelierten sehr gut mit den beobachtbaren Jahresvarven. Kernabschnitte, welche vor über 2500 Jahren abgelagert wurden, zeigten Oszillationen im FeS mit Perioden zwischen 1000 und 1500 Jahren. Ähnliche Muster wurden kürzlich bei Proxi-Indikatoren für Eisbergaktivität im Nordatlantik festgestellt. Diese korrelierten mit kosmogenen Radionukliden als Indikatoren für die solare Aktivität. Zeitreihen für Gletschervorstösse und rückzüge in den Schweizer Alpen zeigen eine ähnliche Periodizität. Die Resultate der Prozessstudie im Baldeggersee an rezenten Sedimentkernen zeigten eine gute Korrelation zwischen Jahrestemperaturen und FeS - Konzentration im Sediment. Zusammengenommen unterstützen diese verschiedenen Beobachtungen aufgrund einer vorläufigen Sedimentdatierung die Hypothese, dass das europäische Klima in den letzten Jahrtausenden ähnlichen Schwankungen unterworfen war, wie die inzwischen gut dokumentierte Eisbergaktivität im Nordatlantik.

Abstract

The goal of this study was the interpretation of iron and sulfur records in the sediment of Baldeggersee. The hypothesis that climatic factors affect deep-water mixing in the lake and leave their mark in the iron sulfide record of the sediments was tested quantitatively on short sediment cores. The speciation of iron and sulfur was analyzed with a combination of wet chemical and spectroscopic methods. Information on the transport and the chemical and microbial transformation of iron and sulfur at the sediment-water interface was obtained from a process study on recent sediments.

The results of these measurements were then used in a second step to interpret the iron sulfide stratigraphy in a long sediment core covering several thousand years. This paleolimnological study was focused on a preliminary analysis of the oscillating varve regime of Baldeggersee. By comparison with recent paleoceanographic literature potential links between the North Atlantic climate oscillations and the iron sulfide record in the partially varved sediments from Baldeggersee were explored. Several sediment cores were taken at the deepest site of Baldeggersee (65m). At this site cores dated by ^{14}C and varve counts were available for correlation. Maximal sulfate reducing bacteria concentrations were found at the sediment water interface and at a sediment depth of 5 cm. From sulfate pore-water gradients a diffusion rate of $0.45 \text{ mmol m}^{-2} \text{ d}^{-1}$ was calculated. With this value a sulfur concentration of about $150 \text{ } \mu\text{mol g}^{-1}$ dry sediment was expected. The average measured value was about $190 \text{ } \mu\text{mol g}^{-1}$. Most of the sulfur (about 70%) was bound as iron sulfide and less than 5% sulfur was found in pyrite. The pyrite concentration profile showed a negative correlation with iron sulfide. Pyrite maxima and FeS minima could be linked to mixing and oxidation events, which occurred when the average yearly temperature was low. The total iron concentration was about $300 \text{ } \mu\text{mol g}^{-1}$ and exceeded the total amount of sulfur. The iron rich sediments acted therefore as an efficient trap for reduced sulfur species. At the sediment - water interface the iron concentration was lower than deeper down core. Pore-water profiles down to the zone deposited before 1885 reached Fe^{2+} concentrations of 0.6 mM and indicated transport of reduced iron from deeper sediments to the hypolimnion. By contrast, the mobility of sulfide was very low due to the efficient precipitation as iron sulfides. Iron reduction was found to occur by two pathways. First, active iron reducing bacteria were found at the

Abstract

sediment-water interface and an additional maximum at 2 cm depth. Second, dissolved sulfide species allowed the chemical reduction of iron oxides at the sediment interface. A fast reaction caused a depletion of these dissolved sulfide phases. Extraction experiments found iron sulfide (FeS) as the dominant phase. Pyrite contributed only little to the total iron content. Small total phosphorus concentrations excluded a significant amount of vivianite.

EXAFS-measurements indicated oxygen as the dominant nearest neighbor of the iron ions. These spectroscopic data revealed two relevant iron phases. One phase was dominant in the deeper sediment. A best fit to the spectra of this unknown phase was obtained with a solid solution model, where Fe(II) and Fe(III) ions replaced the Ca(II) ions in the calcite structure. The second phase was determined as amorphous iron sulfide with a tetrahedral coordination of the iron(II) ions similar to the mackinawite structure. In this case the wet chemical analysis and the spectroscopic results matched very well.

Iron sulfide was found in deeper sediment layers, too. The concentration changed from no detectable sulfide up to about $60 \mu\text{mol g}^{-1}$. Several FeS maxima were found. Sediment deposited before about 2500 years B.P. showed oscillations of iron sulfide concentration with a period of about thousand years. Similar patterns were observed recently for proxies of ice-rafted debris and cosmogenic radionuclides in North Atlantic sediments, suggesting a solar forcing of Northern hemispheric temperature conditions. Records of glacier advances and retreats from the Swiss Alps showed a similar periodicity as the North Atlantic record and the AVS time series of Baldeggersee. Results from the process study on short cores indicated that AVS concentrations in recent sediments correlated with average yearly temperatures with warmer conditions leading to more stratification and higher sulfide concentrations in the sediment. Together, these different lines of evidence suggest that the AVS record in deep meromictic lakes can be used as a sensitive proxy for deep-water mixing and climatic forcing. The 1000-1500 year periodicity of the varved sections from the preliminary age model of Baldeggersee sediments would support the hypothesis that European climatic conditions showed similar fluctuations in the past 8000 years as the sedimentary proxies for the iceberg record of the North Atlantic.

Table of contents

CHAPTER 1: INTRODUCTION	1
Iron sulfides in sediments.....	1
Baldeggersee	2
References	5
CHAPTER 2: BOTT, JOEDICKE, STEINGRUBER AND WEHRLI: VARIATIONS IN SULFIDE DEPOSITION IN SEDIMENTS OF EUTROPHIC BALDEGGERSEE (SWITZERLAND) AND THEIR CORRELATION WITH AVERAGE TEMPERATURES	7
Abstract	8
Introduction	9
Material and Methods	12
Study site	12
Methods.....	13
<i>Sampling</i>	13
<i>Chemical analysis</i>	13
<i>Microbiology</i>	14
Results.....	16
Sediment dating.....	16
Linking peeper measurements to sedimentation rates.....	16
Microbiology.....	18
Iron	19
Sulfur	20
Discussion.....	22
Specificity of the digestion techniques	22
Interpretation of the concentration profiles	23
Biogeochemical processes	24
Correlation with climatic parameters.....	26
References	28
CHAPTER 3: SPADINI, BOTT, WEHRLI, MANCEAU ANALYSIS OF THE MAJOR FE BEARING MINERAL PHASES IN RECENT LAKE SEDIMENTS BY EXAFS SPECTROSCOPY	31
Abstract	32
Introduction	33
Material and methods	35
Sampling site and core description.....	35
Chemical analysis.....	35
X-ray diffraction analysis.....	37
Sample preparation, EXAFS data collection and reduction.....	38
Analysis of bond distances in iron minerals.....	38
Results and Discussion	40
Qualitative spectra analysis.....	40
Quantitative spectra analysis.....	44
Speciation proposition	50
Generation of a $(Ca_x, Fe_{1-x})CO_3$ structure.....	52
Conclusions	56
References	57

Table of contents

CHAPTER 4: BOTT, STURM, WEHRLI IRON SULFIDES IN LAKE SEDIMENTS AS POTENTIAL INDICATORS FOR CONTINENTAL CLIMATE CONDITIONS – A 8000 YEAR RECORD FROM BALDEGGERSEE, SWITZERLAND	59
Abstract	60
Introduction	61
Material and methods	63
Study site	63
Sampling	63
Methods	65
<i>Sediment dating</i>	67
<i>Core description</i>	69
<i>Climate data</i>	70
Results	72
Dry weight	73
AVS	73
Iron speciation	74
Pyrite	76
Discussion	77
Factors governing AVS accumulation	77
AVS accomodation from 1000 to 2000	78
AVS accumulation during the Holocene	79
References	83
CHAPTER 5: CONCLUSIONS AND OUTLOOK	85
Conclusions	86
Goal	86
Results	86
<i>i) Cores</i>	86
<i>ii) sulfur in recent sediments</i>	86
<i>iii) iron in recent sediments</i>	87
<i>iv) the long sediment record</i>	88
Outlook	89
CURRICULUM VITAE	90
ANNEX: TABLES AND RAW DATA OF THE PLOTS	91
Table A1: Age model	91
Table A2: Dry weight in % (Fig. 2.1)	92
Table A3: Sulfate reducing bacteria SRB (Fig. 2.3)	93
Table A4: Active iron reducing bacteria (FeRB) (Fig. 2.3)	93
Table A5: Sulfur contents in $\mu\text{mol/g}$ dried sediment (Fig. 2.4)	94
Tables A6: Iron concentrations in $\mu\text{mol/g}$ dried sediment (Fig. 2.4)	95
Tables A7: Correlation of average temperature and iron sulfides (Fig. 2.6)	96
Table A8a: Procentual iron speciation, page 1 (Fig. 3.1)	97
Table A8b: Procentual iron speciation, page 2 (Fig. 3.1)	98
Table A9a: Correlation of BA97-6 and BA97-4, page 1 (Fig. 4.3)	99
Table A9b: Correlation of BA97-6 and BA97-4, page 2 (Fig. 4.3)	100
Table A10: AVS concentrations in BA97-4 in $\mu\text{mol/g}$ (Fig. 4.4)	101
Table A11a: Dry weight of BA97-6 [g/g], page 1 (Fig. 4.5), sections have romain labels.	102

Table of contents

<i>Table A11b: Dry weight of BA97-6 [g/g], page 2 (Fig. 4.5).....</i>	<i>103</i>
<i>Table A12: Concentration of iron species in $\mu\text{mol/g}$ (Fig. 4.6).....</i>	<i>104</i>

Chapter 1:

Introduction

Here, the current literature on iron sulfides in sediments and the methods to study the relevant speciation and processes is briefly reviewed. Then the reasons for choosing Baldeggersee as a study site are outlined. Finally an overview of the structure of this thesis is given.

Iron sulfides in sediments

The production and settling of organic matter promotes the reduction of oxygen, nitrate, iron(III), manganese(III,IV), sulfate and finally, methanogenesis. Sulfate reduction was found to be the dominant process of organic carbon oxidation in anoxic marine sediments (Jørgensen, 1982). The reaction product hydrogen sulfide may be partially oxidized to elemental sulfur, pyrite, iron sulfide and dissolved sulfate (Schulz et al., 1994 and Ferdelmann et al., 1997). Chemical reoxidation of pyrite and iron sulfide in contact with oxygen was observed (Thamdrup et al., 1994). Mechanisms and kinetics of iron sulfide and pyrite oxidation under chemical conditions are well described in Lawson, 1982, Moses et al., 1987, and Sand et al., 2001. In anoxic sediments pyrite and iron sulfide oxidation is possible with MnO_2 (Aller and Rude, 1998; Schippers and Jørgensen, 2001). Pyrite is oxidized in anoxic marine sediments via polysulfides mainly to elemental sulfur and pyrite is oxidized via thiosulfate and polythionates to sulfate (Schippers and Jørgensen, 2001).

The concentration of mobile dissolved iron(III) is generally too low to allow oxidation of iron sulfides in carbonate buffered systems even when organic ligands allow a higher concentration of iron(III) (Schippers and Jørgensen, 2001). In absence of nitrate, MnO_2 and O_2 , iron sulfide phases are assumed to be preserved in the sediment over longer periods and may therefore serve as a potential proxy for paleo-redox conditions. For the speciation of FeS in sediments, selective chemical extraction procedures are well established. In addition, new spectroscopic techniques are becoming available for the study of sedimentary minerals. Recently,

EXAFS spectroscopy was applied to study the speciation of poorly crystallized sedimentary (Friedl, 1995). Precipitated manganese oxide in the water column was identified as poorly crystallized birnessite. In the sediments, manganese was found to co precipitate with calcite and vivianite.

Baldeggersee

Baldeggersee was recently an object of intense research. Detailed analyses of the water body and the sediment stratigraphy are available. Hill slopes shield the lake against the dominant westerly winds. The deep water therefore exhibited several meromictic periods since the last glaciation. Several varved sections in long sediment cores were observed in previous studies. Two possible pathways of varve formation were considered for Baldeggersee: Eutrophication and reduced mixing during warm winters. Since iron sulfides are preserved in old sediment layers, they may potentially be used as proxies for earlier anoxia and meromictic conditions. An overview of the limnological development of Baldeggersee since about 1950 was given by Wehrli et al. (1997). Maximal total phosphorus and ammonium concentrations were found between 1970 and 1975. The dissolved inorganic nitrogen concentration increased from 1965 to 1993. Between 1960 and 1980 very low oxygen concentrations were found in the hypolimnion over the whole year, indicating meromictic conditions during this period of high eutrophication. Lotter et al. (1997a) applied a freeze core technique for the analysis sediment material with a high spatial resolution. The sediment material was freeze-dried in situ with cooled ethanol and dry ice. The sampling in the cold room allowed obtaining sediment samples from the recent varved section with seasonal resolution. Based on this technique, Lotter et al. (1997) published a detailed sediment stratigraphy of Baldeggersee {TIC, C(tot), N(tot), P(tot), Ca, Mg, water content and dry accumulation}. The dating of the sediment material until 1885 was possible with an accuracy of one year. Due to eutrophication the calcite grain size increased from 1885 to 1965, where about 30% has a grain size of more than 20 μm . After 1975 the grain size decreased until 1993 where only 15% have more than 20 μm diameter.

Schaller et al. (1997a) measured profiles of total Fe, Mn, V, Cr, As and Mo in the freeze core from Baldeggersee. Under oxic conditions high concentrations of Fe, V and Cr were deposited. Under anoxic conditions enriched Mo concentrations were

accompanied with lower iron concentrations. Evidence for a remobilization of Fe in the meromictic lake was presented. In a second study Schaller et al. (1997b) presented a spatial analysis of the Baldeggersee sediments. An oxic water body and anoxic sediment were responsible for a release of dissolved manganese, iron and arsenic. Oxidation in the water body of Mn and Fe and fast horizontal transport of precipitated colloids produced a sediment focusing effect to the deepest site.

Jane Teranes (1998) published her PhD work on stable isotope signatures (^{18}O and ^{13}C) in the carbonate phases from Baldeggersee. She worked with daily sediment material from sequencing sediment traps and samples of the freeze core. The first white calcite layers grown in spring were depleted in ^{18}O and ^{13}C , respectively. For climatic interpretation only the black sediment material, accumulated during late summer and autumn was used. The values of ^{18}O were found to be a convincing proxy for precipitation. In the last 30 years a significant shift of ^{18}O was observed. This shift was interpreted as a result of the variability of the North Atlantic Oscillation. In summary, the recent sedimentation of Baldeggersee is well documented by several studies and first evidence that this site is susceptible to climatic variability has been published. Therefore it was decided to perform a detailed process study on FeS sedimentation in the recent sediments of Baldeggersee and then to apply the results in a paleolimnological study on a long core. The main results of the thesis are presented in three chapters:

Chapter 2 presents the information from the process study on short cores from the deepest site of Baldeggersee. The data on iron and sulfur deposition, chemical and microbial transformation processes and the speciation of iron and sulfur phases are evaluated. A correlation between annual temperatures and the iron sulfide profiles is presented for the period of meromictic conditions in the lake.

Chapter 3 documents the combination of wet chemical techniques and EXAFS spectroscopy for selected samples at different sediment depths. The EXAFS spectra are compared with reference spectra of iron minerals. A solid solution model of a dominant iron species in the CaCO_3 phase is presented together with spectroscopic evidence for the structure of the main FeS phase.

Chapter 4 gives a detailed account of the long core study down to sediment depths of more than 7 m. A preliminary age model for the sedimentation at the deepest site

in Baldeggersee is developed. The FeS profile is closely correlated with varved segments. The oscillations in the FeS record are linked to recent studies of ice-berg records in the North Atlantic and the record of glacier stands in the Swiss Alps.

The summary and outlook at the end of the thesis concentrates the relevant results and identifies the research needs to complete and generalize the present study.

References

- Aller R.C., Rude P.D. (1988); Complete oxidation of solid phase sulfides by manganese and bacteria in anoxic marine sediments, *Geochim. Cosmochim. Acta*, **52**, 751-765.
- Ferdelmann T.G., Lee C., Pantoja S., Harder J., Bebout B.M., Fossing H. (1997); Sulfate reduction and methanogenesis in a Thioploca-dominated sediment off the coast of Chile, *Geochim. Cosmochim. Acta*, **61**, 3065-3079.
- Friedl G. (1995), Die Mineralogie des Mangankreislaufes in eutrophen Seen: Eine Untersuchung mit EXAFS-Spektroskopie, Swiss Federal Institute of Technology (ETH), Zürich, PhD Nr. 10987.
- Jørgensen B.B. (1982); Mineralization of organic matter in the sea bed — The role of sulfate reduction, *Nature*, **296**, 643-645.
- Lotter A.F., Renberg I., Hansson H., Stöckli R. and Sturm M. (1997a); A Remote Controlled Freeze Corer for Sampling Unconsolidated Surface Sediments, *Aquat. sci.*, **59** (4), 295-303.
- Lotter A.F., Sturm M., Teranes J.L., Wehrli B. (1997b); Varve Formation since 1885 and high-resolution varve analyses in hypertrophic Baldeggersee (Switzerland), *Aquat. sci.*, **59** (4), 304-325.
- Lowson R.T. (1982); Aqueous oxidation of pyrite by molecular oxygen, *Chem. Rev.*, **82**, 461-497.
- Moses C.O., Nordstrom D.K., Herman J.S., Mills A.L. (1987); Aqueous pyrite oxidation by dissolved oxygen and by ferric iron, *Geochim. Cosmochim. Acta*, **51**, 1561-1571.
- Niessen F., Sturm M. (1987); Die Sedimente des Baldeggersees (Schweiz) - Ablagerungsraum und Eutrophierungsentwicklung während der letzten 100 Jahre, *Arch. Hydrobiol.*, **108**, 365-383.
- Sand W., Gehrke T., Jozsa P.G., Schippers A. (2001); (Bio)chemistry of bacterial leaching — Direct vs. indirect bioleaching, *Hydrometallurgy*, **59**, 159-175.
- Schaller T., Moor H.C., Wehrli B. (1997a); Reconstructing the iron cycle from the horizontal distribution of metals in the sediment of Baldeggersee, *Aquat. Sci.*, **59**(4), 326-344.
- Schaller T., Moor H.C., Wehrli B. (1997b); Sedimentary Profiles of Fe, Mn, V, Cr, As and Mo as Indicators of Benthic Redox Conditions in Baldeggersee, *Aquat. Sci.*, **59**(4), 345-361.
- Schippers A., Jørgensen B.B. (2001); Oxidation of pyrite and iron sulfide by manganese dioxide in marine sediment. *Geochim. Cosmochim. Acta*, **65**, 915-922.
- Schulz H.D., Dahmke A., Schinzel U., Wallmann K., Zabel M. (1994); Early diagenetic processes, fluxes and reaction rates in sediments of the South Atlantic, *Geochim. Cosmochim. Acta*, **58**, 2041-2060.
- Stadelmann P., Herzog P., Arnold P., Bernegger J. C., Butscher E., Hirsiger F., Koller P. (1993), Sanierung des Baldegger- und Hallwilersees und deren

Einzugsgebiete. Situationsanalyse und Rechenschaftsbericht zuhanden des Gemeindeverbandes Baldegger- und Hallwilersee. Amt für Umweltschutz Luzern.

Teranes J.L. (1998); Climatic Significance and Biogeochemical Controls on Stable Isotopes in a Lacustrine Sequence from Baldeggersee, Switzerland, Swiss Federal Institute of Technology (ETH), Zürich, PhD Nr. 12609.

Thamdrup B., Fossing H., Jørgensen B.B. (1994); Manganese, iron and sulfur cycling in a coastal marine sediment, Aarhus Bay, Denmark, *Geochim. Cosmochim. Acta*, **58**, 5115-5129.

Wehrli B., Lotter A.F., Schaller T., Sturm M. (1997); High-Resolution Varve Studies in Baldeggersee (Switzerland): Project Overview and Limnological Background Data, *Aquat. sci.*, **59(4)**, 285-294.

Chapter 2:

Bott, Joedicke, Steingruber and Wehrli:

Variations in sulfide deposition in sediments of eutrophic Baldeggersee (Switzerland) and their correlation with average temperatures

This chapter is based on a publication submitted to the Journal of Paleolimnology

Abstract

The redox cycling of Fe and S was analyzed in recent sediments of Baldeggersee, an eutrophic lake in Switzerland. The deepest site shows a continuous record of annually varved sediments since 1885. This absolute time scale offers the opportunity to correlate the iron sulfide record with climatic data. The study was aimed at quantifying the actual Fe and S turnover in the recent sediments and to test the hypothesis that warmer average temperatures decrease the hypolimnetic mixing of the lake. As a consequence of a stronger stratification reducing conditions in the deep waters should prevail during a longer time of the year and the accumulation of iron sulfides in the sediment should increase.

A combination of geochemical and microbiological analyses was used to identify the actual fluxes of sulfate reduction across the sediment-water interface and to estimate the extension of the zone with active iron- and sulfate reducing bacteria. Based on seven pore-water profiles from dialysis samplers the average diffusive flux of SO_4^{2-} $0.45 + 0.15 \text{ mmol m}^{-2} \text{ d}^{-1}$ corresponded to an FeS accumulation of $150 + 50 \text{ } \mu\text{mol g}^{-1}$ dry weight. This value agreed well with the analysis of acid volatile sulfur (AVS) in the sediment (average concentration $135 \text{ } \mu\text{mol g}^{-1}$). The chromium reducible fraction (CRS), which is attributed to pyrite, contributed only by 4.3% to the total sulfur in the sediment. Active iron- and sulfate reducing bacteria were concentrated in the top 2 cm. This indicated that FeS and FeS₂-formation were essentially completed within about 5 years after sediment deposition.

Accordingly, FeS accumulation was correlated with 5-year running means of climatic time series. The time window of 1950 to 1980 was chosen for a more detailed analysis. During this time the lake was in highly eutrophic conditions with meromixis in the hypolimnion. Peaks in AVS were clearly correlated with warmer temperatures. Low levels of AVS were accompanied by high levels of CRS, which indicates that sedimentary iron sulfide is partially oxidized in years with cold winters and increased ventilation of the hypolimnion. The sulfide record in meromictic lakes may therefore reveal valuable information about hypolimnetic redox chemistry, deep-water mixing and climatic forcing .

Introduction

In this study we test whether the concentration of sedimentary iron sulfides reveals information on climatic conditions in the past. The analysis was focused on a period of constant eutrophic conditions in Baldeggersee, Central Switzerland (Lotter et al., 1997b and Wehrli et al., 1997). Hypolimnetic oxygen was almost completely consumed during the period between 1955 and 1982 in Baldeggersee. However, during very cold winters with strong winds it remained possible that surface water was partially mixed with the stratified hypolimnion, thus destroying the meromictic conditions. Precipitation of MnO_2 in the sediment could be linked to such mixing events (Schaller et al. 1997). In such cases oxygen should come in contact with the sediment surface, thus reducing sulfide accumulation. Results of alkalinity and oxygen measurements in the hypolimnion of Baldeggersee from 1950 to 1990 are published in Wehrli et al. (1997). We tested our working hypothesis by correlating iron sulfide concentrations in the sediments of Baldeggersee deposited during the meromictic period (1950-1982) with mean air temperature. After starting the lake restoration project in 1982 climate did no longer control the oxygen concentration at the sediment water interface and after 1982 no further correlation was expected. The lake restoration project and data of oxygen concentrations in Baldeggersee are presented in Stadelmann et al. (1997).

Several processes of iron sulfide precipitation and oxidation in lake sediments were well characterized both in field and laboratory studies. Iron(II)-sulfide formation was studied extensively in anoxic sediments (Berner, 1984, Davison, 1985 and Urban et al., 1994). It was controlled by microbial sulfate reduction in different marine and limnic systems (Lovley et al., 1983, Jørgensen, 1989 and Urban et al., 1994). The released H_2S may reduce iron (hydr)oxides also by chemical pathways. Dos Santos et al. (1992) found a linear dissolution rate of hematite as a function of hydrogen sulfide concentration up to a pH of 7 when iron sulfide was not oversaturated. In such systems the reductive transformation of iron(hydr)oxides to dissolved Fe^{2+} by chemical pathways seems to be possible. Iron reducing microorganisms may also contribute to iron(II) mobilization (Lovley and Phillips, 1988).

The solubilities of different iron sulfides have been reviewed by Davison (1991). Based on an analysis of pore-water data he concluded that in typical soft water lakes

amorphous iron sulfide was the dominant phase. In contrast, different minerals such as pyrite and greigite were found in marine sediments (Kasten et al., 1998).

In systems where iron sulfide precipitation is limited by available iron, excess hydrogen sulfide will be lost to the overlying water by diffusive transport. On the other hand, with an excess of sedimentary iron such as in the case of Baldeggersee it is possible that iron(III)-(hydr)oxide particles in deeper sediment strata are not completely reduced. Reduced sulfur will be trapped almost quantitatively as iron sulfide in such systems.

Carignan and Tessier (1988) found that iron sulfide was the dominant phase in eight acidic lakes in Canada. These authors postulated that the lack of available iron lead to free sulfide which inhibited sulfate reducers. In this way, sulfur retention was limited by iron sedimentation. In contrast they found preferential formation of organic sulfur compounds in sediments with high concentrations of oxygen, Mn(III/IV) and Fe(III). The importance of the organic sulfur fraction compared to inorganic sulfur was interpreted as rapid re-oxidation of dissolved hydrogen sulfide in these systems. A similar conclusion was put forward by Rudd et al. (1986). Different field and laboratory studies have analyzed the rapid oxidation kinetics of dissolved sulfide in presence of oxygen (De Vitre et al., 1988, Morse et al., 1987b and Urban et al., 1994). Microorganisms can play a key role in this process (Brune et al., 2000).

In summary, these studies indicate that iron sulfides could act as sensitive tracers of paleo-redox conditions in systems with a slight excess of iron keeping losses of H_2S from the sediments at minimum. On the other hand, electron acceptors such as O_2 , MnO_2 and $FeOOH$ should not dominate the system. In such cases, the FeS record is likely to be buffered by organic sulfur. Baldeggersee during the eutrophic phase represents such a system which is slightly iron dominated, but exhibited a stable anoxic hypolimnion with minimal concentrations of O_2 and MnO_2 . Sulfide preservation was at its optimum when no oxygen was present at the sediment-water interface even during wintertime.

More detailed knowledge on the response time of a paleo-proxy to changes in the environmental conditions is essential for interpreting time series from sediment archives. In order to characterize the typical response times of sedimentary iron sulfides to changes in redox conditions we measured recent pore-water profiles of

dissolved iron(II) and sulfate as well as bacterial distributions of sulfur reducing bacteria and active iron(III) reducing bacteria. With these data, we established the thickness of the reactive zone in the sediments of Baldeggersee, where actual sulfur and iron diagenesis takes place.

Finally, high-resolution concentration profiles of total iron, total sulfur, iron sulfide and pyrite were measured and compared to a time series of meteorological data. The sediment data were calibrated with the absolute time scale of sediment accumulation in Baldeggersee obtained with an in-situ freeze corer (Lotter et al. 1997a and b).

Material and Methods

Study site

Baldeggersee is situated in Central Switzerland at 463 m asl. It has a surface area of 5.2 km² and a maximum depth of 67 m. The volume is 0.173 km³. With an average inflow of 1.28 m³ s⁻¹ the hydraulic residence time is about 4.3 years. The catchment of 67.8 km² is composed of 82% agricultural area, 13% forest and 5% settlement with about 12,000 inhabitants (Stadelmann et al., 1993). The basin stretches in NW - SE direction. It is shielded from the prevalent west winds by hill slopes of 700-800 m elevation. Therefore, Baldeggersee is more susceptible to mixing by cold North-winds than to warmer West-winds during wintertime.

The recent varved sediment section indicates that anoxic conditions prevailed at the deepest site since 1885 (Lotter et al., 1997b). Using the varve chronology Niessen and Sturm (1987) reconstructed the history of eutrophication. Their sediment mapping study revealed that the oxycline reached a water depth of 40 m around 1940. Between 1950 and 1982 the whole hypolimnion was anoxic during most of the year since bioturbation was absent in sediments below 10 m depth (Niessen and Sturm, 1987). A detailed analysis of the last 100 years of varved sediments is given in Lotter et al. (1997b). Before 1885 the sediment showed a homogeneous light grey colour. Between 1885 and about 1905 its colour changed first to dark grey then to grey and after 1905 the stirred sediment appeared black. Trophic indicators such as calcite grain-size (Lotter et al., 1997b) indicate that eutrophication started around 1905. The average phosphate concentration increased to a maximum of about 500 mg P/m³ around 1975. Due to increased efficiency of sewage treatment plants and the ban of polyphosphates in detergents in Switzerland the P-concentration decreased below 100 mg/m³ until the early 1990s (Wehrli et al., 1997).

A lake restoration program with artificial oxygenation during summer and mixing with compressed air during winter started in 1982. This measures successfully reestablished oxic conditions throughout the water column (Gächter and Wehrli, 1998). Therefore, the time frame for the correlation of FeS concentrations in sediments with external factors was restricted to 1955-1982.

Methods

Sampling

Short sediment cores were taken at the deepest site of Baldeggersee (65 m water depth) with a gravity corer. The principles of the coring system have been described by Kelts et al. (1986). Immediately after sampling the cores were closed with gas tight stoppers and transported to the laboratory. The cores were stored for no longer than a few days in a cold room at a temperature of 4 °C and sectioned in a glove box under a nitrogen/hydrogen atmosphere. The sediment was extruded directly into the glove box and cut into slices with a modified petri dish. Wet sediment samples were stored in containers in the glove box until they were analyzed for reduced sulfur compounds. Subsamples were weighted and dried to determine the % dry weight. Dry samples were ground in an agate mortar for analysis of total iron and total sulfur. All chemicals used were of reagent grade quality.

Chemical analysis

Total iron was measured after digestion with H_2O_2 / HNO_3 in a microwave oven using acetylene/air flame AAS. Iron(II) and iron(III) were digested with 5 M HCl in an oxygen free atmosphere following the method of Heron et al. (1994). Reaction time at room temperature was 24 days. This longer extraction time was chosen because tests with only 1 day digestions with 5 M or 0.5 M HCl resulted in smaller iron concentrations. All solutions were filtered through a 0.45 μm cellulose acetate filter and analyzed photometrically with a method adapted from Pehkonen et al., (1992). An aliquote of 20 μl filtrate was added to a mixture of 1.5 ml ethanol, 1 ml of 0.2 M ammonium-acetate solution and 150 μl of 0.02 M di-2-pyridyl-ketone-benzoylhydrazone dissolved in ethanole. Absorption was measured at 660 nm (where only Fe(II) is absorbing) and at 410 nm (where both iron(II) and iron(III) contribute to the signal). Iron(III) concentrations were calculated by correcting for iron(II) absorption at 410 nm.

For the analysis of acid volatile sulfide (AVS, mainly iron sulfides) and chromium reducible sulfur (CRS, corresponds to pyrite) we followed the method described by Morse et al., (1987a). About 3 g of sample were weighted, diluted with 20 ml distilled water and purged with nitrogen (99.999%) for 5 minutes. Then 2.5 g $\text{SnCl}_2 \cdot 6\text{H}_2\text{O}$

were diluted in 10 ml 37% HCl and added to the sample through a serum stopper at ambient temperature. The liberated H₂S was trapped in a solution containing 25 ml 0.15 M zinc-acetate and one drop of sulfur free silicon antifoam agent (available from Fluka). After stirring during one hour the trap was changed and CRS was determined in the same sample by adding 8 ml of 12 M HCl and 20 ml of 1 M Cr²⁺-solution in 0.5 M HCl. The chromium(II)-solution was prepared following Fossing et al., (1989). After stirring for 85 minutes at ambient temperature the CRS collected in the Zn-acetate traps was analyzed. Four drops of saturated starch solution and aliquotes of 1 ml 25 mM iodine solution were added until the brown colour of iodine did not disappear anymore. Then 4 ml 6 M HCl were added and the starch-iodine complex was titrated with a 20 mM thiosulfate solution until the colour in the solution disappeared. The sediment in blank experiments with pure water added instead of reagents did not release any detectable amount of H₂S.

Fe²⁺_(aq)-gradients were measured with dialysis plates (peepers) following Hesslein, (1976) and Urban et al., (1997). Sulfate and iron in the porewater were measured using ion chromatography and AAS, respectively. Total sulfur was measured with a CHNS-elemental-analyzer (Elementar: Vario EL).

Microbiology

Sulfate reducing bacteria were counted by in situ hybridisation (Amann et al., 1995). Samples from a sediment core were preserved in the field with ethanol. Slides were prepared by staining with 4',6-diamidino-2-phenylindol (DAPI). Two RNA probes, EUB338 and SRB385 were used. DAPI detects all bacteria, EUB338 eubacteria and SRB385 sulfate reducing bacteria. A fluorescent dye (Cy3, Amersham) was bound to these probes. Two slides of the same sample were counted under an epifluorescence microscope with a 1000 fold magnification. DAPI shows blue UV fluorescence, Cy3 shows red fluorescence in green light exposure.

Active iron reducing bacteria were counted with a most probable number experiment (Gerhardt et al., 1994). About 2 g of fresh sediment samples were suspended in a sterile 0.1% pyrophosphate solution. For each sediment depth dilutions with factors of 100, 2·10³, 2·10⁴, 2·10⁵ and 2·10⁶ were prepared. The bottles were incubated for 5 months at 30 °C. Active iron reducing bacteria could grow in a medium of 13.7 g iron(III)-citrate, 4.1 g sodium-acetate, 2.0 g sodium-formiate, 2.5 g sodium-

bicarbonate, 1.5 g ammonium-chloride, 0.6 g sodium-dihydrogenephosphate, 0.1 g potassium-chloride as well as trace minerals and vitamins. In positive bottles iron reduction was observed by a color change from red-brown ferric iron to grey ferrous iron. The most probable number of iron reducing bacteria was calculated from the dilution factor at which the color change occurred.

Results

Sediment dating

In 1993 a freeze core was taken on Baldeggersee by Lotter et al. (1997a). Sediment formed after 1885 showed undisturbed varves. By comparing varve dating with ^{137}Cs measurements a precision of one year was confirmed for the time period 1963-1993 (Lotter et al., 1997b). For our analysis, the gravity cores were extruded into an oxygen - free atmosphere. Since the varves were not countable with this technique direct high resolution dating was not possible. Therefore an indirect method was used based on the correlation of the dry weights of the extruded samples and the available data with an absolute time scale from the freeze core. The alignment of the minima and maxima of the dry weight in the gravity core by hand with the freeze core curve allowed a precise dating of the gravity core (Fig 2.1). Linear interpolation between these points produced an age model with an estimated accuracy of about 2 years for a sampling resolution of 5 mm and 5 years for sections of 2 cm.

Linking peeper measurements to sedimentation rates

The porewater profiles of sulfate pointed to an intense sulfate reduction process in the sediment of Baldeggersee. Iron(III) reduction was indicated by the porewater profile of dissolved Fe(II) (Fig. 2.2.). The sulfate concentration in the bottom water was about 150 μM . A typical sulfate penetration depth into the sediment of about 2 cm was observed. Based on seven sulfate gradients (January 1994, March 1994, May 1994, July 1994, September 1994, November 1992 and December 1993) we calculated an average sulfate diffusion flux of about $0.45 \pm 0.15 \text{ mmol m}^{-2} \text{ d}^{-1}$. The average sulfide concentration was estimated assuming that the produced sulfide accumulated completely in the sediment. The density of dry sediment was estimated as 2.3 g cm^{-3} , the mean dry weight between 1920 and 1980 was determined as 28% (Fig. 2.1.) and the average sedimentation rate was 3.3 mm per year during this period. With the average sulfate flux given above, a sulfide concentration in the sediment of about $150 \pm 50 \mu\text{mol/g}$ dry weight was calculated.

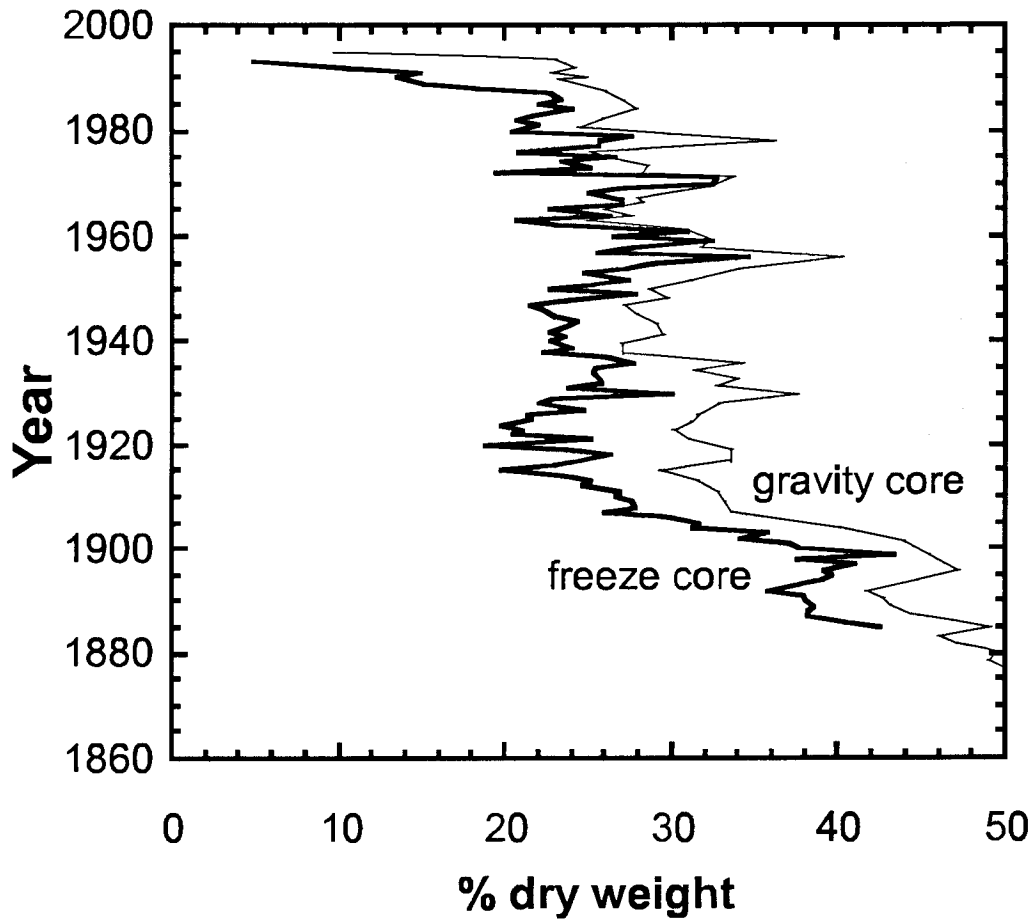


Fig. 2.1.: Dating of a gravity core by correlation with a freeze core. Dry weight data from a gravity core (thin line) were aligned to the data set of individual varve analyses from a freeze core (thick line, Lotter et al. 1997b).

The dissolved Fe^{2+} concentration had a maximum at about 2 cm sediment depth. Obviously iron(III) reduction occurred not only at this depth. Iron(II) in the pore water increased until 30 cm sediment depth to a concentration of 0.6 mM. Therefore, additional iron reduction has to be inferred at greater sediment depth.

Microbiology

Both, sulfate reducing and iron reducing bacteria were quantified in cores from the deepest site in Baldeggersee. The profiles are shown in Fig. 2.3. A maximum of sulfate reducing bacteria at the sediment water interface was found. In addition, a second maximum at about 5 cm sediment depth was observed in a zone, where sulfate was depleted.

The distribution of active iron reducing bacteria was similar to the pattern of sulfate reducers. Within the limits of statistical errors we found a maximum of microbial activity at the sediment-water interface and a second maximum at a sediment depth of about 2 cm.

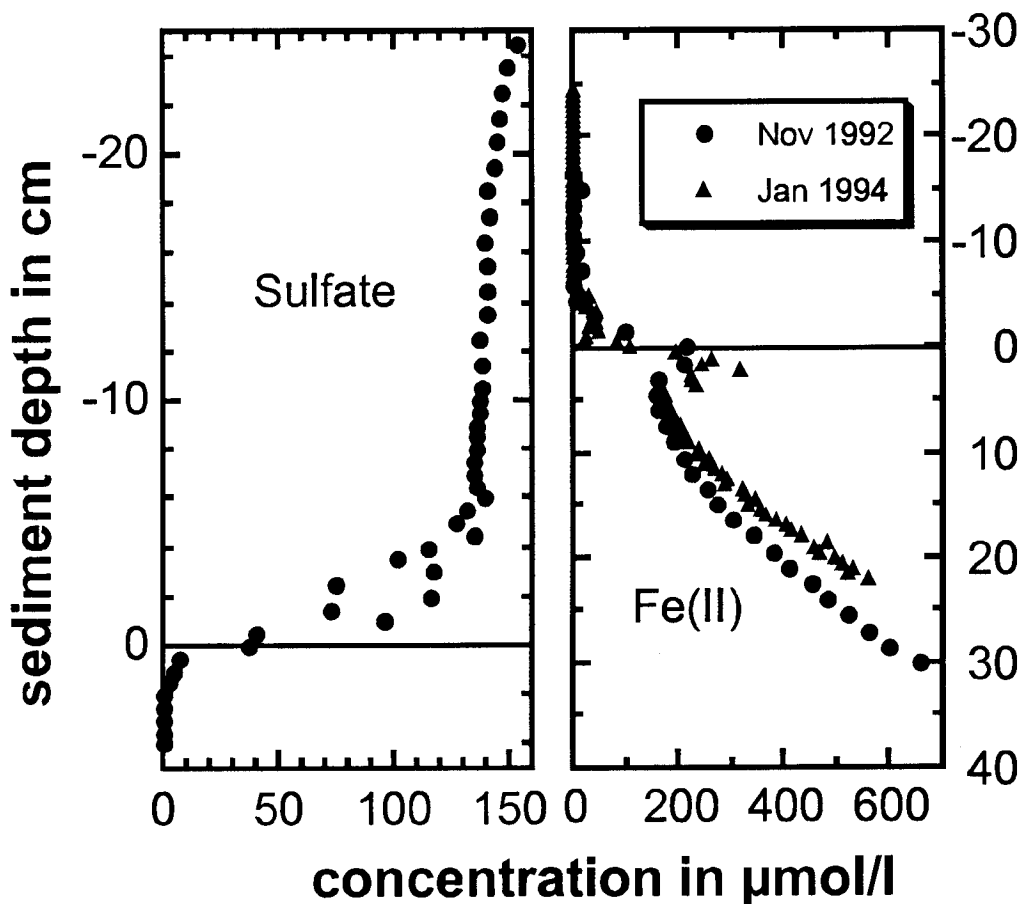


Fig. 2.2.: Porewater profiles of sulfate and iron(II) measured with dialysis plates (peepers) at the deepest site of Baldeggersee (65m).

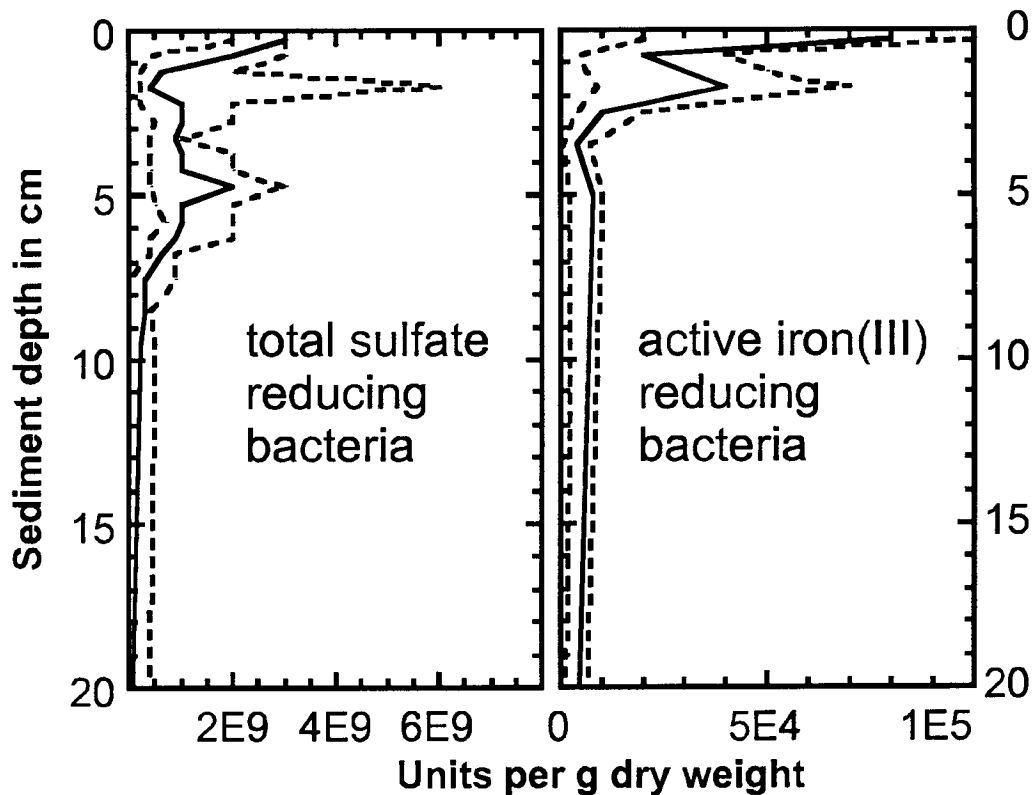


Fig. 2.3.: Number of sulfate and active iron(III) reducing bacteria with upper and lower error bars; significance level 95% for sulfate and 90% for iron reducing bacteria. Sulfate reducers were counted by fluorescent in-situ hybridisation (FISH), iron reducers represent most probable numbers (MPN)

Iron

Iron(II) and iron(III) are usually stable in sediment digestions with HCl (Wallmann et al., 1993). In the presence of hydrogen sulfide, iron(III) could be partially reduced during the procedure (Westrich 1983). More than 90% of iron is present as iron(II) (Fig. 2.4 and Fig. 2.5). Interestingly, the deeper sediment shows an increasing total iron concentration. The mean concentration for iron(III) of 18 $\mu\text{mol/g}$ dry weight in recent sediments represents about 6% of the total iron with a mean concentration of 290 $\mu\text{mol/g}$ dry weight. An iron(III) concentration of up to 50 $\mu\text{mol/g}$ dry weight was found in the older grey sediment deposited in the mesotrophic lake.

Sulfur

The iron(II) concentration was higher than the iron sulfide concentration over the whole section shown in Fig. 2.4. and Fig. 2.5. The total sulfur concentration was smaller than the total iron concentration. Only between 1940 and 1970 the sulfur concentration increased to similar levels as iron. Nevertheless, the system remained iron dominated.

The importance of sulfate reduction was reflected in the AVS and S° profiles (Fig. 2.4. and Fig. 2.5.). Iron sulfides (AVS) were the dominant sulfur phase which correlated very well with the total sulfur profile ($R^2=77\%$). Their mean concentration reached a broad maximum between 1905 and 1982. During this time span AVS had a mean concentration of $135 \mu\text{mol/g}$ dry weight i.e. 71% of total sulfur. Pyrite played a minor role only with about $8.1 \mu\text{mol/g}$ dry weight (4.3% of total sulfur). Interestingly, pyrite showed a negative correlation with AVS during this time period ($R= -0.40$). More than 20% of total sulfur could not be specified with the two extraction methods. This fraction was classified as elemental and organic sulfur. Free hydrogen sulfide did not contribute to the AVS concentration. Tests, where H_2S was trapped in zinc acetate without addition of HCl to the sediment confirmed that the H_2S concentration was controlled by Fe^{2+} in the porewaters (Fig. 2.2.). Sulfur bound to iron(II) $\text{AVS} + 2 \cdot \text{CRS}$ had a mean concentration of $146 \mu\text{mol/g}$ dry weight between 1905 and 1996. This value was very close to the estimated iron sulfide concentration based on the sulfate diffusion gradients $150 \pm 50 \mu\text{mol/g}$ dry weight.

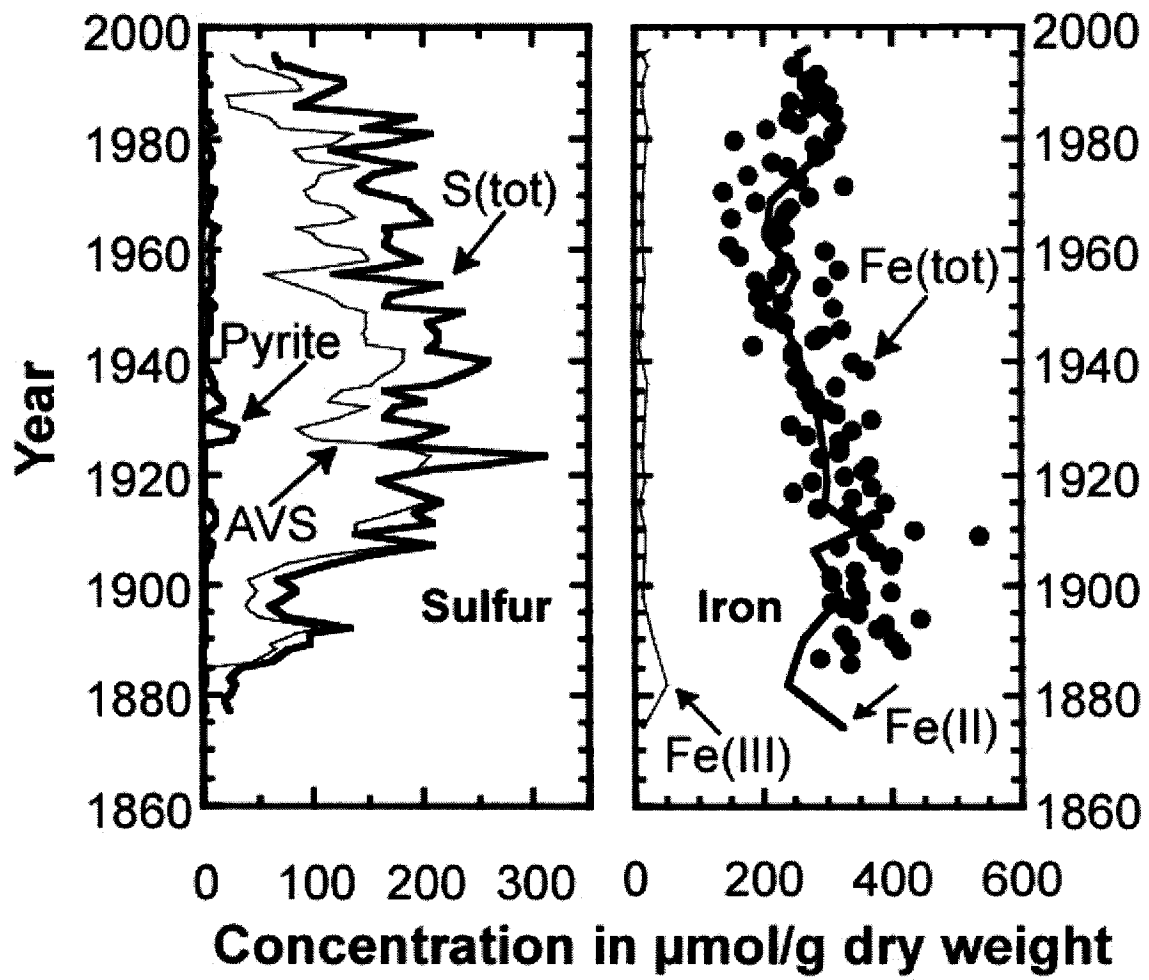


Fig. 2.4.: Concentration profiles of different sulfur and iron species measured with leaching methods

Discussion

Specificity of the digestion techniques

Before any meaningful interpretation of the iron and sulfur data can be done it should be examined how specific the leaching techniques are. The AVS digestion dissolves amorphous iron sulfides. Pyrite is not attacked by this technique. Greigite (Fe_3S_4) represents a difficult phase which can not be digested separately with the AVS or the CRS technique (Morse et al., 1987b). Because the quantity of hydrogen sulfide in the porewater was negligible and the iron concentration was larger than the sulfur concentration it could be assumed that AVS corresponds quantitatively to iron sulfides. A cold CRS digestion after the AVS determination dissolves pyrite and only little elemental sulfur in contrast to a hot CRS digestion (Fossing et al., 1989). Organically bound sulfur such as sulfonates, thioethers, thiols, disulfides and egg-albumine are not dissolved even with a hot CRS digestion (Canfield et al., 1986). In the present study, iron(II) and iron(III) was dissolved by the digestion in cold 5 M HCl during 24 days. The presence of sulfide in the extraction a reduction of iron(III) was possible in our case (Heron et al., 1994). Therefore only the maximum iron(II) concentration could be calculated from the data. EXAFS measurements in the same sediment provided evidence that iron(III) was a minor phase in the section between 1885 and today (See chapter 3). According to Heron et al. (1994) the digestion in 5 M HCl during 21 days dissolves the following phases: Iron sulfides (100%), Siderite (91%), Magnetite (75%) and Pyrite (1%). The following iron(III) phases are dissolved: goethite (100%), akaganeite (98%), hematite (79%) and magnetite (78%). Pyrite can be estimated with the CRS method. In the presence of iron sulfides less iron (hydr)oxides will be measured due to direct reaction of iron(III) with hydrogensulfide.

Interpretation of the concentration profiles

Within the last 120 years the AVS concentration changed by more than one order of magnitude (Fig. 2.4.). Before 1885 only very small iron sulfide concentrations were found. It seems that the lake was only mesotrophic before 1885 and that enough oxygen was present in the bottom water to outcompete sulfate reduction. The calculated sulfate reduction rate at this time was about $8 \mu\text{mol m}^{-2} \text{d}^{-1}$. Between 1885 and about 1905 a first AVS maximum was reached and after 1905 the AVS concentration increased to a maximum around 1920 when the calculated sulfate reduction rate reached $170 \mu\text{mol m}^{-2} \text{d}^{-1}$. After 1920 this value decreased slightly until today. Before 1980 the sulfate reduction rate was about $140 \mu\text{mol m}^{-2} \text{d}^{-1}$. After 1982 the sulfide accumulation decreased more rapidly.

This history of sulfide accumulation closely reflects the development of eutrophication and meromixis in Baldeggersee. The history of eutrophication is described in Stadelmann et al. (1993) and Wehrli et al. (1997). The eutrophication began at the beginning of the last century. Around 1950 the content of phosphorus in the water column was about 0.08 mg P/l. The maximum was reached in 1970 with a phosphorus concentration of over 0.5 mg P/l. In 1967 a water treatment plant was installed in Hochdorf and since then agriculture became the main source of phosphorus in Baldeggersee. 82% of total phosphorus was delivered from agriculture in 1990. After 1982 a lake restoration program started with an artificial aeration to the whole water column.

At the deepest site of Baldeggersee the sediment had no contact with oxygen during longer periods since 1885. Sulfate reduction increased due to the lack of oxygen until approximately 1920. After 1920 the iron sulfide concentration in the sediment decreased even though the phosphorous concentration increased. It must be assumed here that the sulfate concentration in the bottom water decreased due to a high sulfate reduction rate and that the transport of sulfate to the bottom water (e.g. eddy diffusion) limited the sulfate delivery to the sediment. After 1982 less than 50% of the maximal concentration in the year 1920 was found. The supply of oxygen to the bottom water and the enhanced oxic respiration slowed down the reduction rate.

The total iron concentration in the sediment decreased after 1885. Before 1885 oxic conditions at the sediment-water interface prevailed. As a consequence diffusive

losses of Fe^{2+} from the porewaters were minimized. During the meromictic phase between 1950 and 1980 dissolved Fe(II) accumulated in the deep water (Fig. 2.2.). A part of this reservoir was probably oxidized into colloidal Fe(III) and exported via the outflow. Schaller et al. (1997) estimated a yearly loss of 18 t iron via this mechanism. This flux can be compared to an estimated iron accumulation of $84 \text{ t} \cdot \text{a}^{-1}$ during the mesotrophic phase.

Significant iron (III) concentrations were found only in the grey sediment before 1885. Then the oxic conditions allowed a iron(III)-(hydr)oxide deposition in the sediment. Also EXAFS measurements (chapter 3) and leaching experiments in the deeper sediment (chapter 4) provided evidence that iron(III) was present below the strictly reducing black sediment section. The iron(II) profile in the porewater (Fig. 2.2.) indicated that a source of iron(II) existed below 30 cm sediment depth (~1880). The slow reduction of the iron(III) pool increasing before 1880 could explain the iron(II) flux from deeper porewaters.

Biogeochemical processes

The concentration profiles of dissolved iron(II) and sulfate indicated that both sulfate and iron(III) reduction occurred within the top 2 cm of the sediment (Fig. 2.2.). The iron sulfide record therefore represents a signal which is integrated over about 5 years, i.e. the time required to accumulate the top layer of 2 cm of sediment. The abundance of iron reducing bacteria was about 5 orders of magnitude smaller than that of sulfate reducers. This observation indicates that sulfate reduction was probably active at a higher rate than microbial iron reduction. Furrer and Wehrli (1996) reached the same conclusion in a diagenetic modelling study in a neighboring lake. Under these conditions it is likely that the hydrogen sulfide produced by sulfate reducers acts as a chemical reductant for iron hydroxides (Peiffer et al., 1992). A close correlation of sulfate reducing bacteria with the sulfate depletion in the sediment was obvious. The presence of sulfate reducing bacteria at a depth of 5 cm was more difficult to interpret. Two hypotheses could account for this second maximum: Either an internal sulfur cycle could produce sulfate by re-oxidation of H_2S or sulfate reducers could be involved in fermentative processes. This second maximum was not associated with changes in one of the potential electron acceptors like manganese oxides or iron oxides. We therefore conclude that fermentation

associated with methanogenesis is the most likely explanation for the deep maximum in sulfate reducers. With the sulfate diffusion rate the transport of sulfur into the sediment could be calculated. The close match of the resulting iron sulfide concentration with the experimental value indicates that the reduced sulfur remained in the sediment. The iron pool in the sediment was large enough to precipitate the reduced sulfur almost quantitatively. This characteristic is essential for a subsequent interpretation of the iron sulfide record as a proxy for climatic variations.

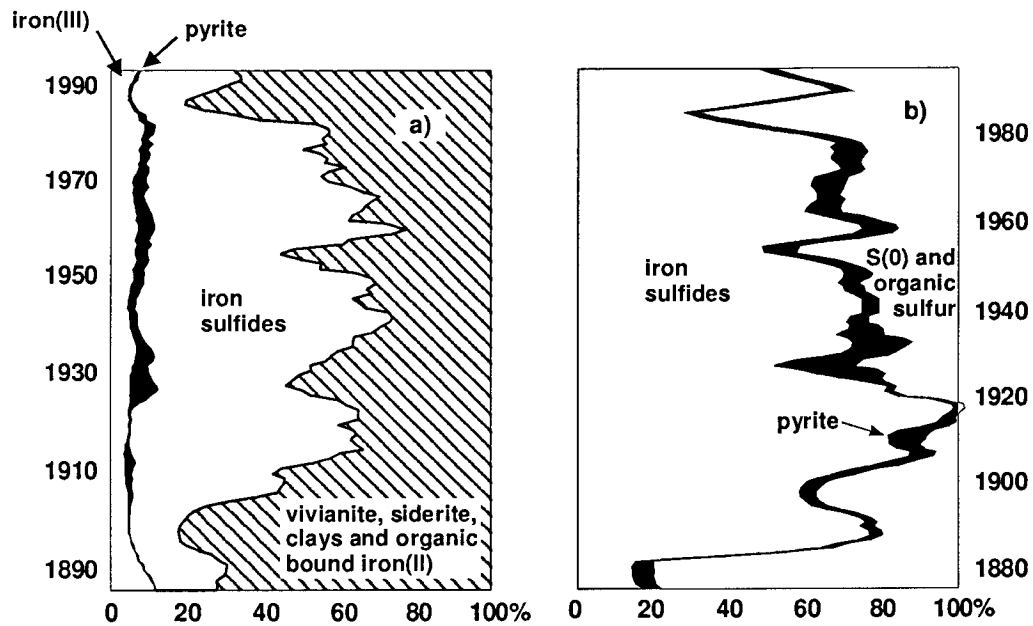


Fig. 2.5.: Iron and sulfur speciation profiles. At left the different iron fractions are shown as percentage of total iron, at right the different sulfur fractions are related to total sulfur in the sediment.

Correlation with climatic parameters

In order to test the sensitivity of the iron sulfide proxy towards climate variability we chose a time window of rather constant limnological conditions. Meromictic conditions in Baldeggersee prevailed between 1950 and 1980. Before 1950 the history of eutrophication was a dominant process and after 1982 the lake restoration program guaranteed a sufficient oxygen supply to the bottom water independent of any climatic conditions. Figure 2.6 compares three-year moving averages of pyrite (CRS) and iron sulfide with the corresponding moving average of yearly temperatures measured at the station of Bern Liebefeld (570 m asl). It is evident from this graph that warmer time periods correspond to higher AVS accumulation rates. Colder periods are correlated with higher pyrite accumulation. The AVS signal is more significant probably because pyrite concentrations are quite low. They are subject to a larger analytical error. An explanation of the slight shift between the AVS and the mean temperature plot is due to the impossibility of an exact sediment dating in our case.

Our process studies on AVS accumulation in the sediments of Baldeggersee support the following connection between average temperature and the AVS proxy in the sediment: Sulfate reduction occurred in the top 2 cm of the sediment and the freshly formed sediment contains about three years in the top 2 cm. Therefore the sulfide formed in this top layer is modulated by oxygenation events during wintertime, which are induced by climatic factors. During cold winter periods the water mixing was enhanced by strong northerly winds when the whole water column had a temperature close to 4 °C. Oxygen came in contact with the sediment water interface. The sulfate reduction rate decreased under these circumstances and the sulfide oxidation in the sediment increased. These processes diminished sulfide accumulation rates in the sediment. During warmer winters the water column was not mixed completely and no oxygen reached the bottom water. Sulfate reduction dominated at the sediment water interface and no sulfide oxidation happens.

In contrast to the positive correlation of iron sulfides with the temperature the pyrite concentration is negatively correlated. Low temperatures enhance the contact of oxygen with the freshly formed sediment. Intermediate reaction products such as thiosulfate, polysulfides and elemental sulfur are formed due to the oxidation of iron

sulfides with oxygen. These species enhance the formation of pyrite whereas under strictly anoxic conditions the iron sulfide formation is dominant.

In summary, AVS and CRS maxima show significant potential as proxies for warm and cold climate conditions respectively in a setting like Baldeggersee. These parameters can yield similar information as $\delta^{18}\text{O}$ in carbonates (Teranes et al.1999). In a subsequent study we have therefore correlated the AVS record from a long core in Baldeggersee with other proxy indicators for climate variability during the Holocene (chapter 4).

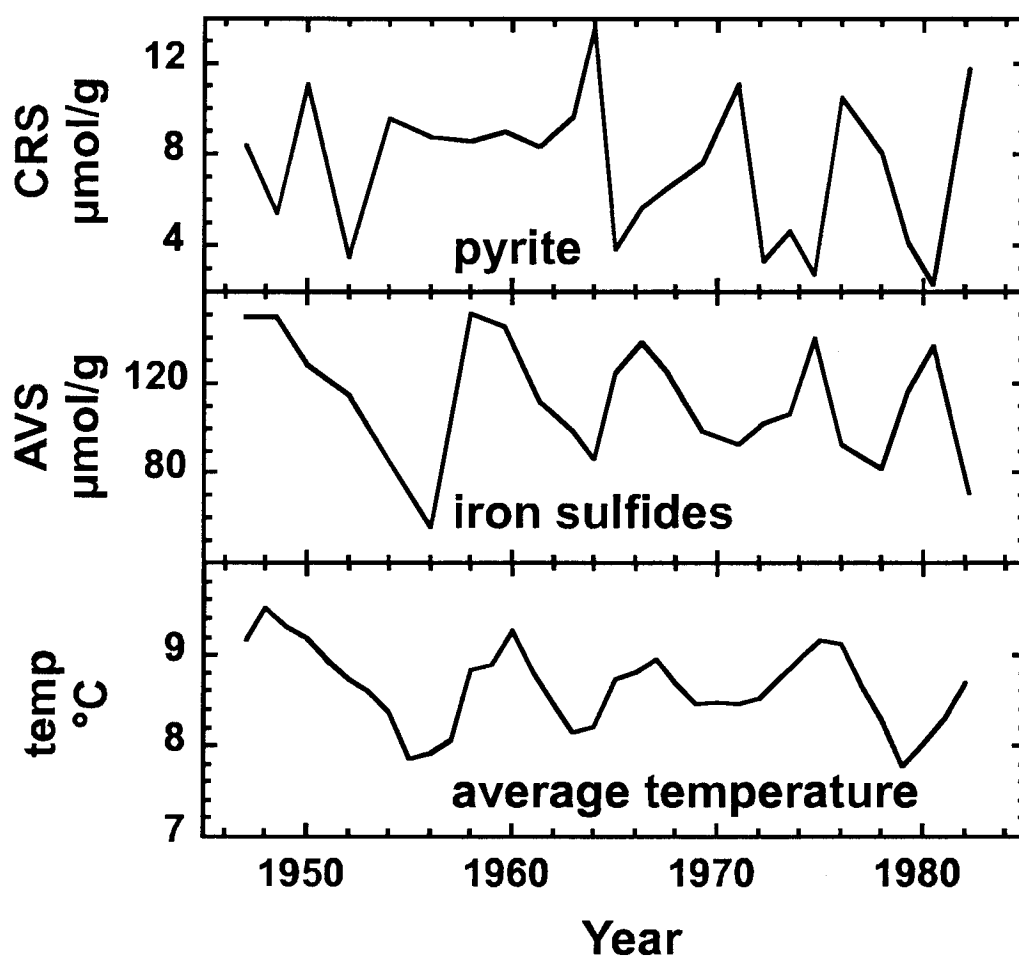


Fig. 2.6.: Comparison of three years moving averages of AVS and CRS (Pyrite) concentrations in sediments from Baldeggersee with the corresponding yearly temperature from the Bern Liebefeld meteorological station.

References

- Amann R.I., Ludwig W., Schleifer K.H. (1995); Phylogenetic identification and in situ detection of individual microbial cells without cultivation, *Microbial Reviews*, **59**, 143-169.
- Berner R.A. (1984); Sedimentary pyrite formation: An update. *Geochim. Cosmochim. Acta*, **48**, 605-615.
- Brune A., Frenzel P., Cypionka H. (2000); Life at the oxic-anoxic interface: microbial activities and adaptation. *FEMS Microbiol. Rev.*, **24**, 691-710.
- Carignan R., Tessier A. (1988); The Co-Diagenesis of Sulfur and Iron in Acid Lake Sediments of Southwestern Québec, *Geochim. Cosmochim. Acta*, **52**, 1179-1188.
- Canfield D.E., Raiswell R., Westrich J.T., Reaves C.M., Berner R.A. (1986); The Use of Chromium Reduction in the Analysis of Reduced Inorganic Sulfur in Sediments and Shales, *Chemical Geology*, **54**, 149-155.
- Davison W., Lishman J.P., Hilton J. (1985); Formation of Pyrite in Freshwater Sediments: Implications for C/S ratios. *Geochim. Cosmochim. Acta*, **49**, 1615-1620.
- Davison W. (1991); The Solubility of Iron Sulfides in Synthetic and Natural Waters at Ambient Temperature, *Aquat. Sci.*, **53(4)**, 309-329.
- Fossing H., Jørgensen B.B. (1989); Measurement of Bacterial Sulfate Reduction in Sediments: Evaluation of a Single-Step Chromium Reduction Method, *Biogeochemistry*, **8**, 205-222.
- Furrer G., Wehrli B. (1996); Microbial reaction, chemical speciation and multicomponent diffusion in porewaters of a eutrophic lake. *Geochim. Cosmochim. Acta*, **60**, 2333-2346.
- Gächter R., Wehrli B. (1998); Ten years of artificial mixing and oxygenation: No effect on the internal phosphorus loading of two eutrophic lakes. *Environ. Sci. Technol.*, **32**, 3659-3665.
- Gerhardt P., Murray R.G.E., Wood W.A., Krieg N.R. (1994); Methods for General and Molecular Bacteriology, American Society for Microbiology, Washington, 257-260.
- Heron G., Crouzet C., Bourg A.C.M., Christensen T.H. (1994); Speciation of Fe(II) and Fe(III) in Contaminated Aquifer Sediments Using Chemical Extraction Techniques, *Environ. Sci. Technol.*, **28**, 1698-1705.
- Hesslein R.H. (1976); An in-situ sampler for close interval pore water studies, *Limnol. Oceanogr.*, **21**, 912-914.
- Jørgensen B.B. (1989); Biogeochemistry of Chemoautotrophic Bacteria: In H.G. Schlegel and B. Bowien (editors), *Autotrophic Bacteria*, Springer, 117-146.
- Kasten S., Freudenthal T., Gingele F.X., von Debenneck T., Schulz H.D. (1998); Simultaneous formation of iron-rich layers at different redox boundaries in sediments of the Amazon Deep-Sea Fan, *Geochem. Cosmochim. Acta*, **62**, 2253-2264.
- Kelts K., Briegel U., Ghilardi K. and Hsu K. (1986); The Limnology-ETH Coring System. *Schweizerische Zeitschrift für Hydrologie*, **48**, 104-115.

- Lotter A.F., Renberg I., Hansson H., Stöckli R. and Sturm M. (1997a); A Remote Controlled Freeze Corer for Sampling Unconsolidated Surface Sediments, *Aquat. sci.*, **59** (4), 295-303.
- Lotter A.F., Sturm M., Teranes J.L., Wehrli B. (1997b); Varve Formation since 1885 and high-resolution varve analyses in hypertrophic Baldeggersee (Switzerland), *Aquat. sci.*, **59** (4), 304-325.
- Lovley D.R., Klug M.J. (1983); Sulfate Reducers can Outcompete Methanogens at Freshwater Sulfate Concentrations; *Appl. Environ. Microbiol.*, **45**, 187-192.
- Lovley D.R., Phillips E.J.P. (1988); Manganese inhibition of microbial iron reduction in anaerobic sediments. *Geochim. Cosmochim. Acta*, **46**, 2665-2669.
- Morse J.W., Cornwel J.C. (1987a); Analysis and Distribution of Iron Sulfide Minerals in Recent Anoxic Marine Sediments, *Marine Chemistry*, **22**, 55-69.
- Morse J.W., Millero J.M., Cornwell J.C., Rickard D. (1987b); The Chemistry of the Hydrogen Sulfide and Iron Sulfide Systems in Natural Waters, *Earth Science Reviews*, **24**, 1-42.
- Niessen F., Sturm M. (1987); Die Sedimente des Baldeggersees (Schweiz) - Ablagerungsraum und Eutrophierungsentwicklung während der letzten 100 Jahre, *Arch. Hydrobiol.*, **108**, 365-383.
- Pehkonen S.O., Erel Y., Hoffmann M.R. (1992); Simultaneous Spectrophotometric Measurement of Fe(II) and Fe(III) in Atmospheric Water, *Environ. Sci. Technol.*, **26**(9), 1731-1736.
- Peiffer S., dos Santos Afonso M., Wehrli B., Gächter R. (1992); Kinetics and mechanism of the reaction of H₂S with lepidocrocite, *Environ. Sci. Technol.*, **26**, 2408-2412.
- Rudd J.W.M., Kelly C.A., Furutani A. (1986); The Role of Sulfate Reduction in Long Term Accumulation of Organic and Inorganic Sulfur in Lake Sediments, *Limnol. Oceanogr.*, **31**(6), 1281-1291.
- Dos Santos Afonso M., Stumm W. (1992); Reductive Dissolution of Iron(III)-(Hydr)oxides by Hydrogen Sulfide, *Longmuir*, **8**, 1671-1675.
- Schaller T., Moor H.C., Wehrli B. (1997); Sedimentary Profiles of Fe, Mn, V, Cr, As and Mo as Indicators of Benthic Redox Conditions in Baldeggersee, *Aquat. Sci.*, **59**(4), 345-361.
- Stadelmann P., Herzog P., Arnold P., Bernegger J. C., Butscher E., Hirsiger F., Koller P. (1993), Sanierung des Baldegger- und Hallwilersees und deren Einzugsgebiete. Situationsanalyse und Rechenschaftsbericht zuhanden des Gemeindeverbandes Baldegger- und Hallwilersee. Amt für Umweltschutz Luzern.
- Stadelmann P., Butscher E., Bürgi H.-R. (1997), Massnahmen zur Seesanieung: Beispiel des Baldeggersees. Amt für Umweltschutz Luzern.
- Teranes J.L., McKenzie J.A., Lotter A.F. (1999); Stable isotope response to lake eutrophication: Calibration of a high-resolution lacustrine sequence from Baldeggersee, Switzerland, *Limnol. Oceanogr.*, **44**(2), 320-333.

- Urban N.R., Brezonik P.L., Baker L.A., Sherman L.A. (1994); Sulfate Reduction and Diffusion in Sediments of Little Rock Lake, Wisconsin, *Limnol. Oceanogr.*, **39(4)**, 797-815.
- Urban N.R., Dinkel C., Wehrli B. (1997); Solute Transfer Across the Sediment Surface of a Eutrophic Lake: I. Porewater Profiles from Dialysis Samplers, *Aquat. Sci.*, **59**, 1-25.
- De Vitre R.R., Buffle J., Perret D., Baudat R. (1988); A Study of Iron and Manganese Transformations at the O₂/S(-II) Transition Layer in a Eutrophic Lake (Lake Bret, Switzerland): A Multimethod Approach, *Geochim. Cosmochim. Acta*, **52**, 1601-1613.
- Wallmann K., Hennies K., König I., Petersen W., Knauth H.-D. (1993); New procedure for determining reactive Fe(III) and Fe(II) minerals in sediments, *Limnol. Oceanogr.*, **38(8)**, 1803-1812.
- Wehrli B., Lotter A.F., Schaller T., Sturm M. (1997); High-Resolution Varve Studies in Baldeggersee (Switzerland): Project Overview and Limnological Background Data, *Aquat. sci.*, **59(4)**, 285-294.
- Westrich J.T. (1983); The Consequences and Controls of Bacterial Sulfate Reduction in Marine Sediments, PhD University Yale.

Chapter 3:

Spadini, Bott, Wehrli, Manceau

Analysis of the major Fe bearing mineral phases in recent lake sediments by EXAFS spectroscopy

This chapter is based on a publication submitted to aquatic geochemistry

Abstract

EXAFS spectroscopy and chemical analysis were combined to determine the Fe bearing minerals in recent lake sediments from Baldeggersee (Switzerland). The upper section of a laminated sediment core deposited under eutrophic conditions was compared to the lower part from an oligotrophic period. Qualitative analysis of Fe_K EXAFS agreed well with chemical data: In the oligotrophic section the presence of Fe(II)-O and Fe(III)-O species was evident, whereas a significant fraction of Fe(II)-S sulfides was strongly indicated in the eutrophic part. A statistical analysis was performed by least square fitting of normalized reference spectra. The set of reference minerals included Fe(III) oxides, Fe(II) sulfides, Fe(II) carbonates and Fe phosphates. In the eutrophic section mackinawite appeared as the dominant phase among the Fe(II) sulfides. This observation was in agreement with the significant fraction (18-40%) of acid volatile iron sulfides resulting from specific chemical extraction in sediment samples from the eutrophic period. In the oligotrophic regime no satisfying fit was obtained using the set of reference spectra. It was shown that siderite ($FeCO_3$) was not present in major amount in these carbonate-rich sediments. However, simulations of EXAFS spectra of solid solution (Ca_x, Fe_{1-x}) CO_3 allowed reconstructing the specific patterns of the observed spectra. This phase was therefore proposed to be the dominant Fe form in the oligotrophic section of the core.

Introduction

In complex environmental systems like soils, aquifer material and sediments iron is typically present as a mixture of different mineral phases. Dissolution and precipitation of iron is controlled by redox conditions and different microbial and geochemical processes (Davison 1993, Cornell and Schwertmann 1996, Burdidge, 1993). There is a considerable interest to analyze the dominant mineral form of iron present in these environments. Important parameters such as the adsorption capacity of iron minerals or their bioavailability for iron reducing organisms depend on the mineral phase. On the other hand, information on the oxidation state of Fe and the dominant phase provides important clues to the past and present redox conditions prevailing in a particular system (Chapter 2, Chapter 4 and Schaller et al. 1997).

So far mainly chemical extraction methods were used as operational tools to distinguish different fractions of iron in soils and sediments. For a quantitative analysis of iron sulfides the extraction methods of acid volatile sulfide (AVS) and chromium reducible sulfide (CRS) proved to be quite reliable for the determination of iron sulfides and pyrite, respectively (Morse et al. 1987b) In addition to these *specific* extractions the *sequential* extraction schemes were often used to discriminate between iron oxide, carbonate and phosphate phases. However, Nirel and Morel (1990) summarized the pitfalls of such methods. Recent studies proposed to combine chemical extractions with more direct methods such as diffraction, spectroscopy or microprobe analysis (Manceau et al. 2000). Among the spectroscopic methods Mössbauer (König, 1989) and EXAFS spectroscopy (Friedl et al. 1997) showed significant potential to identify poorly crystallized Fe minerals in sediments.

In this study we addressed the question whether EXAFS is a favourable method to determine the dominant iron phases in recent lake sediments. We characterized sediment samples deposited under different redox conditions in a 65 m deep hardwater lake by selective extraction methods. EXAFS spectra of sediment samples were recorded under strictly anaerobic conditions. In order to analyze the EXAFS data in detail, we compiled a broad database containing the EXAFS spectra of Fe reference minerals. This analysis was focused on the main sedimentary Fe minerals

(excluding silicates), namely the oxides, sulfides, phosphates and carbonates. On the basis of this data set we performed an extensive regression analysis from the EXAFS spectra to evaluate the dominant Fe bearing phases in these recent lake sediments. The comparison of these EXAFS analysis with the results from selective chemical extraction methods allows to formulate a valuable speciation hypothesis for the major Fe bearing species in the lake sediment.

Material and methods

Sampling site and core description

Sediment cores were taken at the deepest site (65 m) of Baldeggersee, a eutrophic hardwater lake near Lucerne, Switzerland. The sediments at this site are continuously varved since 1885 (Niessen and Sturm, 1987). Lotter et al. (1997) and Schaller et al. (1997) analyzed the sediment characteristics of this varved section in detail. The 1.3 m long and 6 cm wide sediment cores were retrieved with an UWITEC gravity corer. They were used for the geochemical analysis as described in detail in chapter 4. A second core was taken on September 1997 for the EXAFS analysis. A simplified sedimentological core profile is shown in Fig. 3.1. The samples #1 to #3 were collected in the 39 cm long black section from the recent eutrophic period. The remaining samples #4 to #10 came from the light grey section deposited earlier, when the lake was oligotrophic. Five of these samples (#5, #6, #7, #9 and #10) corresponded to varve bundles deposited under anoxic conditions and 2 others (#4 and #8) were from homogeneous (bioturbated) sediments from oxic periods in the deep water (Fig. 3.1).

Chemical analysis

The eutrophic section corresponded to the first 39 cm of the core and to the time span between 1885 and 1997. In this section selective extraction methods were applied in order to determine the Fe and S speciation. The Fe(III) and Fe(II) fractions relative to total Fe with the method of Heron et al. (1994). The acid-volatile Fe(II)-sulfides (AVS) and the chromium-reducible Fe(II)-sulfides (CRS) were analysed following Fossing et al., (1989) and Morse et al. (1987a). The AVS fraction is commonly assigned to mackinawite, troilite and pyrrhotite, and CRS compounds are attributed to the FeS₂ minerals pyrite and marcasite (Morse et al. 1987b). Details are described in Chapter 4. The resulting Fe speciation profile is given in Fig 3.1. Fe(III) and CRS minerals represent only minor fractions of total Fe. More precisely, 2.6% to 12.9% of the total Fe is bound as iron(III) (average 5.7%), and 0.3% to 11.0% with an average of 2.5% are bound in the CRS fraction.

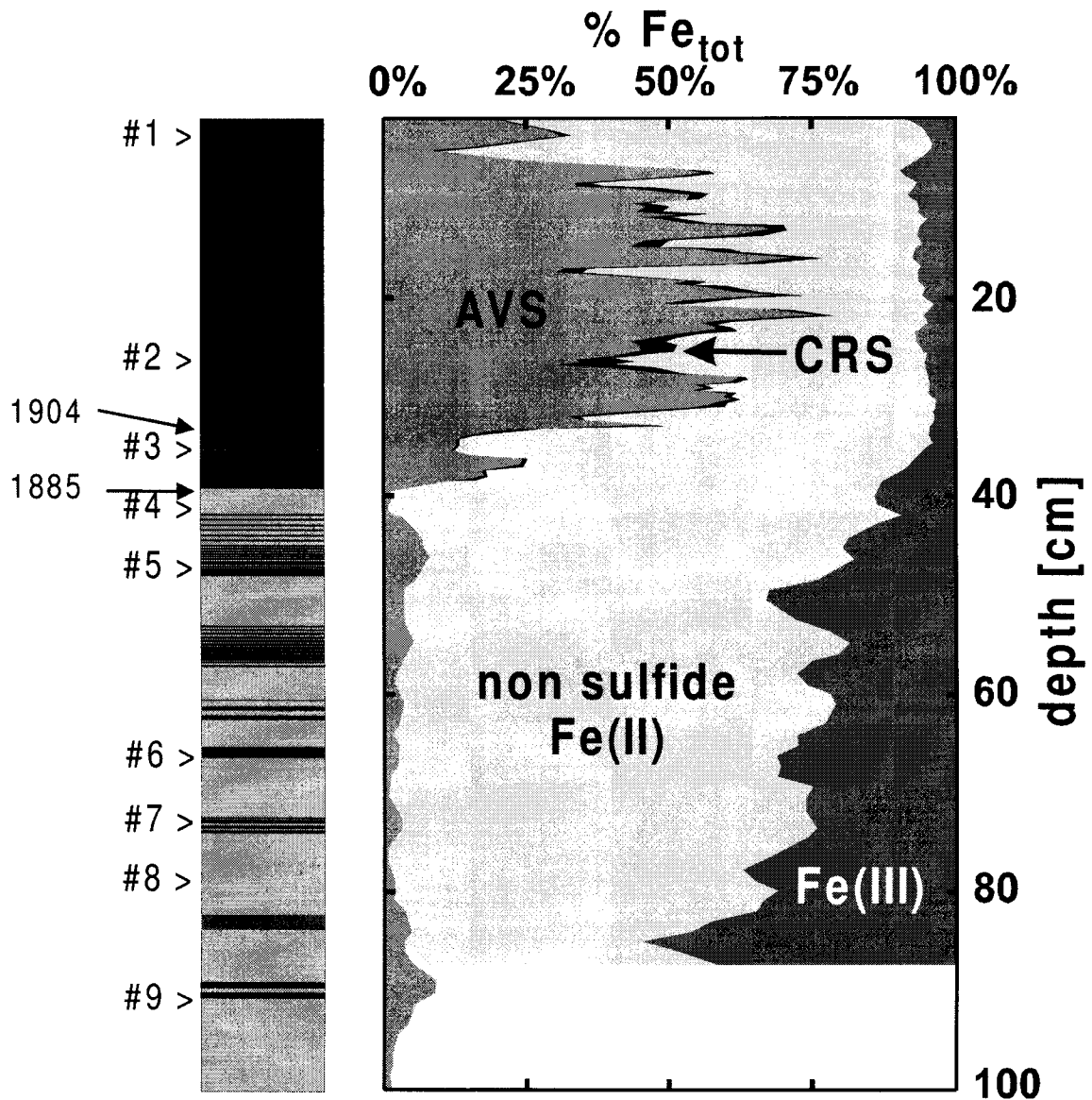


Fig. 3.1: Schematic sedimentological profile recovered from the deepest station (65 m) in Baldeggersee (left). The eutrophic section is given in black, the oligotrophic section in light gray, respectively. Black line bundles indicate the locations of visible varves (annual laminations). '>' indicates the sampling locations of the EXAFS samples #1 to #9. The diagram at right shows the mol-% of different iron fractions obtained by selective extraction. AVS = acid volatile sulfides, CRS = chromium reducible sulfides.

The important fractions are AVS sulfides and the remaining non-sulfide Fe(II) fraction. They bind both together at least 82%, on average 91% of the total iron. In the oligotrophic section the non sulfide Fe(II) fraction dominates the speciation. The Fe(III) mineral fraction increases with depth and becomes the second important fraction. Fig. 3.1 documents also the locations of the EXAFS samples #1 to #10. Table 3.1 displays for each sample the corresponding mean Fe speciation, and the total concentrations of Fe, P and CaCO₃. The Fe speciation and the P content are expressed relative to the total Fe concentration. It is evident from the data in Table 3.1 that the eutrophic samples have generally low CRS, Fe(III) and phosphate concentrations (up to 11% of total iron). As a consequence, iron oxides, pyrite and iron phosphates will be difficult to detect in these sediment samples by EXAFS spectroscopy. By contrast, the Fe(II) sulfides and the undetermined Fe(II) fraction are significant with respect to EXAFS sensitivity.

Table 3.1: Chemical analysis and extraction results related to the EXAFS samples.

#	Depth interval [cm]	Time span year	Fe(III)	[Fe(II)]	[Fe(II)]	Fe (II)	Fe _{tot} μmol/g dry wt.	P _{tot} /Fe _{tot} Mol%	CaCO ₃ % dry wt.
			% [Fe _{tot}]	CRS % [Fe _{tot}]	AVS % [Fe _{tot}]	non sulfide % [Fe _{tot}]			
1	0.2–0.7	1996-97	7.7	0.8	21.5	70.0	265	10.8	62
2	24-27	1927-35	5.7	5.9	40.4	48.0	294	5.6	69
3	35-38	1888-96	7.3	0.5	18.0	74.2	371	4.8	60
4	40-41	1880-82	13.5	0.3	1.0	85.2	346		
5	45-46	~1840	19.8	0.0	7.4	72.8	373		
6	66-67	~1660	33.1	0.0	3.3	63.6	421		
7	71-72	~1580	26.2	0.0	2.4	71.4	529		
8	77-78	~1530	38.9	0.0	1.6	59.5	602		
9	90-91	~1440					599		
10	102-103	~1340					535		

X-ray diffraction analysis

Powder diffraction spectra were recorded on a SIEMENS D5000 spectrometer with a rotating sample disk and a solid state detector. The sample powder was dried under inert atmospheric conditions. Dominant signals were those of quartz and calcite. The minor signals could be attributed to feldspar (albite), mica (muscovite), chlorite (chlinochlore) and dolomite. Other minerals, noticeably Fe compounds, were not found in the diffraction spectra.

Sample preparation, EXAFS data collection and reduction

Immediately after retrieving the cores on the lake the sediment tubes were closed by airtight rubber stoppers and transported to the synchrotron laboratory. EXAFS analysis took place no later than 60 h after coring. The sample preparation was performed under an inert atmosphere in a glove box at the synchrotron laboratory. Adequate core sampling in vertical position was achieved by means of an airtight core gate and a core crank. Fe_K edge EXAFS measurements were performed at the EXAFS D42 station of the L.U.R.E synchrotron radiation facility in Orsay, Paris. Spectra were recorded in fluorescence or transmission mode depending on the metal concentration. X-ray absorption spectra were treated following a standard procedure (Koningsberger and Prins, 1988). The terminology used here corresponds to that given in Sarret et al. (1998).

Analysis of bond distances in iron minerals

The analysis of Fe_K edge EXAFS data from heterogeneous sediment samples is based on the hypothesis that Fe-carbonates, -phosphates, -sulfides and -oxides may be discriminated according to their Fe-1^{st} shell distances. This working hypothesis needs to be verified. The interatomic distances of reference minerals are thus compared in Fig. 3.2: gray-shaded areas mark the distribution of the Fe-1^{st} shell distances of the given mineral groups. Effectively, the gray box for the Fe-sulfide 1^{st} shell distances reflects the largest distances. Almost all individual Fe-sulfide 1^{st} shell distances are longer than those of other groups. In more detail, octahedrally coordinated Fe(II)-S(-II) minerals (smythite, pyrrhotite, troilite) form a distinguished group of maximum Fe-S bond length as compared to Fe(II)-S(-I) minerals - as is expected from crystal chemical rules. Shortest Fe-S distances are found for tetrahedrally coordinated S atoms (mackinawite, greigite). Compared to Fe-sulfides, Fe(II)-O carbonate and phosphate distances are shorter, and the Fe(III)-O group exhibits the shortest bond lengths. Average first shell distances can be determined with a precision of $\geq 0.1 \text{ \AA}$ from EXAFS spectra at the Fe_K edge. Fig. 3.2 therefore shows that a coarse speciation of the main mineral groups is possible for mineral phases which contribute significantly to sediment material.

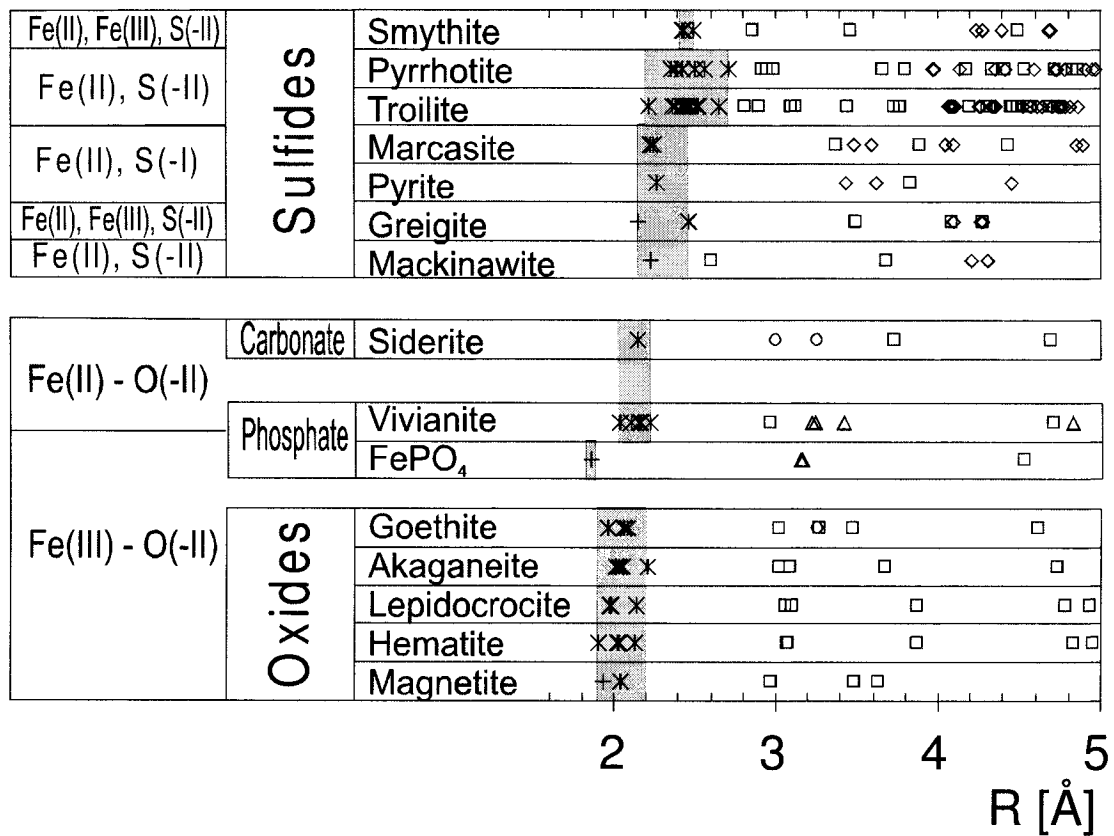


Fig. 3.2: Interatomic distances d_{Fe_c-N} . Fe_c represents the central Fe atom and N the neighboring atom. Oxidation states and the mineral groups are given in the left column. The gray areas mark the individual first shell Fe_c-O and Fe_c-S distances of the given minerals. (*) and (+) indicate their octahedral or tetrahedral coordinations. (\square), (Δ), (\diamond), (\circ) refer to Fe, P, S and O neighbors in next-nearest shells, respectively. Oxygen atoms were plotted up to an Fe_c-O distance of 3.4 Å only.

Results and Discussion

Qualitative spectra analysis

The normalized EXAFS Fe_{K} edge $k^2\chi(k)$ spectra of the sediment samples are shown in Fig. 3.3. The spectra represent the Fe_{K} edge X-ray absorption fine structure of the sediment samples, recorded with increasing wave number, i.e. with increasing energy relative to the Fe_{K} edge. The top three samples #1 to #3 relate to the eutrophic lake regime whereas the seven lower samples #4 to #10 come from sediment strata deposited under oligotrophic conditions. Generally all 10 spectra are close in shape. The signal seems essentially composed from a single oscillation thus probably related essentially to the first coordination shell of the central Fe atom. A particular beating pattern is observed in all spectra at 8 \AA^{-1} . The generalized occurrence of this signal could indicate the occurrence of a unique mineral phase in all of these samples, i.e. in both the eutrophic and oligotrophic range. This feature will be discussed in more detail later. Some of the spectra differ nevertheless significantly in the low k range at $k < 7 \text{ \AA}^{-1}$. The raw spectra of the oligotrophic group (#4 to #10) look almost identical, they have all a $k^2\chi(k)$ maxima at 4.0 \AA^{-1} . By contrast, the spectra of the eutrophic group (#1 to #3) show this phase maxima slightly shifted towards higher k values (Fig. 3.3, see arrows). Visibly this k shift changes continuously in going from sample #1 to #4. Thus roughly two groups of spectra can be identified: (i) The seven spectra of the oligotrophic section are almost invariant, which indicates a constant speciation with depth. (ii) The three spectra of the eutrophic section change continuously with depth.

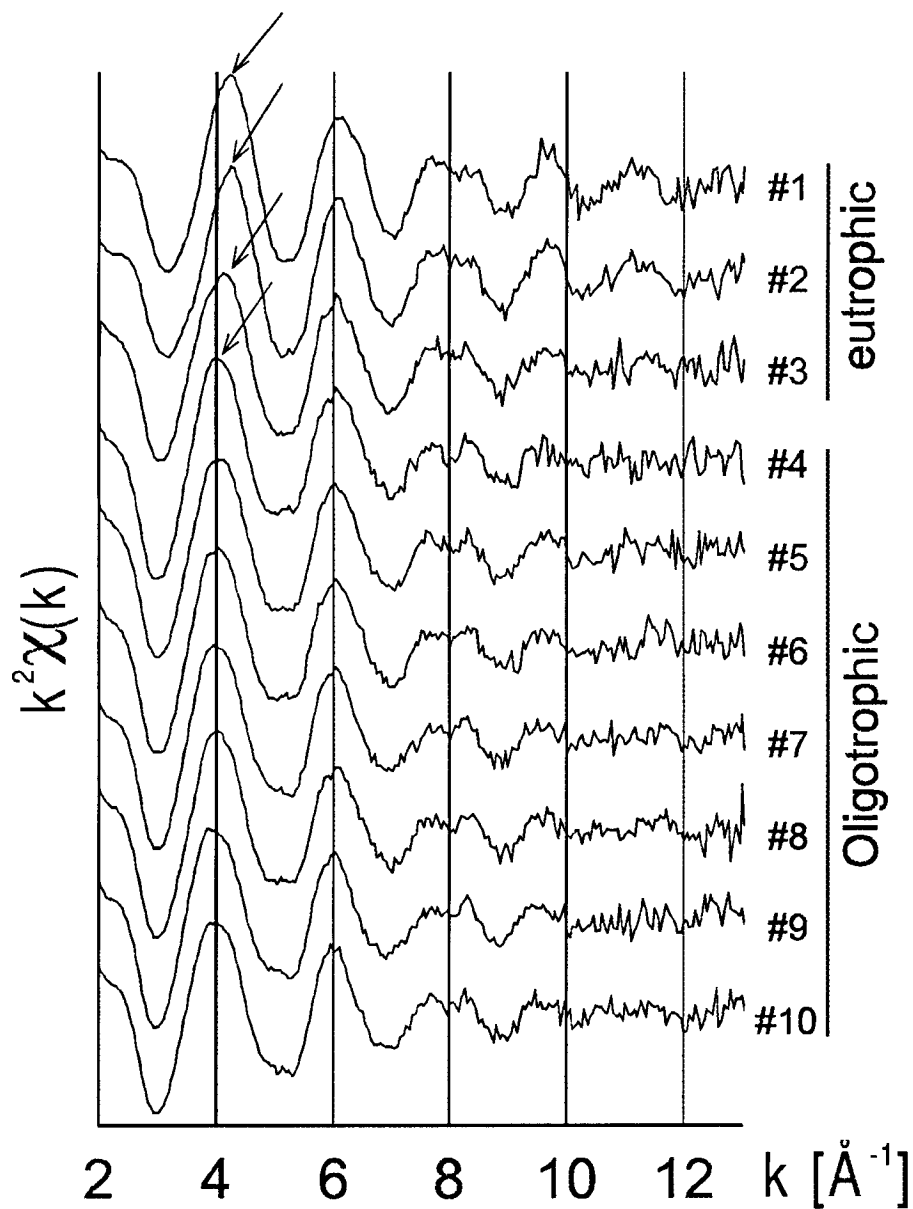


Fig. 3.3: Normalized $k^2\chi(k)$ spectra of the 10 analyzed sediment samples. #1 to #3 relates to the eutrophic core section whereas samples #4 to #10 are collected in the deeper oligotrophic core fraction.

The samples of the oligotrophic group were alternatively recovered from varved and unvarved sections. Thus the spectra of samples #4 and #8 were recovered from sections of homogeneous light grayish color whereas samples #5, #6, #7, #9 and #10 instead were from darker varved zones (Fig. 3.1). The corresponding EXAFS spectra showed no variation with depth. Thus the EXAFS records seemed not to be sensitive to the speciation change related to core colouring. The black colour related to the presence of Fe-sulfides. Chemical analyses indicated a relative increase of Fe bound AVS minerals in varved sections (Fig. 3.1, Table 3.1). However the corresponding Fe fraction was low, the maximum Fe sulfide concentration in the oligotrophic section of interest was on average only 3.1% with a maximum of 11.2% of total Fe. This fraction was clearly too low to be discriminated by EXAFS from the predominant contributions. The EXAFS signal in the oligotrophic section is therefore certainly dominated by other non-sulfide Fe species.

The oligotrophic and eutrophic samples thus certainly differ fundamentally with respect to mineralogy. These differences can be qualitatively observed when comparing their radial distribution functions RDF, obtained by Fourier transforming the Fe_K EXAFS spectra (Fig. 3.4). These RDF provide information of the Fe-oxygen or Fe-sulfur bond distances in the first coordination shell of Fe which will be discussed in more detail. The RDF of the samples #1 and #8 are plotted in Fig. 3.4 together with some relevant reference compounds. The RDF position of the maxima of the 1st peak relates to the mean Fe-1st shell distance. The sample #1 exhibits a maximum at 1.9 Å and the #8 maximum is at 1.75 Å respectively. This indicates that the mean Fe-1st shell distance in sample #1 is longer than that of #8.

A first speciation hypothesis can be formulated when comparing these RDF to those of the reference minerals given in Fig. 3.4. The positions of the 1st shell maxima of both #1 and #8 compare best to those of vivianite and siderite. Both are Fe(II) minerals with an oxygen lattice. Thus major concentrations of Fe(II)-O minerals are supposed to be present in both #1 and #8. In comparison the 1st peak positions of Fe-sulfides (the Fe(II)-S group) appear at longer distances, and inversely the Fe(III)-oxides distances (Fe(III)-O group) are shorter.

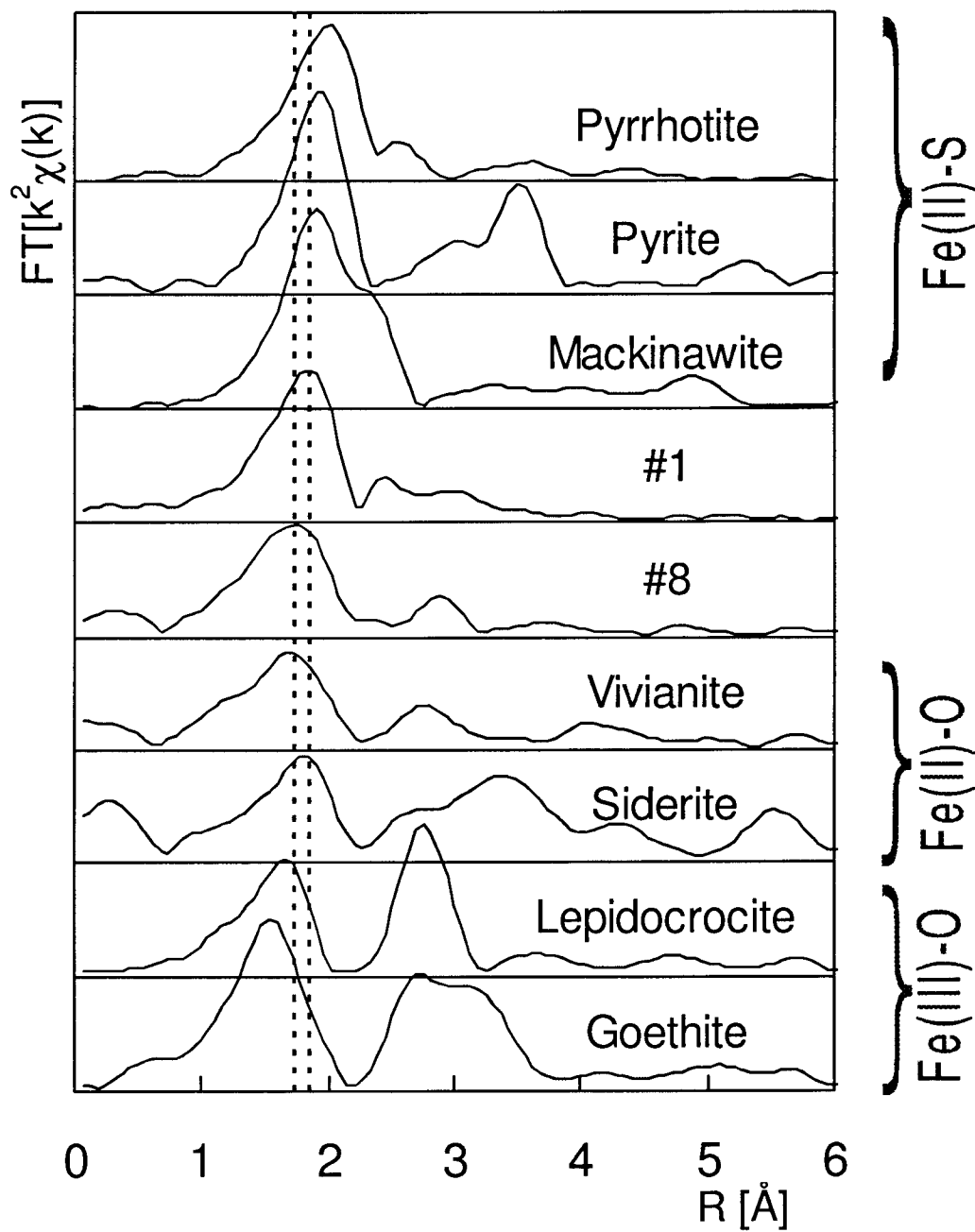


Fig. 3.4: Radial distribution functions (RDF) of samples #1, #8 and reference compounds.

In more detail, the #1 peak points to longer distances compared to the peak of #8. It approaches positions of Fe(II)-S minerals. The spectrum #1 from the eutrophic lake may thus incorporate simultaneously significant fractions of both Fe(II)-S and Fe(II)-O minerals. This first speciation proposition matches results of the chemical analysis (Fig. 3.1, Table 3.1). In the eutrophic range two major Fe fractions were detected with specific chemical extraction methods. The first fraction consisted of AVS minerals contributing with 7.3 to 85% to the speciation of Fe (sample #1 had 22% AVS). This AVS fraction can be related to the Fe(II)-S group contributing to the EXAFS data in Fig. 3.4. The second important fraction could be assigned to non sulfide Fe(II) minerals (15 to 86%, sample #1 had 70% of this fraction). This fraction corresponds to the dominant contribution of the Fe(II)-O group in the RDF of Fig. 3.3. There are two important mineral groups, which could correspond to this Fe(II)-O group: phosphates and carbonates. The P/Fe ratios reach maximum levels in the 4-22% range of total Fe for the eutrophic section. In sample #1 the P/Fe ratio is 10.8 mol%. In the oligotrophic sections lower P/Fe ratios are observed. In general the total P concentration is too low to bind a significant fraction of the iron in the Fe(II)-O group. The carbonates are therefore the most likely candidate for iron binding in these sediments.

Quantitative spectra analysis

Statistical analyses of EXAFS data were performed with linear combinations of reference and sample $k^2\chi(k)$ spectra and subsequent least square regression analysis. In a first round a systematic but uncritical fit procedure was applied: all possible pair combinations of reference spectra (marcasite & siderite, marcasite & goethite etc.) were fitted to the sample spectra #1 and #8, respectively. The results are presented as a two dimensional map of the number of merit in Fig. 3.5. Crosses on a white background correspond to the best correspondence. The merit of the other squares decreases with increasing darkness.

In these uncritical approach the least square sum U was minimized as $U = \sum (k^2\chi_{\text{exp}} - k^2\chi_{\text{th}})^2$ with $k^2\chi_{\text{exp}}$ representing the sample $k^2\chi$ value and $k^2\chi_{\text{th}}$ the value of the summed and optimized contributions of the two reference spectra. Greigite, troilite and smythite EXAFS spectra were not available and consequently generated with the FEFF7 code (label FEFF). The adequate FEFF7 simulation parameters were

determined by comparing the available experimental spectra to their FEFF7 simulations. Well crystallized reference compounds yield good agreement with FEFF7 standard parameters and an overall σ^2 value $SIG2=0.0064$ at the exception of siderite. For this compound and pyrrhotite $SIG2$ was fixed to 0.0144 to take account of the relatively low spectral amplitude. Crystal chemical parameters for pyrrhotite were taken from Nakano et al., 1979. The given simulation of mackinawite is based on the idealized vacancy-free FeS structure proposition of Uda et al, 1968. The simulated spectrum can thus not be taken as representative for iron deficient $Fe_{1-x}S$ mackinawite. It nevertheless yields a comparable merit of fit to the lc mackinawite spectrum. The low crystalline (lc) mackinawite compound was synthesized at pH 8 (Berner, 1964) and verified by X-ray diffraction analysis.

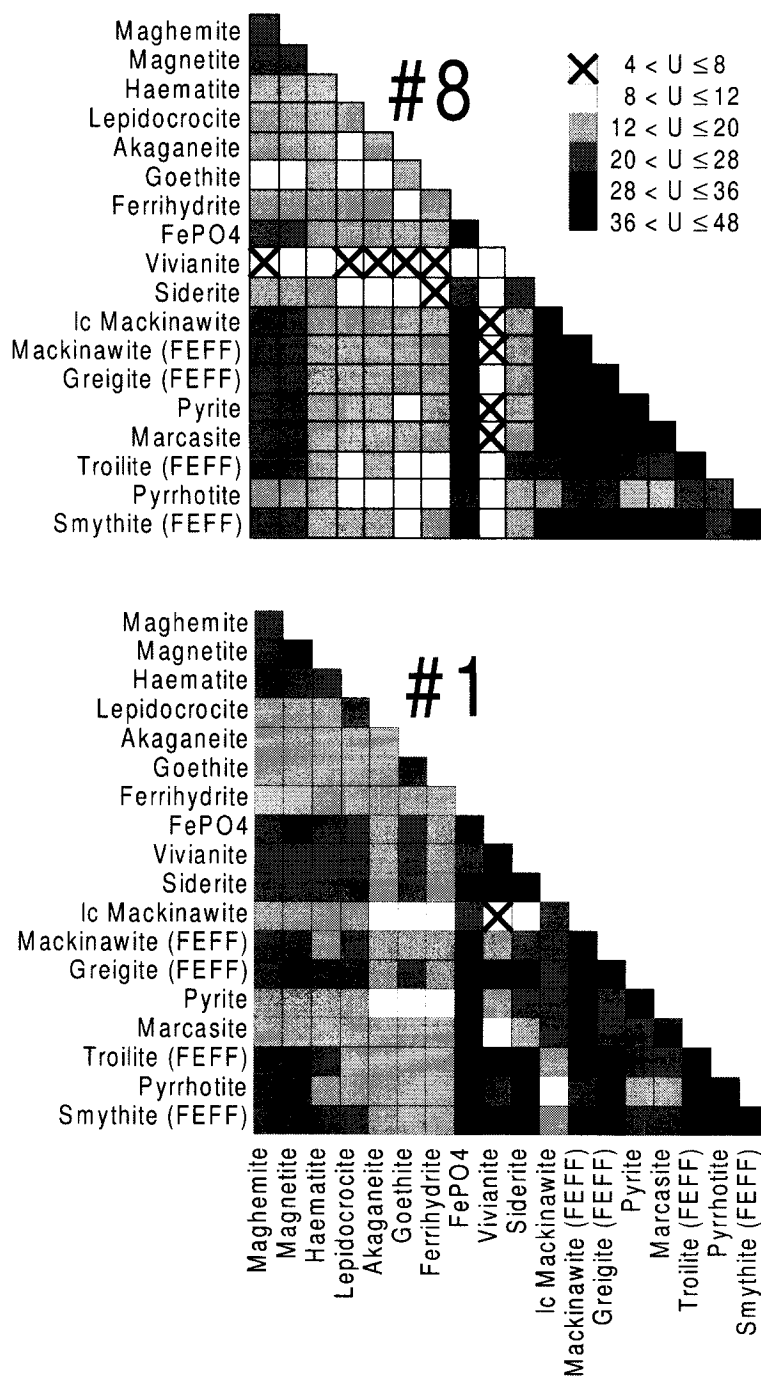


Fig. 3.5: Map of least square error sums for a fit of sample spectra #8 and #1 with two reference compounds. Crossed squares indicate optimal fits, darker squares indicate increasing least square errors.

Oligotrophic section: Vivianite itself fits very well to #8, all combinations including vivianite have correspondingly a good merit. Most of the best solutions marked with a cross in Fig. 3.5 include this reference mineral. The only competitive alternative combines siderite and ferrihydrite. Further linear combinations with good numbers of merit are found when combining two iron oxides (goethite, ferrihydrite, lepidocrocite and akaganeite) or one oxide with siderite or some of the Fe-sulfide references (pyrrhotite, pyrite, troilite). This statistical approach identifies primarily vivianite, and then also siderite, some Fe oxides and Fe sulfides as potential major Fe bearing minerals in the oligotrophic section of the sediment. Most of these propositions do not agree with the chemical findings. As already noticed Fe-phosphates and Fe sulfides are potentially present as a minor fraction only. In the oligotrophic regime the uncritical systematic fitting fails to identify relevant mineral species. On the other hand, the best fitting mineral vivianite belongs to the Fe(II)-O group. At this group level the fit result compares well to the speciation scheme expected from RDF findings in the oligotrophic section. While not predicting the major mineral species, the approach nevertheless results in a valuable proposition for the dominant mineral group.

Eutrophic section: All 'best' (cross) and 'good' (white square) combinations in sample #1 involve Fe-sulfides. Effectively the presence of Fe(II)-S minerals in #1 is indicated from chemical and comparative RDF findings. In particular the best solution combines mackinawite and vivianite, thus an Fe-sulfide and a Fe(II)-O compound. As for #8, uncritical systematic fitting leads to valuable propositions with respect to the dominant mineral groups. But, uncritical fitting fails again in delivering reasonable mineral species combinations. Vivianite can only represent a minor Fe bearing fraction according to the chemical analysis results. On the other hand mackinawite as an AVS compound is compatible with both chemical and RDF results. The repeated occurrence of mackinawite in several good fits (white squares) indicates that this species systematically improves the linear regression fits. The combined evidence suggests that mackinawite is effectively a major Fe-bearing sediment compound. However, the repeated presence of the only marginally important vivianite spectrum in best fits indicates that this species behaves as a placeholder for an Fe species not included in the reference data with similar first shell properties as vivianite. This hypothetical species would then necessarily subsist in both trophic

ranges. More generally, the repeated presence of vivianite points to the strong similarity of all of the sample spectra and further to the suggested predominance of one or several so far not identified Fe(II)-O minerals.

Experimental and reference $k^2\chi(k)$ spectra were systematically compared to obtain more information. The four top fits in Fig. 3.6 (1a to 1d) compare sample #8 individually to each of the four references vivianite, ferrihydrite, siderite and goethite found in the best solutions of Fig. 3.5. A common systematic deviation between #8 and each of these four references is indicated at 5.3 \AA^{-1} by a vertical line in Fig. 3.6: the $k^2\chi(k)$ value of the #8 spectrum is always significantly lower than those of the four references. It is thus mathematically not possible to solve this misfit by linearly combining these four reference spectra. The same significant misfit can still be observed in the fit 6e. In this 3-component fit all species which could be major Fe bearing species were included (siderite, ferrihydrite, goethite, akaganeite, hematite, maghemite, magnetite, lepidocrocite). In Fig. 3.6f, a 4-component fit, all non-sulfide references were included. Also in this case the 5.3 \AA misfit prevails. We therefore conclude that the database is not representative for the speciation in sample #8. EXAFS spectra of major Fe species may be missing, or sample and reference species may have a different local Fe order. The following section is dedicated to the solution of this specific problem.

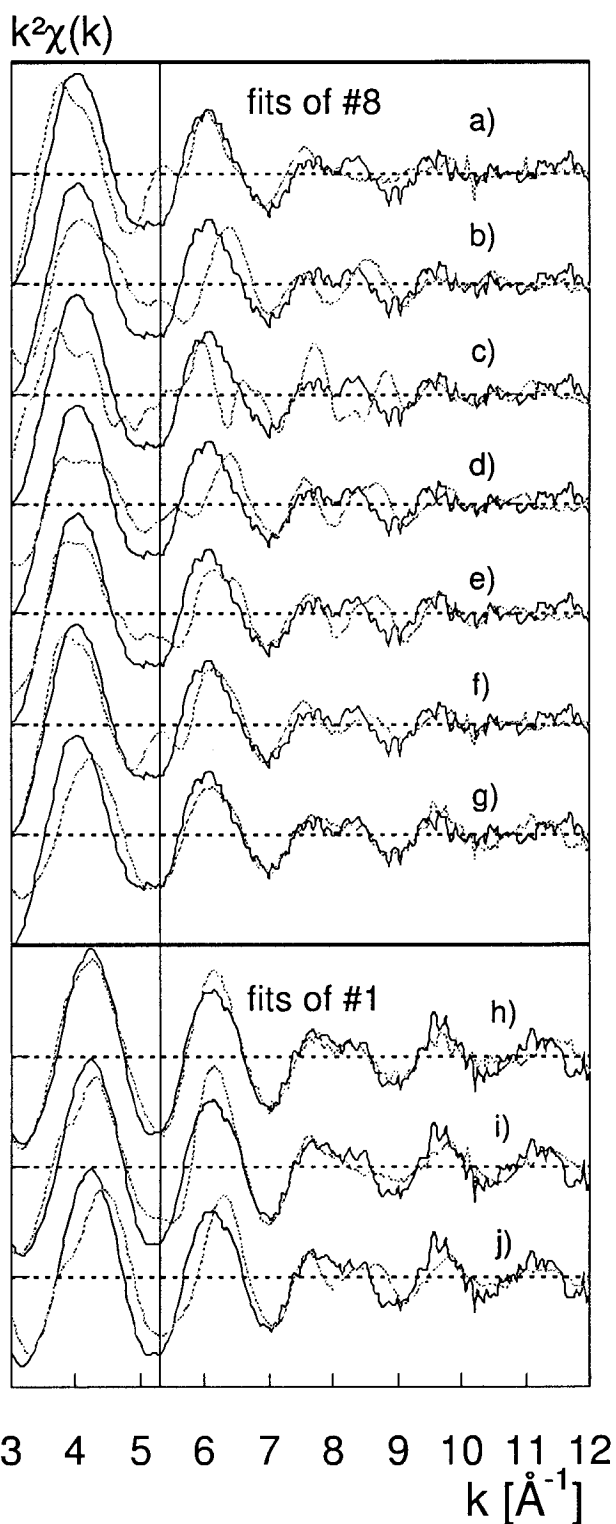


Fig. 3.6: Spectra #8 and #1 (black lines) compared to fitted spectra (grey lines). The following references were used in calculating the fits: a) vivianite, b) ferrihydrite, c) siderite, d) goethite, e) siderite, ferrihydrite and lepidocrocite, f) vivianite, ferrihydrite, lepidocrocite and siderite, g) spectrum #1 used as reference, h) spectrum #8 and lc mackinawite, i) vivianite and lc mackinawite and j) goethite and lc mackinawite. Table 3.2 list the relevant amplitude factors and compares the figures of merit of the fits.

Speciation proposition

It was already mentioned that all ten sample spectra are close in shape. This observation and in particular the beating pattern between 7.7 and 8.3 Å⁻¹ (Fig. 3.3) common to all spectra are indicative for a unique species in both trophic regimes. Further, the repeated presence of vivianite in the best eutrophic *and* oligotrophic fit results justifies the hypothesis of a unique major Fe(II)-O species. In the oligotrophic regime EXAFS spectra were found to be invariant. This points to one single and dominating Fe bearing compound. The #8 spectrum is thus supposed to represent the EXAFS spectrum of this unique and dominating species, referred to thereon as #8 species. In a first round the spectrum #1 was fitted to the #8 spectrum (Fig. 3.6g). This yields the best merit when compared to other one-component fits 6a to 6d. This reflects the strong similarity of oligotrophic and eutrophic spectra and further indicates that possibly the dominant Fe species generating the #8 spectrum exists also in #1. Considering the #8 spectrum as potential signal of a major Fe species this spectrum was thus included in the reference database for fitting the #1 spectrum. The best two-component fit (Fig. 3.6h) incorporates consequently the #8 spectrum and the spectrum of low crystalline (lc) mackinawite. This mineral was already determined in other lake sediments by classical microscopic techniques. The suggestion of #8 being representative for a major Fe bearing species existing in both trophic regimes thus leads to an acceptable speciation proposition. The two dominant phases corresponding to the chemically predicted AVS and the non-sulfide Fe(II) fraction would thus consist of mackinawite and the so far undetermined species #8. All other two-component fits compatible with the chemical analysis results have a significantly lower merit. For comparison the best two-component fit not including the #8 spectrum is given in Fig. 3.6i and includes vivianite and lc mackinawite. 6j finally is the best two-component fit which does not include the #8 spectrum and which is compatible with the chemical analysis results. Obviously, this fit does not match the experimental #1 spectrum. The calculation of 3- and 4-component fits did not lead to further coherent information: the #8 spectrum and lc mackinawite were constantly found in best and compatible fits, but no further components could be unambiguously determined. Minor Fe phases were thus not further investigated.

Table 3.2: EXAFS fits of spectra #1 and #8 with reference data (Fig. 3.6). Merit of the spectral fit: $V = \Sigma(k^2\chi_{exp} - k^2\chi_{th})^2 / \Sigma(k^2\chi_{exp})^2$

#	Fit	References	Amplitude factors	Figure of merit V
8	a	Vivianite	0.86	0.0733
8	b	Ferrihydrite	0.54	0.1048
8	c	Siderite	0.42	0.1523
8	d	Goethite	0.45	0.1062
8	e	Siderite, ferrihydrite and lepidocrocite	0.32, 0.28 and 0.16	0.0721
8	f	Vivianite, ferrihydrite, lepidocrocite and siderite	0.58, 0.25, 0.58 and 0.52	0.0492
8	g	Spectrum #1 used as reference	0.71	0.0562
1	h	Spectrum #8 and lc mackinawite	0.78 and 0.49	0.035
1	i	Vivianite and lc mackinawite	0.67 and 0.74	0.053
1	j	Goethite and lc mackinawite	0.32 and 0.59	0.0959

The next question of interest concerns the mineralogical nature of the #8 species. Fe replacing Ca in the calcite structure seems to be a valuable proposition to be tested: CO_3^{2-} ligands are abundant in the sediment, calcite and thus also a $(\text{Ca}_x, \text{Fe}_{1-x})\text{CO}_3$ solid solutions may form in both eu- and oligotrophic conditions. Also, the central Fe atom is in a Fe(II)-O environment as required from RDF findings. A final important argument relates to the variation of the chemically determined molar ratio of the Fe(III) to the non sulfide Fe(II) fraction (Fig. 3.1). In the oligotrophic range, this ratio increases from 0.16 (#4) to 0.67 (#9). This significant change has no influence on the series of invariant EXAFS spectra #4 to #10. A change of the spectral habit would be expected in case of formation of a specific mineral species incorporating the Fe(III) ions. The independency of the EXAFS signal to this change could indicate the incorporation of both Fe(II) and Fe(III) ions in a unique local environment – as could be in the case of a Fe-Calcite solid solution formation. An EXAFS spectrum of Fe containing calcite was not available. Therefore a hypothetical $(\text{Ca}_x, \text{Fe}_{1-x})\text{CO}_3$ structure was generated step by step with the FEFF7 code (Rehr et al. (1991), Zabinsky et al., (1995))

Generation of a $(\text{Ca}_x, \text{Fe}_{1-x})\text{CO}_3$ structure

The siderite FeCO_3 and calcite CaCO_3 structures are isomorph. In both the central Me(II) ion is coordinated in an equidistant manner to 6 oxygen atoms (1st shell), 6 carbon (2nd shell), 6 oxygens (3^d shell) and 6 Ca(II), Fe(II) (4th shell) atoms. The related Me-interatomic distances of siderite and calcite are 2.14, 3.00, 3.26, 3.73 Å, and 2.36, 3.21, 3.46, 4.05 Å, respectively. In a first step the siderite spectrum was simulated with the FEFF7 code (Rehr et al. (1991), Zabinsky et al., (1995)) to test the validity of the simulation. Calculated and measured siderite spectra do not compare adequately (Fig. 3.7a): At $k < 7 \text{ \AA}^{-1}$ a significant phase shift is observed, increasing with decreasing k values. In addition calculated and experimental beating patterns do not compare at $k < 5 \text{ \AA}^{-1}$. Such strong differences are not acceptable, specifically when considering the sensitivity of linear combination fitting to phase shifts. The calculation of the same structure but with removed next-nearest 2nd C and 3rd O shells (Fig. 3.7b) leads to a better match between calculation and experiments. Thus next-nearest inner shells were not considered in the following calculations. In Fig. 3.7c, the #8 spectrum is compared to a calculation of a siderite FeO_6 octahedra ($d_{\text{Fe-O}} = 2.144 \text{ \AA}$). The comparison shows that the two spectra do not compare. A better fit is obtained for a FeO_6 octahedra with a shortened Fe-O distance $d_{\text{Fe-O}} = 2.080 \text{ \AA}$ (Fig. 3.7d). The calculated spectrum matches the experimental phase at $k < 7 \text{ \AA}^{-1}$. This model octahedron replaces in the next calculation (Fig. 3.7e) a central CaO_6 ($d_{\text{Ca-O}} = 2.36 \text{ \AA}$) in calcite. The measured and calculated spectra are relatively close, in particular the characteristic beating pattern at 8 \AA^{-1} is reproduced. However, the pattern is partly out of phase. Relaxation of the inner Ca shell surrounding the central Fe atom can be expected from crystal chemical rules. The spectrum with $d_{\text{Fe-Ca}}$ shortened to 3.94 \AA^{-1} (4th shell) as compared to the calcite $d_{\text{Ca-Ca}} = 4.05 \text{ \AA}$ and to the siderite $d_{\text{Fe-Fe}} = 3.73$ - is given in fig. 3.7f. This model reproduces the 8 \AA^{-1} beating pattern more closely. The relaxation corresponds to a distance shift of 1/3 from the calcite $d_{\text{Ca-Ca}}$ 4th shell distance toward the siderite $d_{\text{Fe-Fe}}$ 4th shell distance. The Ca shell thus approaches Ca-Ca calcite rather than Fe-Fe siderite distances - which is considered reasonable for this 4th shell. Nevertheless the spectrum is still out of phase when considering the beating patterns at 6 and 4 \AA^{-1} respectively. These patterns relate to Fe - Ca contributions as indicated in fig. 3.7h. In this simulation all O and C shells, including the first one, are removed. This pattern

difference was not analyzed further. The disagreement is possibly linked to shell-related disorder of the solid solution. Fig. 3.8g finally presents a simulation of a complete $(\text{Ca}_x, \text{Fe}_{1-x})\text{CO}_3$ structure with all O, C, shells included. For this, 2nd O and 3^d C shells were placed at halfway between siderite and calcite Me-shell distances. This spectrum is slightly shifted to lower k values in the low k range when compared to the simulation given in fig. 3.8f. As explained above, a comparable effect was observed when comparing the experimental and calculated siderite spectra. We thus propose the simulation 8f as the most representative for the #8 spectrum.

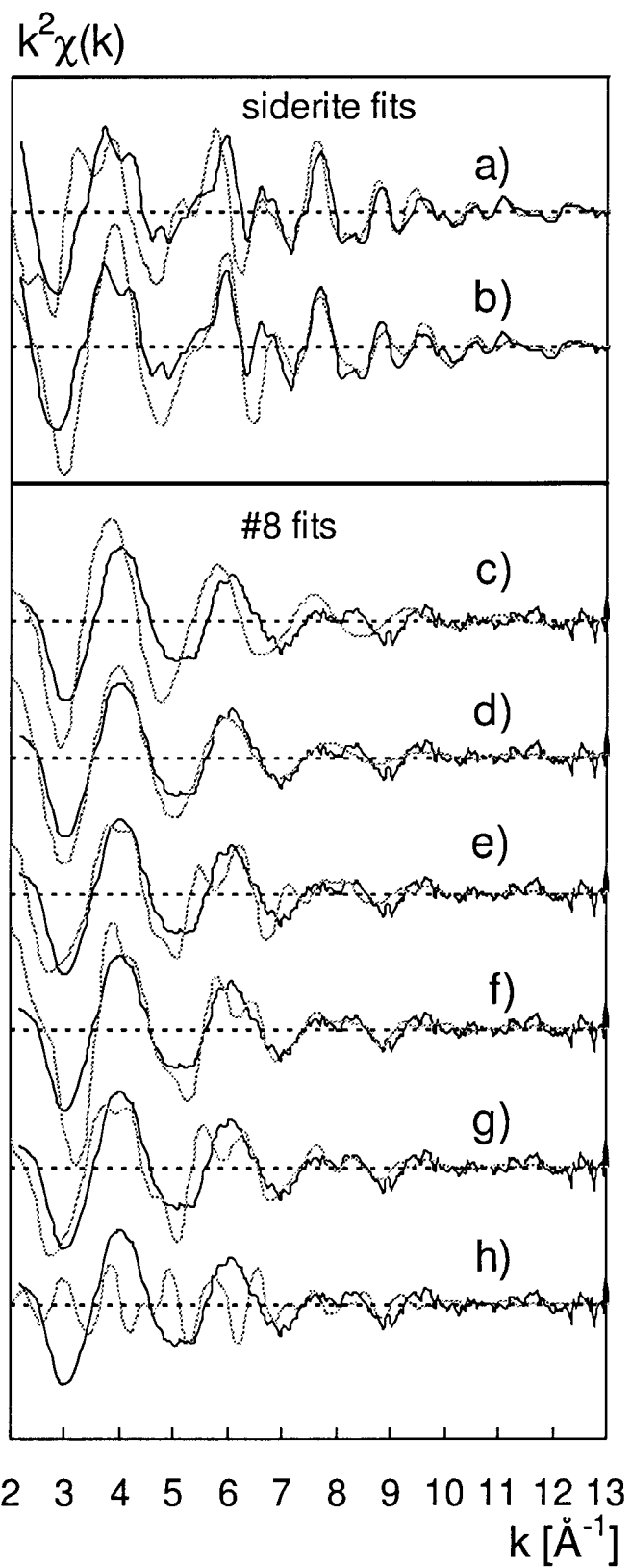


(Fig. 3.7.)

Fig. 3.7: *Experimental spectra (black lines) compared to simulated spectra (grey lines) obtained with the FEFF7 code. a) and b): experimental and calculated siderite spectra. In the calculation a) all shells surrounding the central Fe atom are taken into account. In b) the 2nd and 3d C, O shells were removed. c) and d): The experimental #8 spectrum compared to simulations of FeO₆ octahedra. The c) FeO₆ octahedra was calculated at a Fe-O distance $d_{\text{Fe-O}} = 2.144 \text{ \AA}$ which equals that in siderite. In d) this distance was shortened to $d_{\text{Fe-O}} = 2.08 \text{ \AA}$. e) to g): The #8 spectrum compared to (Ca_x, Fe_{1-x})CO₃ solid solution structure models. The simulation is based on a calcite cluster in which the central CaO₆ octahedra is substituted by a FeO₆ octahedra at $d_{\text{Fe-O}} = 2.08 \text{ \AA}$. In e) the 2nd and 3d O, C shells of the cluster were removed. In f) the 4th Ca shell of the cluster was additionally relaxed as given in the text. In g) all shells were taken into account, the 2nd to 4th shells are relaxed as given in the text. h) represents a calculation of the f) cluster but with all C, O shells removed, including the first one.*

Clearly this simulation does not perfectly fit the experimental spectrum. Also, the calculated short Fe-O 1st shell distance is confusing when considering the expected relaxation of a siderite FeO₆ octahedra within a calcite cavity. Considering the compatibility of the proposed structure to chemical and fit-related findings we nonetheless propose this species as being the dominant Fe bearing species in the oligotrophic Baldeggersee sediment. In the eutrophic section, mackinawite adds as second major species to this Fe-Calcite solid solution.

Conclusions

The present work applies EXAFS spectroscopical methods to analyse a complex natural lake sediment. The study allows us to test the potential of EXAFS spectra analysis linked to linear combination techniques to decipher the Fe speciation in a lake sediment. In the given case the method proved successful in identifying the major Fe species in the lake sediment when combined to chemical selective AVS, CRS and Fe(II), Fe(III) extraction methods. Information from EXAFS chemical analysis allowed us to distinguish major *individual* mineral species whereas specific chemical extraction methods deciphered major *groups* of minerals species such as AVS and CRS minerals. The two methods are thus clearly complementary. Also the combination of the two methods allows us to enhance the validity of speciation hypotheses. EXAFS alone is found to have limited methodological functionality to discriminate the dominant existing species in a complex system such as the given lake sediment. In particular the linear combination fit approach requires a priori knowledge of the reference compounds and the associated EXAFS spectra. Thus major species not included in the database may be disregarded. In the given case the $(\text{Ca}_x, \text{Fe}_{1-x})\text{CO}_3$ solid solution compound was not evident in a statistical analysis of reference compounds. Its existence was revealed from the combination of EXAFS and chemical analysis results. Also natural compounds may be more or less substituted and their EXAFS spectra may correspondingly differ significantly from well crystallized reference compounds. Limits of validity of fit merits are consequently difficult to fix, the validation of fits by chemical analysis results is thus essential. In summary, EXAFS and selective extraction working methods complements each other with respect to mineralogical information and reliability of speciation information, the combination of several investigation tools is generally strongly indicated when solving speciation problems in complex natural systems.

References

- Berner, R. A., *J. Geol.*, **72**, 293-306 (1964)
- Burdridge D. J. (1993) The biogeochemistry of manganese and iron reduction in marine sediments. *Earth –Science Reviews*, **35** 249-284.
- Cornell R. M. and Schwertmann U. (1996) The Iron Oxides. Structure, Properties, Reactions, Occurrence and Uses. VCH Verlagsgesellschaft, Weinheim. 573 pp.
- Davison W. (1993) Iron and manganese in lakes. *Earth-Science Reviews*, **34**, 119-163.
- Fossing H., Jørgensen B.B. (1989); Measurement of Bacterial Sulfate Reduction in Sediments: Evaluation of a Single-Step Chromium Reduction Method, *Biogeochemistry*, **8**, 205-222.
- Friedl G., Wehrli B. and Manceau, A. (1997) The role of solids in the cycling of manganese in eutrophic lakes - new insights from EXAFS spectroscopy. *Geochim. Cosmochim. Acta* **61**, 275-290.
- Heron G., Crouzet C., Bourg A.C.M., Christensen T.H. (1994); Speciation of Fe(II) and Fe(III) in Contaminated Aquifer Sediments Using Chemical Extraction Techniques, *Environ. Sci. Technol.*, **28**, 1698-1705.
- König, I. (1989) ⁵⁷Fe-Mössbauer-Spektroskopie an jungen Sedimenten. Ph.D. Thesis. University Hamburg. 132 pp.
- Koningsberger, D. C., and Prins, R., Ed. "X-ray Absorption", John Wiley & Sons, New York, 1988
- A.F. Lotter, M. Sturm, J.L. Teranes, B. Wehrli (1997) Varve formation since 1885 and high-resolution varve analyses in hypertrophic Baldeggersee (Switzerland), *Aquat. Sci.* **59**, 304-325,.
- Manceau A. , Lanson B. , Schlegel M. L. , Harge J. C. , Musso M. , Eybert-Berard L. , Hazemann J.-L. , Chateigner D. , Lambelle G. M. (2000) Quantitative Zn speciation in smelter-contaminated soils by EXAFS spectroscopy *Am. j. sci.* (1880). **4**, 289-343
- Morse J.W., Cornwell J.C. (1987a); Analysis and Distribution of Iron Sulfide Minerals in Recent Anoxic Marine Sediments, *Marine Chemistry*, **22**, 55-69.
- Morse J. W., Millero J. M., Cornwell J. C., Rickard D. (1987b); The Chemistry of the Hydrogen Sulfide and Iron Sulfide Systems in Natural Waters, *Earth Science Reviews*, **24**, 1-42.
- Nakano, A., *Acta crist.*, **35B**, 722 (1979)
- Niessen F., Sturm M. (1987); Die Sedimente des Baldeggersees (Schweiz) - Ablagerungsraum und Eutrophierungsentwicklung während der letzten 100 Jahre, *Arch. Hydrobiol.*, **108**, 365-383.
- Nirel P. M. V., and Morel F. M. M. (1990) Pitfalls of sequential extractions. *Water Res.* **24**, 1055-1056.
- Rehr, J. J., Mustre de Leon, J., Zabinsky, S. I., Albers, R. C. (1991) Theoretical X-ray Absorption Fine Structure Standards. *J. Am. Chem. Soc.*, **113**, 5135-5145

Sarret, G., Manceau, A., Spadini, L., Roux, J.-C., Hazemann, J.-L., Soldo, Y., Eybert-Bérard, L., and Menthonnex (1998) J.-J., *Envir. Sci. Technol.*, **32**, 1648-1655

Schaller T., Moor H. C. and Wehrli B. (1997) Sedimentary profiles of Fe, Mn, V, Cr, As and Mo recording signals of changing deep-water oxygen conditions in Baldeggersee. *Aquatic Sciences* **59**, 345-361.

Uda, L., *Zeitschr. anorg. allg. Chem.* **361**, 94-97 (1968)

Zabinsky S. I., Rehr J. J., Ankudinov A, Albers R. C., and Eller M. J. Multiple Scattering Calculations of X-Ray Absorption spectra. *Phys. Rev. B.* **52**, 2995 (1995)

Chapter 4:

Bott, Sturm, Wehrli

Iron sulfides in lake sediments as potential indicators for continental climate conditions – a 8000 year record from Baldeggersee, Switzerland

This chapter is based on a publication submitted to the Journal of Paleolimnology

Abstract

Iron sulfide accumulation was studied on a long sediment core from the deepest site of Baldeggersee, Switzerland. The study addressed the question whether old varved sediment sections deposited over the 8000 years reflect eutrophication events or changes in deep-water mixing. Recent varves from the anthropogenic eutrophication period starting around 1885 were used as a reference. The old varved sediment sections were characterized by a high acid volatile sulfur (AVS) concentrations of $60 \mu\text{mol g}^{-1}$ dry weight compared to baseline AVS values of $0\text{-}5 \mu\text{mol g}^{-1}$ dry weight. Varved sections showed lower compaction (65% water content compared to 50% in non-varved sections). The AVS maxima in laminated sections suggest that the sediment-water interface remained anoxic over decades to centuries. The recent sediment from the anthropogenically eutrophied lake shows AVS values which are three times higher than the maxima observed during the past 8000 years. Lower concentrations during the past clearly indicate that primary production, organic carbon deposition and hypolimnetic anoxia in Baldeggersee were significantly lower compared to the present.

A preliminary age model was established by correlation with ^{14}C AMS dates on a core taken in 1978. The model indicates that varved sections occur with a period of 1000 - 1500 years. A similar pattern was observed recently for proxies of ice-rafted debris and cosmogenic radionuclides in North Atlantic sediments, suggesting a solar forcing of Northern hemispheric temperature conditions. Records of glacier advances and retreats from the Swiss Alps show a similar periodicity as the North Atlantic record and the AVS time series of Baldeggersee. Results from a previous study showed that AVS concentrations in recent sediments correlated with average yearly temperatures with warmer conditions leading to more stratification and higher sulfide concentrations in the sediment. Together, these different lines of evidence strongly suggest that the AVS record in deep meromictic lakes can be used as a sensitive proxy for deep-water mixing and climatic forcing. The 1000 - 1500 year periodicity of the varved sections in Baldeggersee sediments supports the hypothesis that European climatic conditions showed similar fluctuations in the past 8000 years as the iceberg record of the North Atlantic.

Introduction

Climatic conditions in the past are recorded in several environmental archives such as tree rings, ice cores and lake sediments. The density of annual tree rings is now established as a proxy for warm summer temperatures (Schweingruber et al. 1979). Cold summers rich in precipitation trigger the advancement of glaciers. Ice moraines are used to reconstruct the position of glaciers in the past (Hantke 1958 and Maisch et al., 1993). Ice cores contain a wealth of climatic information (Lorius et al. 1990). Isotope measurements such as $\delta^{18}\text{O}$ values of calcite in lake sediments are also used to quantify climatic changes such as the transition from cold conditions during the Younger Dryas to warmer temperatures at the end of the last ice-age (Fischer et al. 1997).

In the present study we examined whether iron sulfide concentrations in the sediment of Baldeggersee (Switzerland) represent an adequate climate proxy for temperature or precipitation during the last 8000 years. The formation and preservation of iron sulfides depend on the oxygen concentration at the sediment-water interface. When no oxygen is present in the bottom water reduction of sulfate and iron(III) occurs and the resulting hydrogen sulfide and ferrous iron precipitate as iron sulfide (Chapter 2). Oxygen competes with sulfate reduction in mineralization processes and reoxidizes iron sulfides. Oxygenation of bottom water is possible during winter when the water column has a constant temperature of about 4°C (Wüest et al. 1992). Because of a small density gradient in the water column a turn over followed by an intense mixing of oxygen into the hypolimnion is possible. Two factors may modify deep-water mixing and therefore sulfide deposition in the sediments: 1) Intense winter storms and rapid cooling of the water column both support the mixing process during the cold season. Mild weather conditions and low wind activity during winter, however, can lead to permanent stratification of the water column. As a consequence a salt gradient in the deep water builds up and promotes anoxic conditions in the hypolimnion. Baldeggersee is shielded against westerly winds by hills on the eastern shore. Therefore it reacts sensitively to climatic forcing. 2) Intense precipitation washes phosphates from the soils. P-loading enhances productivity and may also lead to anoxia in the hypolimnion. High iron sulfide concentrations in the sediment may therefore indirectly indicate low mixing (mild

weather) or enhanced productivity (P-leaching from soils by heavy rainfall). In chapter 2 we found that average temperatures of 3 years correlate well with iron sulfide and pyrite concentrations in sediment strata between 1950 and 1982. The climatic signal in the sediment was clearly discernible because of the stable highly eutrophic state of the lake. Before 1950 the shift in trophic changed also the oxygen consumption. Under these conditions not only climatic factors determined the iron sulfide formation. The goal of this consecutive work is to examine whether climatic conditions in the past can be reconstructed from iron sulfide concentrations in the older sediment from periods where the lake was in a stable mesotrophic state and anthropogenic nutrient fluxes were small.

Material and methods

Study site

Baldeggersee was formed in the catchment of the ancient Reuss-glacier during the Würm glaciation about 20'000 ago. At the end of this cold period a branch of the glacier reached from Lucerne over Hochdorf (at the south end of the lake today) to Seon (Hantke 1958). During its retreat two end moraines were formed which dammed the river. Lacustrine deposits in 135-180 m depth in these moraines indicate that a previous lake existed at a similar location before the last glaciation took place. First the lake basin was filled with „dead“ ice without any connection to the retreating glacier. The early sediments contain a sequence of allochthonous clays and silt material. Alluvial soils show that the early Baldeggersee originally had twice the extension of today (Niessen and Sturm, 1987). Baldeggersee today is 67 m deep, it has a surface area of 5.2 km² and a volume of 0.173 km³ (Fig. 4.1). The hydraulic residence time is on average 4.3 years. The catchment of 67.8 km² consists of steep hillslopes and a large wetland area at the southern end of the lake, which is now drained for agricultural use. A more detailed overview of the limnology of Baldeggersee is given by Wehrli et al. (1997) and Gächter and Wehrli (1998).

Sampling

Sediment samples were taken from the deepest site in the lake with a modified Kullenberg corer. The principles of the coring system have been described by Kelts et al. 1986. Fig. 4.2 illustrates the coring procedure. A short pre-fall corer (length about 1.5 m) is fixed to the main corer with a rope. It takes a short undisturbed sediment sample of the recent sediment. When it reaches the sediment, the end of the main corer is positioned close to the sediment-water interface. A piston is fixed inside the main tube at the sediment surface and is initially positioned at the lower end of the tube. The main corer with its mass of about 400 kg is released when the pre-fall enters the sediment. The fixed position of the piston prevents a buildup of pressure in the tube. A core catcher at the bottom end holds the sediment core during retrieval.

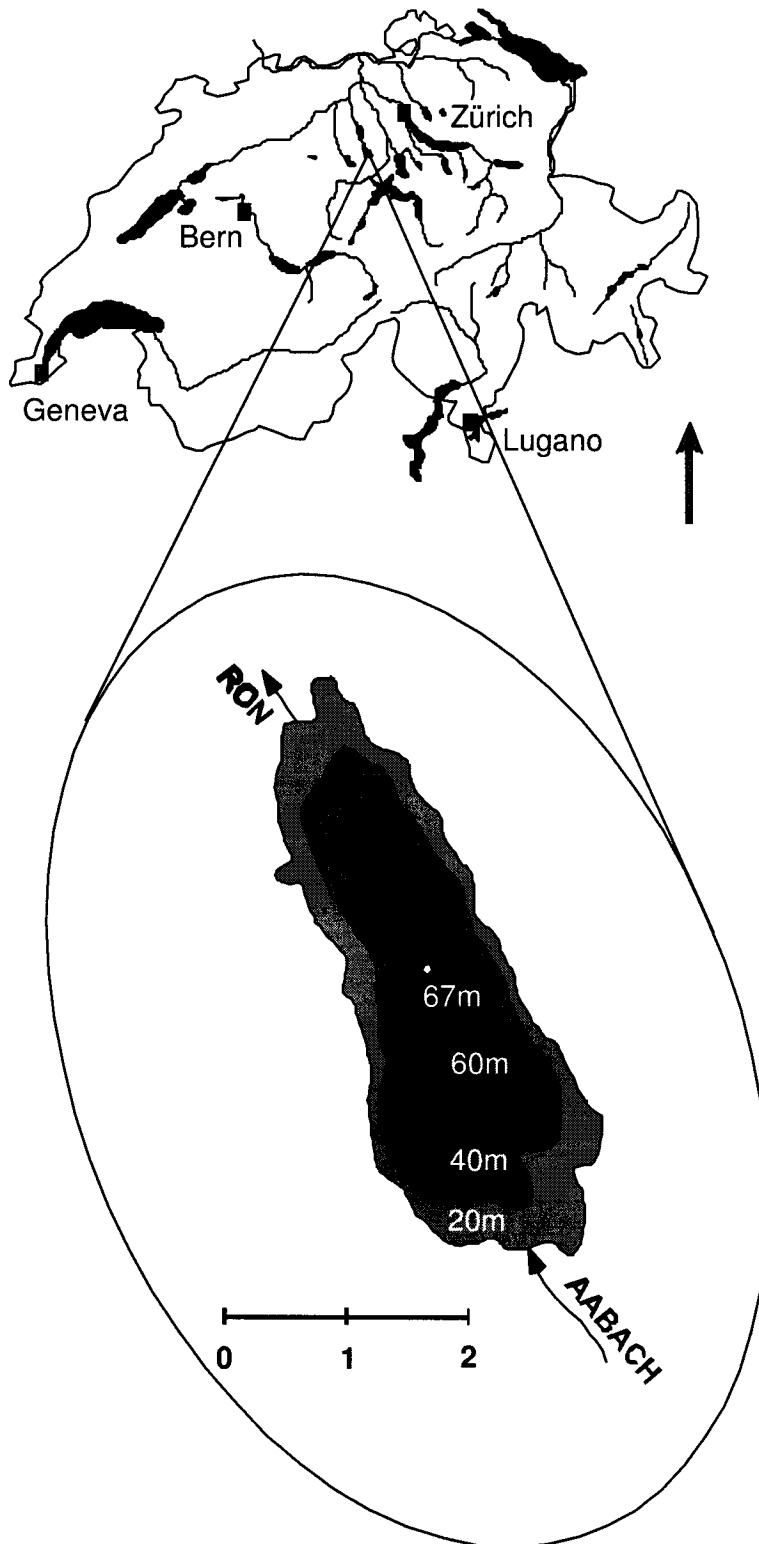


Fig. 4.1: Baldeggersee in central Switzerland. The deepest site at about 67 m.

Table 4.1: Overview of sediment cores from the campaign in November 1997 on Baldeggersee.

core	BA97-1	BA97-2	BA97-3	BA97-4	BA97-5	BA97-6
date/time of sampling	4.11.97 10:45	4.11.97 13:00	4.11.97 15:30	5.11.97 10:00	5.11.97 12:30	5.11.97 13:45
coordinates (Swiss map)	662 027 227 256	662 109 227 706	662 114 227 770	662 354 227 733	662 277 227 861	662 277 227 861
water depth	45m	66m	65m	66m	60m	67m
# of sections	6	10	?	10	?	8
pre-fall	no	yes	no	no	no	Yes
Measurements	-	activity of methanogenesis	-	in situ hybridisation AVS	magnetic measurements	dry weight, elemental analysis, sedimentological analysis

With this technique it was possible to take cores with a length of about 8 m. The coring campaign in Baldeggersee took place from November 4 to 5 1997. Six cores were retrieved. The coordinates and water depths of the stations are summarized in Table 4.1. In this study we analyzed core BA97-4 from the deepest part of the lake (66m). It was correlated with core BA97-6 from the same site in order to include dry weight data.

Methods

Immediately after recovery, sediment cores were cut into sections of about 90 cm length and gastightly closed in the field with plastic caps and tape. After transport to the laboratory the cores were cut longitudinally by using Cu-bronze plates. One half was used for fotografic documentation and measurements of sediment dry weight. The other half of the core sections BA97-4 was immediately transferred to the glove box without removing the copper plate. Sampling for sulfide analysis was performed in the glove box with a nitrogen atmosphere. These sections were stored in the cold room for further sedimentological analysis. The water content was determined on sections of core BA97-6 with a resolution of 1 cm by lyophilisation. For chemical analysis of iron and sulfur the half-cores were cut into slices with a round copper bronze plate and transferred to small labeled plastic boxes in an oxygen free

atmosphere. All chemicals used were of reagent grade quality. Iron(III) was digested with 5 M HCl following the method of Heron et al. (1994). The digestion time was 24 days. All solutions were analyzed photometrically with the method of Pehkonen et al. (1992, see chapter 2). For the analysis of acid volatile sulfide (AVS, mainly iron sulfides) and chromium reducible sulfur (CRS, corresponds to pyrite) we followed the method described by Morse (1987). About 1.2 g of sample and 1.2 g of $\text{SnCl}_2 \cdot 2\text{H}_2\text{O}$ were weighted into a stoppered glass vessel. Outside the glovebox 20 ml of 4 M HCl were added in a nitrogen atmosphere. The liberated H_2S was caught in a trap containing 25 ml 0.15 M zinc-acetate.

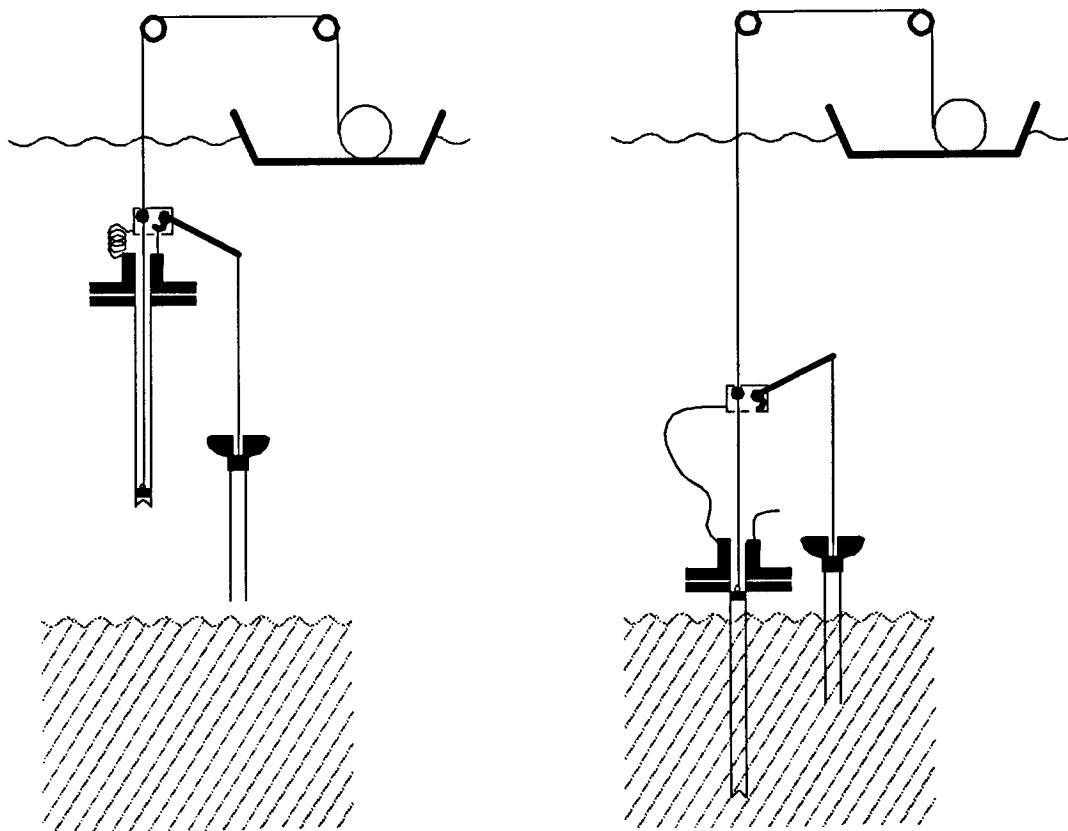


Fig. 4.2: Kullenberg piston corer with prefall before free fall (left) and after free fall (right). First the prefall is fixed to the arm of the lever which carries the heavy long corer. After entering into the sediment of the prefall the fall down of the heavy corer is induced by losing the force at the lever. A core catcher in the corer holds the sediment material during retrieval.

After stirring during one hour the trap was changed and CRS was determined in the same sample by adding 5 ml of 12 M HCl and 12 ml of 1 M Cr^{2+} -solution in 0.5 M HCl. The chromium(II)-solution was prepared following Fossing et al. (1989). After stirring for 60 minutes at ambient temperature the CRS collected in the Zn-acetate traps was analyzed by redox titration (see chapter 2).

Sediment dating

A series of ^{14}C -AMS dates will be measured on core BA00-3. A detailed lithological description of this core has already been performed (by Monecke and Sturm, in prep.). It can be correlated to the two other cores from the deepest site (BA97-4 → AVS and BA97-6 → dry weight) used in the present study. Since the new radiocarbon dates are not yet available our preliminary analysis had to rely on an age model from an earlier coring campaign. Six long cores were already retrieved in 1978 in Baldeggersee along a longitudinal transect (Giger et al. 1984). Core BA78-8 from the deepest site was analyzed in more detail. A lithological description is available together with ^{14}C dating on biomarkers (Sturm, unpublished). Colour and position of stratigraphic markers such as varved sections were aligned to produce an approximate age model of cores BA97-4. Figure 4.3 presents a coarse lithological overview and the correlation between the three cores BA78-8, BA97-4 and BA97-6. The ^{14}C -age was rectified to calendar age by dendrochronological data from Stuiver and Kra (1986) and Kromer and Becker (1993). However, since the radiocarbon dating on BA78-8 was done on biomarkers our preliminary age model includes the error of the ^{14}C reservoir effect. This means that the real dates might be up to a few hundred years younger than our age model predicts. For a preliminary discussion of millennial-scale features these uncertainties are still acceptable. The first reference point dated by ^{14}C is about 1190 years old (110 cm depth) and the time scale between this date and 1885 (39 cm depth) was interpolated assuming constant sedimentation rate. Further it was assumed that the end of one sediment section is adjacent to the beginning of the next section even though some sediment material was lost during cutting (approximately 1 cm). High methane concentrations caused gas expansion by gas bubbles in some parts of the core. Such effects may explain part of the discrepancy between the two cores shown in Figure 4.3. The time interval for the prominent varved sections was estimated by varve counts.

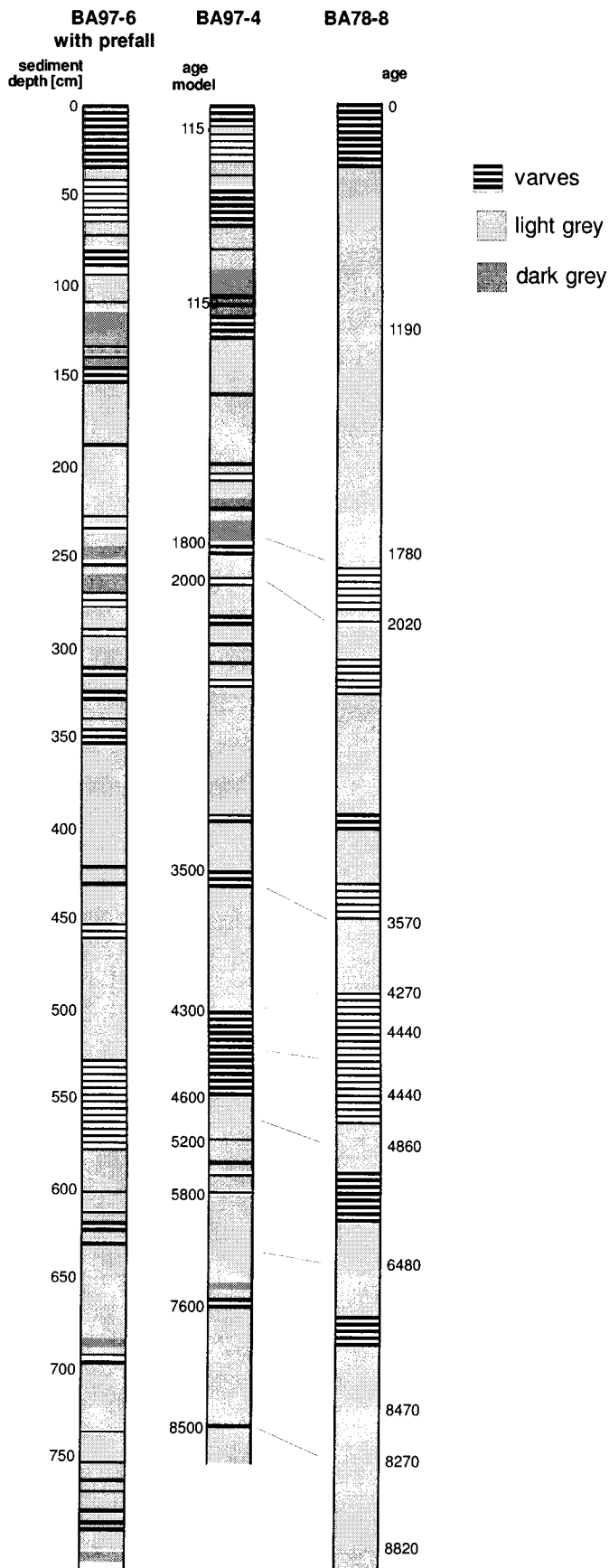


Fig. 4.3: Correlation of the cores BA97-4, BA97-6 and BA78-8. Core BA78-8 was dated with the ^{14}C -method. The correlations with core BA97-4 are marked with lines.

Core description

The core BA97-4 contains varved sections, light gray strata and dark gray sequences. Furthermore thin brown layers, strata with leaves and in the deeper part of the core sections with sand, silt and marl were found. Of central interest in this study are the dark and usually varved sections of the core which indicate absence of bioturbation and long-term anoxia in the deep hypolimnion. An overview of the varved, the dark gray and the light gray sections is given in Tab 4.2. The recent sediment since 1885 is varved (Lotter et al., 1997b). The next section downcore contains various changes with light gray, dark gray and varved layers until about 1250 years ago. Before that age the sediment is usually light gray with some dark layers. Many dark sections are found in the period from 1600 until 2500 years, in the 3500-year-old sediment. An extensive section with very well preserved varves appears in the 4400 year old sediment. Only thin dark layers are present in the older sediment.

Table 4.2: Preliminary age model and description of AVS trends for core BA97-4. For comments on age model see text, AVS = acid volatile sulfide

age [years]	age top [years]	Age bottom [years]	thickness [cm]	description	AVS concentration [$\mu\text{mol/g}$ dry weight]
	0	115	37	varves	Maximal 200
	115	1260	120	many changes in colour	All maxima < 60
	1260	1580	65	light grey	All values < 8
	1580	2500	125	many changes in colour	All maxima < 40
	2500	3250	80	light grey	< 10
3250			5	varves	20
	3250	3550	30	light grey	< 10
3550			11	varves	60
	3550	4300	65	light grey	< 10
4300-4600			50	clear varve sequence	60
	4600	5500	37	light grey	< 10
5500			3	black laminations	< 25
	5500	7300	75	light grey	< 10
7300			about 10	black laminations	< 20
>7500				light grey	< 10

Climate data

The AVS record was compared with several other proxy data from the literature. Table 4.3 gives an overview of the different proxies.

Table 4.3: *Climate records*

proxy	method	time window	Authors
CH winter temperature	weather observations	years 1525-1980	Pfister (1994)
CH annual precipitation	weather observations	years 1525-1980	Pfister (1994)
northern hemisphere temperature	diverse, mainly dendro-chronology	years 1000-2000	Crowley+Lowrey (2000) and Mann et al. (1999)
alpine climate	glacier positions	since 10'000 B.P.	See referencies in Broecker (2001)
north atlantic climate	ice-rating debris	since 10'000 B.P.	Bond et al. (2001)

Semiquantitative indices for temperature and precipitation in Switzerland back to the year 1525 were compiled from historical sources by Pfister (1994). Their resolution is one month and the relative scale reaches from -3 to +3 normalized to average temperature and precipitation. For comparison a 5 year running mean of the climatic indices was calculated. For temperature comparison only the months December to the following February were considered. November temperatures are quite uniform and in March the stratification of the lake often starts already. For precipitation Pfisters annual mean index was used.

Temperature records for the last millenium were recently reconstructed from different records such as dendrochronology, pollen, isotopes, etc). Here we use the recent reconstruction by Mann et al. (1999). The average different observations for the northern hemisphere cover both the cold little ice age (approx. 1580-1850 AD) and the medieval warm period (approximately 1000-1300 AD). We will use these records of the last millenium to test the sensitivity of varve formation towards small average temperature changes. For long-term reconstructions of the climate we have to rely on proxies from the Alps – mainly geomorphological observations on glacier positions. These regionally quite diverse and sometimes conflicting data have been summarized by Maisch et al. (1999) and recently by Broecker (2001). Important

glacier retreats corresponding to warmer temperatures and/or less precipitation were centered around the medieval warm period and 2400, 4300, 6600 and 8700 years ago (Broecker, 2001).

A continuous record of North Atlantic climate has been reconstructed from sedimentological signals of ice-rafting debris in sediment cores south of Labrador (Bond et al, 2001). The oscillations in this records were successfully correlated to proxies for solar activity such as ^{10}Be in Greenland ice cores. We will use these records to test the hypotheses that varve sections in Baldeggersee are linked to changes in North Atlantic climate.

Results

The concentration of acid volatile sulfur decreases drastically at the boundary of the recent varved sediment. Figure 4.4 compares the AVS curve with a photograph of the short core. The sulfide concentration in the homogenized bioturbated sediment is typically on the order of $10 \mu\text{mol/g}$ dry sediment, i.e. twenty times lower than in the varved section of the eutrophic lake. Varve couplets correlate very well with AVS peaks. These observations confirm that high AVS values are a sensitive indicator for meromictic conditions with anoxia at the sediment surface and for the absence of bioturbation. The AVS peaks before never exceed $60 \mu\text{mol/g}$ dry sediment through the Holocene. The complete AVS record from core BA97-4 is compared in Fig. 4.6 to the dry weight measurements of core BA97-6.

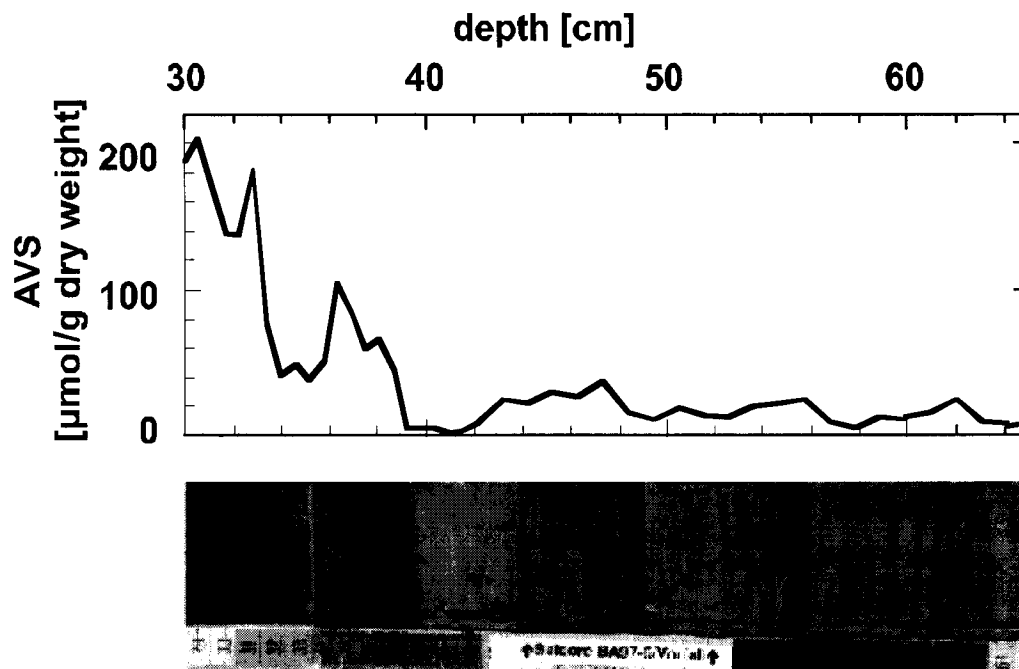


Fig. 4.4: The black colour of the core is accompanied by higher AVS concentrations.

Dry weight

Interestingly the dry weight plot correlates very well with the AVS plot. This validates the correlation of the two cores. Gray marl sections have a much smaller porosity than AVS rich sections. Sections with one mass-% AVS contain about 15% dry material. An increased partition of organic matter in these sections may be accompanied with more water. Further analyses will show whether organic matter or other components in the sediment cause those dry weight changes.

AVS

Before 1885 AVS varies within one order of magnitude. From bottom to top of the sediment core a first peak with high AVS-concentrations appears in the approximately 7500 years old sediment. Since then the AVS concentration oscillates from low baseline levels (about 4 $\mu\text{mol/g}$ dry weight) to AVS maxima with up to about 60 $\mu\text{mol/g}$ dry weight (Fig. 4.5 and Table 4.2) In the older part of the sediment the period between the different AVS maxima is about 1000 years. A very thick varved layer with high AVS concentrations is present in the 4400 year old sediment. Similar high concentrations appear again in the 3500 year old layers. In the timespan between 2500 B.P. and 1885 the frequency of the oscillations increases significantly. A section with low AVS-concentrations is found at about 1.5 m depth in the 1300 to 1600 year old sediment. A high number of AVS-peaks is present in the most recently deposited 1000 year old part of the sediment. The most recent varved section from the eutrophic phase exhibits the highest AVS concentrations during the last 8000 years.

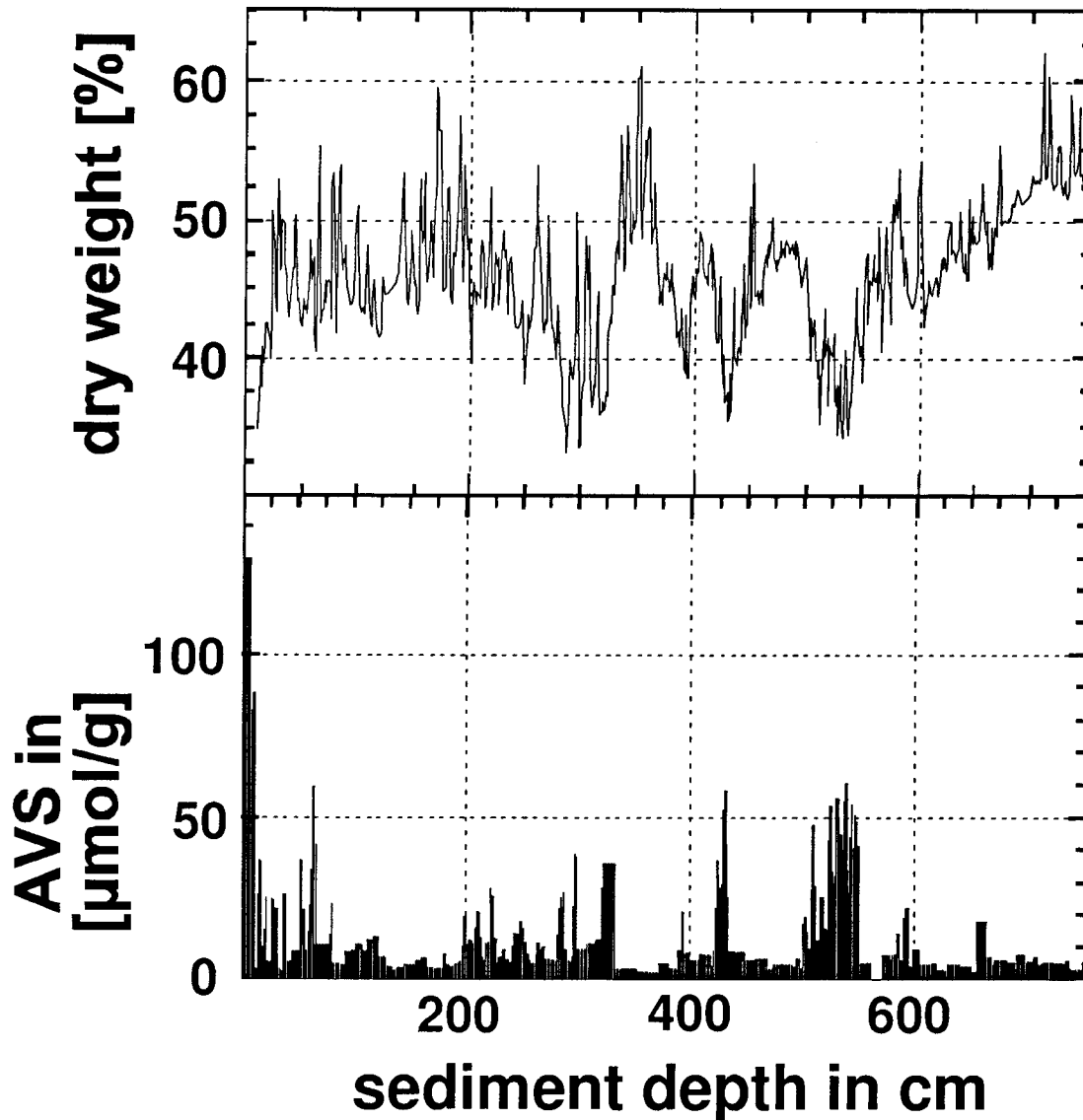


Fig. 4.5: Dry weight profile of core BA97-6 and AVS profile of core BA97-4. The AVS concentration varies about one order of magnitude. The negative correlation between AVS and dry weight is obvious.

Iron speciation

Interestingly, iron(III) was found in the older sediment sections (Fig 4.6). Before 1905 the baseline of its profile increases constantly up to a value of more than 50% of total iron which is in the gray marl about $370 \mu\text{mol/g}$ dry weight (Schaller et al. 1997). In this range AVS maxima are accompanied by iron(III) minima. The extraction method may underestimate the Fe(III)-concentrations in the sediment. Iron(III) can be reduced during the digestion (in 5M HCl for 3 weeks) when free hydrogen sulfide is

present (Dos Santos, 1992). Reduction of iron(III) by hydrogen sulfide during the digestion might cause these negative bumps in the iron(III) plot. It seems that the iron(III) in sections older than 115 years will be transformed by reductants from the overlying younger sediment. Slowly reducing organic matter or even the diffusion of hydrogen sulfide could be responsible for the reduction of iron(III) at the varve boundary around 1885 AD.

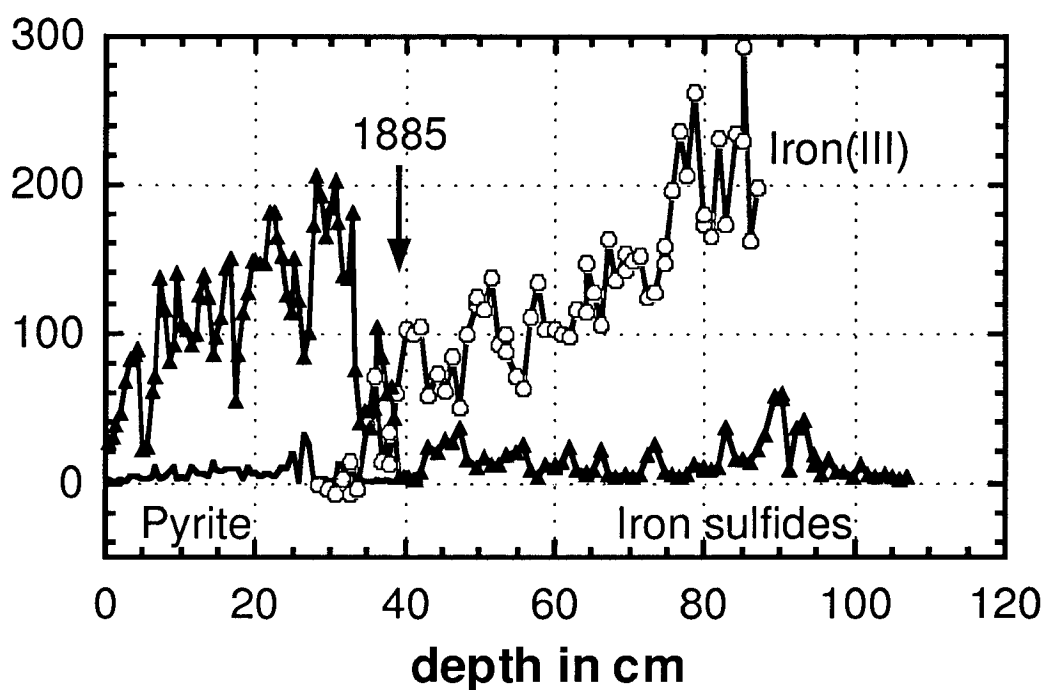


Fig. 4.6: Concentration profile of iron sulfides, pyrite and iron(III). The pyrite concentration is near to the detection limit of the CRS method. Iron sulfide exhibits the eutrophication after 1885. The iron(III) concentration increases when less iron sulfides prevail from 40 cm to deeper sites. This iron(III) gradient may be the source of dissolved iron(II) (Fig. 2.2).

Pyrite

In the earlier study (chapter 2) we found a negative correlation between AVS and pyrite in the younger sediment from 1885 to 1982. In the deeper sediment where less AVS is present no pyrite concentrations could be estimated because of its very low concentrations. The detection limit of the titration method is about 2 $\mu\text{mol/g}$ dry weight.

Discussion

The following discussion is divided into two parts. Based on the results of our previous study (chapter 2) on recent sediments and the new data from long cores we first evaluate the concepts of iron sulfide in lacustrine sediments as a proxy for environmental change. In the second part we compare the time series of AVS data with climatic records for two periods:

- from the medieval warm period (~1000 AD) to the present and
- from about 8000 B.P. to 1000 B.P.

This second part of our discussion relies on a preliminary age model of the Baldeggersee long-cores.

Factors governing AVS accumulation

A correlation of AVS, CRS and average temperature values was found in a previous study (chapter 2) in the section between 1982 when the lake restoration project started and 1950 when the lake reached a rather constant state. The following hypothesis was suggested: Cold winter periods enhanced the mixing of oxygen down the whole water column and oxidized iron sulfide at the sediment-water interface. This process formed pyrite as a byproduct. Therefore the pyrite concentration was positively correlated with the temperature data and negatively correlated with the AVS values. In the older sediment sections pyrite concentrations were below the detection limit. This may indicate that reoxidation of AVS at the sediment surface was of minor importance. The AVS signal in the long core seems to be modulated by the production of sulfide rather than by consumption.

The sulfate reduction rate (SRR) depend on the oxygen penetration into the sediment. Sulfate reduction occurs only in anoxic layers. The consequence is a longer diffusive pathway through the sediment and a slower SRR. The sulfate diffusion rate was estimated for some typical conditions of core BA97-4.

The following boundary conditions were assumed:

- constant sulfate concentration in the water body of Baldeggersee over the Holocene
- an approximately linear sulfate gradient in the sediment
- no AVS losses in the sediment (100% burial of the reduced sulfate)

A minimal concentration of hydrogen sulfide of 4 $\mu\text{mol/g}$ dry weight provides evidence for a slow sulfate reduction rate in the past. The calculated values with Ficks law of diffusion is 19 $\mu\text{mol m}^{-2} \text{d}^{-1}$ for the sulfate diffusion rate. AVS maxima with about 60 $\mu\text{mol/g}$ dry weight correspond to a much higher diffusion rate of 440 $\mu\text{mol m}^{-2} \text{d}^{-1}$. The data of the recent eutrophic situation of the lake at about 1950 result in highest value of 3100 $\mu\text{mol m}^{-2} \text{d}^{-1}$.

Because sulfate diffuses down to older sediment layers the AVS record is shifted in time for some years. This time shift can be estimated from the penetration depth and the accumulation rate of sediment. It is about 9 months for the recent sediment, about 500 years for the AVS baseline with 4 $\mu\text{mol/g}$ dry weight and about 15 years at AVS maxima with 60 $\mu\text{mol/g}$ dry weight in the past. For the following discussion this time lag is not important because the error in our age model is several 100 years. It is important to note that the AVS peaks are formed under conditions which allow for a geochemical response to external changes on the time scale of decades.

In the analyzed part of the sediment the transitions from varved sections and gray "homogeneous" sections are very sharp, dark layers have always high AVS concentrations. The sharp changes indicate that the iron sulfides are geochemically stable as long as no bioturbation destroys the varves and introduces oxygen by advective processes.

AVS accomodation from 1000 to 2000

The recent AVS record from Baldeggersee is compared in Fig. 4.7 to the precipitation and temperature data of Pfister (1994). The precipitation index reveals dry periods centered around 1750, 1820, 1870 and 1950. The dry periods seem to be more pronounced than wet periods. Drought reduces phosphorus inputs to a lake and enforces strongly oligotrophic conditions. The first two dry periods of 1750 and 1820 correspond to AVS minima in our record. Later however the anthropogenic eutrophication takes over. The AVS record increases dramatically in the second half

of the 19th century. This human induced eutrophication produced AVS concentrations, which are three times larger than all other maxima observed during the Holocene.

The winter temperature index for Switzerland calculated from Pfister (1994) as well as the temperature variability after Mann et al. (1999) show the well-known minima of the little ice age but again less pronounced warm periods. The AVS record has been shown to be sensitive for warm periods (especially mild winters, see chapter 2). Therefore it is not surprising that the AVS peaks for the period 1000-1800 calendar years show little correlation with the temperature variability. Land use changes in the catchment were probably the stronger forcing factors for the limnological conditions of Baldeggersee than the temperature variability.

AVS accumulation during the Holocene

Holocene climate proxies from Greenland ice cores are remarkably constant. The North Atlantic hydrography, however, is characterized by a series of shifts during which drift ice was transported southwards. This record of ice rafted debris has been reconstructed in detail from proxies such as hematite coated grains. Bond et al. (2001) found a cycle of roughly 1500 years for this southward penetration of cold waters from Labrador. The cycle was successfully correlated to proxies for solar activity (^{10}Be and $\Delta^{14}\text{C}$). Rough correlations between this North Atlantic climate record and the quite heterogeneous observations of glacier retreats and advances are also intensively discussed at present (Bond et al., 2001 and Broecker, 2001).

Figure 4.8 represents a comparison between these Atlantic and Alpine climate variabilities and the AVS record from Baldeggersee using our preliminary age model. Bond et al. (2001) found three distinct minima for ice-rafted debris between 2000 and 6000 B.P. The minima are centered around 2500, 3500 and 4800 B.P. The AVS record shows three maxima at quite similar ages (~2500, 3500 and about 4500). The event around 4500 represents most extended series of natural Holocene varves in this lake. The period lasted about 200 years.

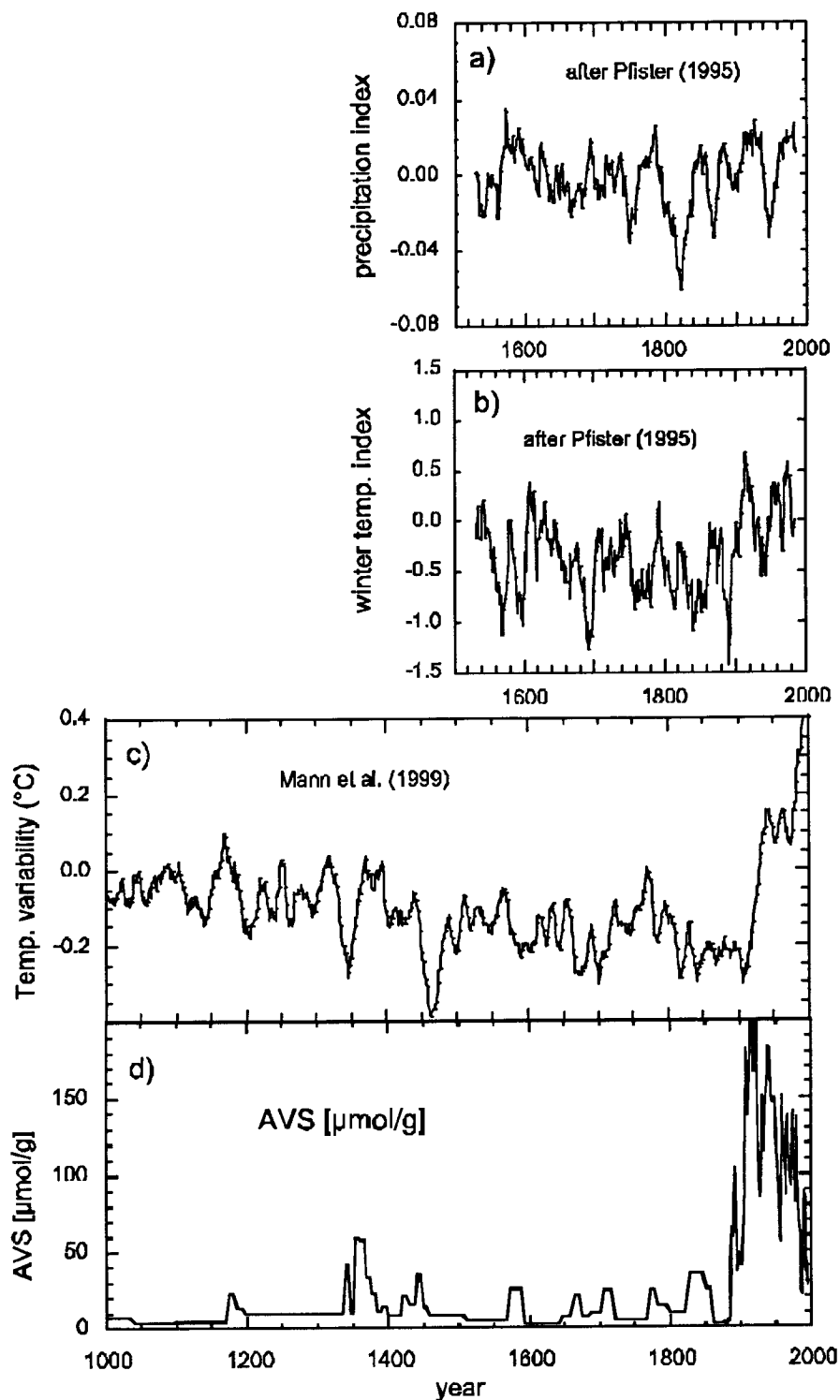


Fig. 4.7: Climate parameters during the last 1000 calendar years compared to the AVS record from Baldeggensee. Index for precipitation (a) and temperature (b) for Switzerland based on historical sources (see text for details). The time series represent 11 year running means. (c) Average temperature reconstruction for the northern hemisphere (Mann et al., 1999). (d) AVS time series from Baldeggensee using a preliminary age model.

The older record shows AVS maxima with smaller amplitude. Similarly the North Atlantic record is less pronounced before 6000 B.P.

The strong coincidence of solar factors with the ice-berg record encouraged Bond et al. (2001) to hypothesize that changes in the production rate of North Atlantic deep water could have amplified the variability of solar irradiance. Such a link could have changed average climate conditions in western Europe.

We have shown previously that the AVS record can react sensitively to average temperature changes (chapter 2). The good coincidence with climate proxies and the sensitive response in the AVS record supports two conclusions:

- a) The hydrographic changes observed in the North Atlantic are observed with similar frequencies in the sediment record of Baldeggersee.
- b) Lakes such as Baldeggersee which can switch from dimictic to meromictic conditions and back may represent very sensitive recorders for continental climate variability.

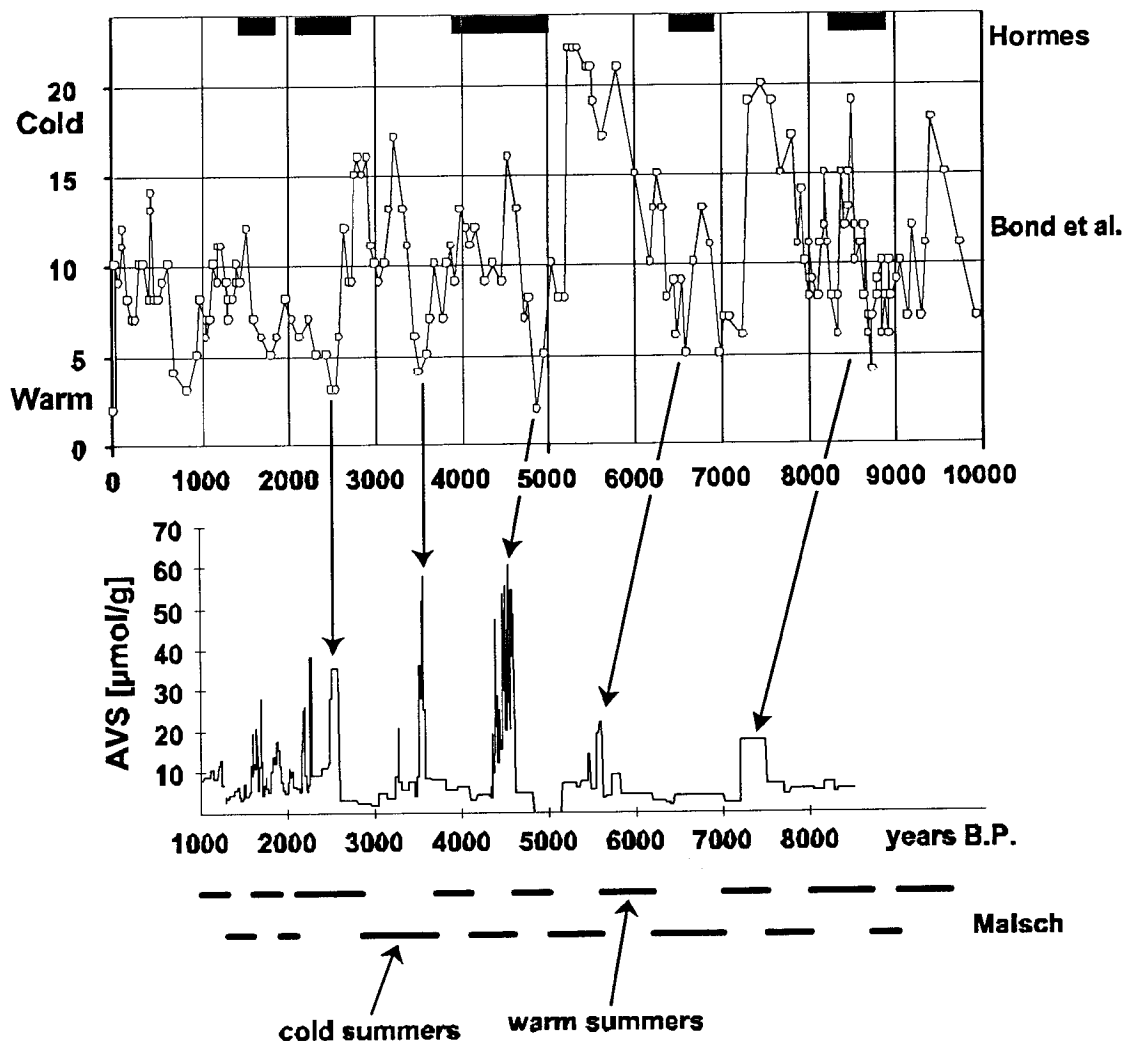


Fig. 4.8: Variability of % hematite stained grains in core VM 29-191 from the North Atlantic. This proxy reflects the input of ice-rafted debris from icebergs. High values indicate colder conditions (Bond et al., 2001). The dark bars represent stages of glacier retreats in the Alps cited after Broecker (2001). Similar information is given in the record from the Morteratsch glacier by Maisch et al. (1993) at the bottom. Warm summers lead to glacier retreats. The roughly 1500 year cycle shown in the North Atlantic record can be tentatively linked to the AVS time series from Baldeggersee.

References

- Bond G., Kromer, B., Beer, J., Muscheler R., Evans M.N., Showers W., Hoffmann S., Lotti-Bond R., Hajdas I., Bonani G., Persistent solar influence on North Atlantic climate during the Holocene, *Science*, **294**, 2130-2136, (2001).
- Broecker W.S., Was the Medieval Warm Period Global?, *Science*, **291**, 1497-1499, (2001).
- Crowley T.J., Lowery T.S., How warm was the medieval warm period?, *Ambio*, **29(1)**, 51-54, (2000)
- Dos Santos Afonso M., Stumm W.; Reductive Dissolution of Iron(III)-(Hydr)oxides by Hydrogen Sulfide, *Longmuir*, **8**, 1671-1675, (1992).
- Fischer A.; Isotopengeochemische Untersuchungen ($\delta^{18}\text{O}$ und $\delta^{13}\text{C}$) im Wasser und in den Sedimenten des Soppensees; Klimaveränderungen und Entwicklungsgeschichte des Sees seit dem Spätglazial, Dissertation ETH Zürich Nr. 11'924, (1997).
- Fossing H., Jørgensen B. B.; Measurement of Bacterial Sulfate Reduction in Sediments: Evaluation of a Single-Step Chromium Reduction Method, *Biogeochemistry*, **8**, 205-222, (1989).
- Gächter, R., Wehrli, B.; Ten years of artificial mixing and oxygenation: No effect on the internal phosphorus loading of two eutrophic lakes. *Environ. Sci. Technol.* **32**, 3659-3665, (1998).
- Giger, W., Sturm, M., Sturm, H., Schaffner, C., Bonani, G., Batzer, R., Hofmann, H.J., Morenzoni, E., Nessi, M., Suter, M., Wölfli, W.; $^{14}\text{C}/^{12}\text{C}$ -Ratios in Organic Matter and Hydrocarbons Extracted From Dated Lake Sediments. *Nuclear Instruments & Methods B5*, 394-297, (1984).
- Hantke R.; Die Gletscherstände des Reuss- und Linthsystems zur ausgehenden Würmeiszeit. Mit 2 Tafeln (I und II); *Eclogae Geologicae Helvetiae*, **51(1)**, 119-150, (1958).
- Heron G., Crouzet C., Bourg A.C.M., Christensen T.H.; Speciation of Fe(II) and Fe(III) in Contaminated Aquifer Sediments Using Chemical Extraction Techniques, *Environ. Sci. Technol.*, **28**, 1698-1705, (1994).
- Kelts K., Briegel U., Ghilarde K. and Hsu K. (1986); The Limnology-ETH Coring System. *Schweizerische Zeitschrift für Hydrologie*, **48**, 104-115.
- Kromer B., Becker B.; German oak and pine ^{14}C calibration 7400 BC to 9400 BC; *Radiocarbon*, **35**, 125-135, (1993).
- Lorius C., Jouzel J., Raynaud D., Hansen J., Le Treut H. (1990); The ice core record: climate sensitivity and future greenhouse warming; *Nature*, **347**, 139-145.
- Lotter A.F., Renberg I., Hansson H., Stöckli R. and Sturm M. (1997a); A Remote Controlled Freeze Corer for Sampling Unconsolidated Surface Sediments, *Aquat. sci.*, **59 (4)**, 295-303.

- Lotter, A. F., Sturm, M., Teranes, J. L., Wehrli, B.; Varve formation since 1885 and high-resolution varve analyses in hypertrophic Baldeggersee (Switzerland); *Aquat. sci.*, **59(4)**, 304-325, (1997b).
- Maisch M., Burga C. A., Fitze P.; Lebendiges Gletschervorfeld: Von schwindenden Eisströmen, schuttreichen Moränenwällen und wagemutigen Pionierpflanzen im Vorfeld des Morteratschgletschers: Führer und Begleitbuch zum Gletscherlehrpfad Morteratsch; Editor: Physische Geographie, Institute of geography, University of Zürich, Engadin press AG Samedan, 138p., (1993).
- Maisch M., Wipf A. Denneker B., Battaglia J., Benz C., In: Die Gletscher der Schweizer Alpen: Gletscherhochstand 1850, Aktuelle Vergletscherung, Gletscherschwund-Szenarien, vdf Verlag, 1. Auflage, 376 Seiten, ISBN 3-7281-2568-7, (1999)
- Mann M.E., Bradley R.S., Northern hemisphere temperatures during the past millenium: Inferences, uncertainties and limitations, *Geophysical Research Letters*, **26(6)**, 759-762, (1999).
- Morse J.W., Cornwel J.C.; Analysis and Distribution of Iron Sulfide Minerals in Recent Anoxic Marine Sediments, *Marine Chemistry*, **22**, 55-69, (1987).
- Niessen F., Sturm M.; Die Sedimente des Baldeggersees (Schweiz) — Ablagerungsraum und Eutrophierungsentwicklung während der letzten 100 Jahre / The sediments of Lake Baldegg (Switzerland) — sedimentary environment and development of eutrophication for the last 100 years; *Arch. Hydrobiol.*, **108(3)**, 365-383, (1987).
- Pehkonen S.O., Erel Y., Hoffmann M.R.; Simultaneous Spectrophotometric Measurement of Fe(II) and Fe(III) in Atmospheric Water, *Environ. Sci. Technol.*, **26(9)**, 1731-1736, (1992).
- Pfister C., Kington J., Kleinlogel G., Schuele H., Siffert E., The creation of high resolution spatio- temporal reconstructions of past climate from direct meteorological observations and proxy data. Methodological considerations and results. In: Frenzel, B., Pfister C., Glaeser, B. (eds), *Climate in Europe 1675-1715* (1994).
- Schaller T., Moor H.C., Wehrli B. (1997), Sedimentary Profiles of Fe, Mn, V, Cr, As and Mo as Indicators of Benthic Redox Conditions in Baldeggersee, *Aquat. Sci.*, **59(4)**, 345-361.
- Schweingruber F. H., Bräker O. U., Schär E.; Dendroclimatic studies on conifers from central Europe and Great Britain; *Boreas*, **8**, 427-452, (1979).
- Stuiver M., Kra R.; Radiocarbon calibration issue; *Radiocarbon*, **28**, 805-1030, (1986)
- Wehrli B., Lotter A. F., Schaller T., Sturm M.; High-resolution varve studies in Baldeggersee (Switzerland): Project overview and limnological background data; *Aquat. sci.*, **59(4)**, 285-294, (1997).
- Wüest A., Aeschbach-Haertig W., Baur H., Hofer M., Kipfer R., Schurter M.; Density structure and tritium-helium age of deep hypolimnetic water in the northern basin of Lake Lugano; *Aquat. sci.*, **54**, 205-218, (1992).

Chapter 5:

Conclusions and outlook

Conclusions

Goal

The goal of this study was the interpretation of iron and sulfur records in the sediment of Baldeggersee. The hypothesis that climatic factors affecting deep-water mixing in the lake leave their mark in the iron sulfide record of the sediments was tested quantitatively on short sediment cores. The speciation of iron and sulfur was analyzed with a combination of wet chemical and spectroscopic methods. Information on the transport and the chemical and microbial transformation of iron and sulfur at the sediment-water interface was obtained from a process study on recent sediments. The results of these measurements were then used in a second step to interpret the iron sulfide stratigraphy in a long sediment core covering several thousand years. This paleolimnological study was focused on a preliminary analysis of the oscillating varve regime of Baldeggersee. By comparison with recent paleoceanographic literature potential links between the North Atlantic climate oscillations and the iron sulfide record in the partially varved sediments from Baldeggersee were explored.

Results

i) Cores

Several sediment cores were taken at the deepest site of Baldeggersee (65m). The cores were correlated with different data sets such as dry weights, sediment descriptions and photographs. In 1993 a freeze core was dated by varve counts and ^{137}Cs and an absolute time scale with a resolution of one year back to 1885 was established. These data were used for the correlation of short cores. Before 1885 and down to a sediment depth of up to 8 meters a ^{14}C -dating from a core taken in 1978 was used.

ii) sulfur in recent sediments

Baldeggersee has a sulfate concentration of about $150\ \mu\text{M}$. Even though a lake restoration project started in 1982 high sulfate diffusion rates into the sediment are still observed. Maximal sulfate reducing bacteria concentrations were found at the

sediment water interface and at a sediment depth of 5 cm. From sulfate porewater gradients a diffusion rate of $0.45 \text{ mmol m}^{-2} \text{ d}^{-1}$ was calculated. With this value a sulfur concentration of about $150 \text{ } \mu\text{mol g}^{-1}$ dry sediment was expected. The average measured value was about $190 \text{ } \mu\text{mol/g}$. Most of the sulfur (about 70%) was bound as iron sulfide. Less than 5% sulfur was found in pyrite. Free hydrogen sulfide was not detected because the Fe^{2+} concentration in the porewater reaches up to 0.6 mM. The pyrite concentration profile shows a negative correlation with iron sulfide. Pyrite is an oxidation product of iron sulfides. Under oxidizing conditions the iron sulfide concentration decreases and the pyrite concentration increases.

iii) iron in recent sediments

The total iron concentration was about $300 \text{ } \mu\text{mol g}^{-1}$ and exceeded the total amount of sulfur. The iron rich sediments acted therefore as an efficient trap for reduced sulfur species. At the sediment water interface the iron concentration was lower than deeper down core. A pore-water gradient down to the zone deposited before 1885 reached Fe^{2+} concentrations of 0.6 mM and allowed a transport of reduced iron from deeper sediments to the hypolimnion. By contrast the mobility of sulfide was very low due to the efficient precipitation as iron sulfides.

Iron reduction was found to occur by two pathways. First, we found active iron reducing bacteria at the sediment water interface and an additional maximum at 2 cm sediment depth. Second, dissolved sulfide species allow the chemical reduction of iron oxides at the sediment interface. A fast reaction caused a depletion of these dissolved sulfide phases. Extraction experiments found iron(II) as the dominant iron oxidation state in this upper part of the sediment. A dominant phase was iron sulfide. Pyrite contributed only little to the total iron content. Small total phosphorus concentrations revealed only a negligible potential amount of vivianite (Fe(II)phosphate). With EXAFS-measurements we found oxygen as the dominant nearest neighbor of the iron ions. These spectroscopic data revealed two dominant iron phases. One phase was the major phase in the deeper sediment. A best fit of this unknown phase was obtained with a solid solution model, where Fe(II) and Fe(III) ions replaced the Ca(II) ions in the calcite structure. A slight correction in the Fe-O distance was applied because the siderite shows a more compact structure compared to calcite. The second phase was determined as amorphous iron sulfide

with a tetrahedral coordination of the iron(II) ions similar to the mackinawite structure. In this case the wet chemical analysis and the spectroscopic results match very well.

iv) the long sediment record

Iron sulfide was found in deeper sediment layers, too. The concentration changes from no detectable sulfide up to about $60 \mu\text{mol g}^{-1}$. Several FeS maxima were found. Changes with a period of hundreds of years were found in the younger sediment. Sediment deposited before about 2500 years B.P. shows oscillations of iron sulfide concentration with a period of about thousand years.

A similar pattern was observed recently for proxies of ice-rafted debris and cosmogenic radionuclides in North Atlantic sediments, suggesting a solar forcing of Northern hemispheric temperature conditions. Records of glacier advances and retreats from the Swiss Alps show a similar periodicity as the North Atlantic record and the AVS time series of Baldeggersee. Results from the process study on short cores showed that AVS concentrations in recent sediments correlated with average yearly temperatures with warmer conditions leading to more stratification and higher sulfide concentrations in the sediment. Together, these different lines of evidence strongly suggest that the AVS record in deep meromictic lakes can be used as a sensitive proxy for deep-water mixing and climatic forcing. The 1000-1500 year periodicity of the varved sections from the preliminary age model of Baldeggersee sediments would support the hypothesis that European climatic conditions showed similar fluctuations in the past 8000 years as the sedimentary proxies for the iceberg record of the North Atlantic.

Outlook

Two major points need additional work for a more conclusive picture of Fe speciation in sediments and FeS sedimentation during the last several thousand years:

1) The solid solution model for Fe in carbonate phases should be verified experimentally and with additional sediment extractions. Treatment of fine calcite crystals with iron(II) solutions could produce an important reference material for further EXAFS measurements. Leaching experiments such as a carbonate extraction with acetate should provide more information on the iron content in calcite in the sediments of Baldeggersee. In the future micro - EXAFS will allow determining the local coordination of elements in particles of a few micrometers in diameter. This method already serves as an important complement to bulk - EXAFS studies on sediment material.

2) The preliminary age model for Baldeggersee sediments should be refined with new ^{14}C dates. Katrin Monecke at ETH is currently improving the sediment description and dating. Her improved stratigraphy will allow a more conclusive comparison between the Baldeggersee sediment record and the recent studies on climate variations based on North Atlantic sediments, Greenland ice-cores and the glacier record of the Swiss Alps.

Besides these incremental improvements of the results presented in this thesis, a broader survey comparing the Baldeggersee record to FeS records in other varved sediments would help to generalize our results. It could answer the question whether the potential climate oscillations during the last several thousand years are a general phenomenon in different environmental archives across Europe or if there are significant regional differences. New analytical approaches such as scanning X-ray fluorescence on whole cores could facilitate such a comparative study.

Curriculum vitae

name: Bott Markus
address: Untermosenstrasse 10
CH-8820 Wädenswil
phone private: +41 1 780 60 27
birthday: 11th december 1968
nationality: Swiss
citizenship: married, three children
confession: roman catholic

1975 - 1981: primary school
1981 - 1983: secondary school
1983 - 1987: high school
1988: military service
1988 - 1989: practicum in electronics
1989 - 1990: employment in electronics. My proposition was to test and repair electronic devices in a production process. 4th semester of the engineering school for electrical engineering and 1st previous diploma.

1990 - 1994: study in physical chemistry at the Swiss Federal Institute of Technology (ETH), Zurich. Diploma in autumn 1994. I visited the additional course in analytical chemistry.

1994: Diploma work: Working with a Ca²⁺-selective optode-membrane. The work was focused on the processes in the PVC membrane. The aim was to optimize the properties of a mechanically more stable membrane. Measurements of the membrane thickness and the diffusion constant of different membrane components were made.

1994-2002: PhD (this study)
1998-2001: Employment as teacher in chemistry and physics at the Lyceum Alpinum Zuoz AG (gymnasium).

2002: Diploma for teaching chemistry at the college level
languages: German, French, Italian, English

Annex: Tables and raw data of the plots

Table A1: Age model

¹⁴ C age (1978)	BA78-8	¹⁴ C age (today)	calculated age	BA97-6
1170 yrs	125 cm	1190 yrs	1190 yrs	110 cm
1760 yrs	250 cm	1780 yrs	1780 yrs	240 cm
2000 yrs	285 cm	2020 yrs	2020 yrs	265 cm
3400 yrs	455 cm	3420 yrs	3570 yrs	435 cm
3900 yrs	490 cm	3920 yrs	4270 yrs	480 cm
4000 yrs	510 cm	4020 yrs	4440 yrs	500 cm
4000 yrs	550 cm	4020 yrs	4440 yrs	540 cm
4320 yrs	570 cm	4340 yrs	4860 yrs	560 cm
5760 yrs	645 cm	5780 yrs	6480 yrs	630 cm
7770 yrs	720 cm	7790 yrs	8470 yrs	705 cm
7600 yrs	750 cm	7620 yrs	8270 yrs	735 cm
8200 yrs	805 cm	8220 yrs	8820 yrs	790 cm

Table A2: Dry weight in % (Fig. 2.1)

Freeze core (FC) and gravity core (GC)

Year	FC	GC	Year	FC	GC	Year	FC	GC
1995		9.7	1957	25.5		1918	26.4	
1994		19.6	1956	34.7	40.2	1917	24.4	33.5
1993	4.8	22.9	1955	28.7		1916	23	
1993		23.5	1954	27.3	34.1	1915	19.7	29.4
1992	10.6	24.2	1953	24.7		1914	23.6	
1991	14.9	22.8	1952	27.5	31.3	1913	25.2	31.5
1990	13.5	24.8	1951	25.3		1912	24.6	
1990		23.3	1950	22.6	28.7	1911	26.9	32.7
1989	15.1		1949	27.8	29.8	1910	26.6	
1988	18.3	25.9	1948	23.7		1909	27.6	33.1
1987	22.7		1947	21.5	27.2	1908	27.8	
1986	23.4	27	1946	22.3		1907	26	33.5
1985	22		1945	23	27.9	1906	29.7	
1984	24	27.8	1944	24.3		1905	31.7	
1983	21.6		1943	23.8	29.1	1904	31.2	40.1
1982	20.6	25.9	1942	22.7	29.5	1903	35.8	
1981	22	24.4	1941	23.6		1902	34	
1980	20.4		1940	22.7	27	1901	37.1	43.9
1979	27.6	29.8	1939	24		1900	37.6	
1978	25.7	36.1	1938	22.3	27.1	1899	43.3	45.4
1977	25.6		1937	26.1		1898	37.5	
1976	20.8	25.1	1936	27.7	34.2	1897	41	
1975	26.6	26.6	1935	25.4	31.4	1896	39.1	47.1
1974	23.3	28.6	1934	25.2		1895	39.7	
1973	25.1		1933	25.7	34	1894	39	44.8
1972	19.5	28.2	1932	25.8	32.8	1893	37.6	
1971	32.8	33.7	1931	23.8		1892	35.8	41.7
1970	32.4		1930	30.1	37.5	1891	37.9	42.7
1969	26.7	32.4	1929	22.9		1890	38	
1968	25	28	1928	22.1	32.9	1889	38.6	43.1
1967	27		1927	24.8		1888	38.2	44.3
1966	27.1	28.2	1926	21.3	31.6	1887	38.2	
1965	22.6	26	1925	21.6	31.3	1886	40.5	46.8
1964	26.3	27.6	1924	19.8		1885	42.6	49
1963	20.7	24.9	1923	21	30.2	1883		46.1
1962	23.1		1922	20.4		1882		47
1961	31	30.9	1921	25.1	31	1880		49.4
1960	26.4	32.3	1920	18.7		1879		49
1959	32.5		1919	24.1	33.5	1877		49.9
1958	27.4	31.8						

Table A3: Sulfate reducing bacteria SRB (Fig. 2.3)

depth in cm	active SRB up	active SRB low	active SRB mean
0	2'000'000'000	3'000'000'000	3'000'000'000
1	400'000'000	3'000'000'000	2'000'000'000
1	200'000'000	2'000'000'000	600'000'000
2	200'000'000	6'000'000'000	400'000'000
2	200'000'000	2'000'000'000	1'000'000'000
3	500'000'000	2'000'000'000	1'000'000'000
3	400'000'000	1'000'000'000	900'000'000
4	400'000'000	2'000'000'000	1'000'000'000
4	400'000'000	2'000'000'000	1'000'000'000
5	400'000'000	3'000'000'000	2'000'000'000
5	500'000'000	2'000'000'000	1'000'000'000
6	700'000'000	2'000'000'000	1'000'000'000
6	400'000'000	2'000'000'000	900'000'000
7	400'000'000	900'000'000	600'000'000
8	0	900'000'000	300'000'000
9	0	400'000'000	300'000'000
10	0	500'000'000	200'000'000
20	0	400'000'000	90'000'000
30	0	100'000'000	10'000'000
40	0	300'000'000	90'000'000

Table A4: Active iron reducing bacteria (FeRB) (Fig. 2.3)

depth [cm]	FeRB low	FeRB up	FeRB mean
0.25	20000	100000	80000
0.75	5000	40000	20000
1.25	6000	50000	30000
1.75	9000	70000	40000
2.5	4000	20000	10000
3.5	800	7000	4000
5	2000	10000	8000
20	800	6000	4000

Table A5: Sulfur contents in $\mu\text{mol/g}$ dried sediment (Fig. 2.4)

Year	AVS	CRS	S(tot)	Year	AVS	CRS	S(tot)	Year	AVS	CRS	S(tot)
1995	27	2	66	1956	56	9	119	1916	194	2	202
1994	31	1	68	1955	71	9	168	1915	203	3	216
1993	39	1	70	1954	86	10	217	1914	189	8	204
1993	47	3	79	1953	100	7	194	1913	175	12	192
1992	68	1	100	1952	115	3	171	1912	157	12	200
1991	84	4	127	1951	121	7	168	1911	140	12	208
1990	87	4	130	1950	128	11	165	1910	139	7	173
1989	89	4	119	1949	150	5	237	1909	138	2	138
1988	22	3	108	1948	149	7	220	1908	160	5	174
1987	23	2	97	1947	149	8	203	1907	182	9	210
1986	24	2	85	1946	148	6	209	1906	147	7	179
1985	43	3	139	1945	147	4	214	1905	112	5	148
1984	62	4	192	1944	147	5	213	1904	76	4	117
1983	66	8	170	1943	148	6	211	1903	65	3	101
1982	71	12	147	1942	182	6	204	1902	53	3	85
1981	137	2	206	1941	182	5	233	1901	41	3	69
1980	127	3	184	1940	182	5	261	1900	45	2	77
1979	117	4	162	1939	174	6	249	1899	49	1	85
1978	82	8	117	1938	166	6	236	1898	45	1	77
1977	88	9	138	1937	159	9	223	1897	41	2	70
1976	93	11	160	1936	152	11	210	1896	38	2	62
1975	140	3	192	1935	126	9	165	1895	44	2	69
1974	106	5	155	1934	120	14	183	1894	50	1	76
1973	104	4	148	1933	114	19	202	1893	77	2	106
1972	103	3	142	1932	151	19	175	1892	104	2	135
1971	93	11	148	1931	137	10	170	1891	85	2	98
1970	96	9	168	1930	123	1	166	1890	72	2	98
1969	99	8	187	1929	104	17	194	1889	60	2	98
1968	126	6	190	1928	86	32	221	1888	66	1	77
1967	132	6	196	1927	94	29	207	1887	55	1	69
1966	138	6	202	1926	102	26	192	1886	44	1	61
1965	125	4	207	1925	173	3	163	1885	4	1	34
1964	86	14	167	1924	190	3	238	1884	4	1	30
1963	99	10	171	1923	206	3	312	1883	4	1	25
1962	105	9	169	1922	200	3	260	1882	5	1	29
1961	112	8	166	1921	194	3	207	1881	3	1	27
1960	145	9	173	1920	180	3	184	1880	2	1	25
1959	148	9	185	1919	166	2	160	1879	3	1	21
1958	151	9	197	1918	175	2	174	1878	4	1	22
1957	103	9	158	1917	185	2	187	1877	5	1	24

Tables A6: Iron concentrations in $\mu\text{mol/g}$ dried sediment (Fig. 2.4)

Year	Fe(tot)	Year	Fe(tot)	Year	Fe(tot)
1993	246	1957	315	1921	354
1992	284	1956	222	1920	324
1991	271	1955	188	1919	276
1990	269	1954	292	1918	368
1989	289	1953	205	1917	246
1988	300	1952	193	1916	338
1987	242	1951	229	1915	388
1986	272	1950	309	1914	285
1985	307	1949	198	1913	329
1984	237	1948	214	1912	370
1983	255	1947	234	1911	348
1982	204	1946	319	1910	432
1981	311	1945	293	1909	534
1980	153	1944	279	1908	357
1979	278	1943	185	1907	318
1978	296	1942	248	1906	374
1977	282	1941	244	1905	399
1976	214	1940	338	1904	397
1975	238	1939	358	1903	342
1974	177	1938	251	1902	306
1973	254	1937	262	1901	306
1972	327	1936	311	1900	343
1971	138	1935	268	1899	398
1970	271	1934	278	1898	350
1969	188	1933	277	1897	305
1968	242	1932	296	1896	323
1967	233	1931	314	1895	348
1966	152	1930	366	1894	441
1965	225	1929	241	1893	390
1964	214	1928	338	1892	375
1963	235	1927	268	1891	320
1962	218	1926	317	1890	399
1961	145	1925	315	1889	334
1960	295	1924	317	1888	411
1959	164	1923	286	1887	287
1958	234	1922	362	1886	335

Year	Fe(II)	Fe(III)
1996	271	25
1995	254	13
1993	257	22
1990	259	11
1987	274	12
1982	325	20
1976	273	18
1969	215	11
1963	206	13
1956	256	15
1949	225	12
1943	252	10
1936	272	20
1930	287	15
1923	297	15
1919	301	15
1915	295	10
1910	350	15
1906	281	16
1898	319	14
1890	262	31
1882	239	51
1874	327	15

Tables A7: Correlation of average temperature and iron sulfides (Fig. 2.6)

year	average temperature [°C]
1982	8.7
1981	8.3
1980	8.0
1979	7.8
1978	8.3
1977	8.6
1976	9.1
1975	9.2
1974	9.0
1973	8.7
1972	8.5
1971	8.5
1970	8.5
1969	8.5
1968	8.7
1967	9.0
1966	8.8
1965	8.7
1964	8.2
1963	8.2
1962	8.5
1961	8.8
1960	9.3
1959	8.9
1958	8.8
1957	8.1
1956	7.9
1955	7.9
1954	8.4
1953	8.6
1952	8.7
1951	8.9
1950	9.2
1949	9.3
1948	9.5
1947	9.2

year	AVS [$\mu\text{mol/g}$]	CRS [$\mu\text{mol/g}$]
1982.3	71	11.7
1980.5	137	2.4
1979.3	117	4.2
1978.0	82	8.1
1976.0	93	10.5
1974.7	140	2.8
1973.5	106	4.7
1972.3	103	3.4
1971.0	93	11.1
1969.3	99	7.7
1967.5	126	6.5
1966.3	138	5.7
1965.0	125	3.8
1964.0	86	13.7
1963.0	99	9.7
1961.3	112	8.4
1959.7	145	9.0
1958.0	151	8.6
1956.0	56	8.7
1954.0	86	9.6
1952.0	115	3.5
1950.0	128	11.1
1948.5	150	5.5
1947.0	149	8.4

Table A8a: Procentual iron speciation, page 1 (Fig. 3.1)

Depth is in cm, Fe(tot) in $\mu\text{mol/g}$

depth	Fe(tot)	AVS	CRS	Fe(II)	Fe(III)	depth	Fe(tot)	AVS	CRS	Fe(II)	Fe(III)
2.0	246	19.0%	1.1%	71.0%	8.9%	20.6	293	49.7%	1.7%	44.7%	3.8%
2.6	284	24.7%	1.0%	67.4%	6.5%	20.9	279	60.9%	2.1%	32.5%	3.9%
3.2	271	29.1%	1.1%	64.4%	5.5%	21.2	185	68.7%	2.4%	24.1%	5.7%
3.8	269	31.4%	1.4%	62.7%	4.2%	21.8	248	76.0%	2.6%	16.1%	4.8%
4.4	289	23.5%	1.2%	71.3%	4.0%	22.1	244	67.3%	2.0%	25.8%	5.4%
4.9	300	15.9%	1.0%	78.8%	3.9%	22.4	338	59.1%	1.8%	34.4%	4.3%
5.2	242	8.6%	0.8%	85.9%	5.0%	22.7	358	56.2%	1.9%	36.7%	4.5%
5.5	272	10.9%	0.9%	83.3%	5.0%	22.9	251	58.4%	2.5%	33.0%	6.9%
5.8	307	16.3%	1.2%	76.8%	5.0%	23.2	262	58.5%	3.2%	31.5%	7.1%
6.1	237	22.0%	2.0%	69.5%	7.2%	23.5	311	52.1%	3.5%	37.4%	6.5%
6.4	255	29.0%	3.5%	59.3%	7.4%	24.1	268	46.4%	4.1%	42.8%	7.2%
6.7	204	35.0%	3.2%	53.8%	10.0%	24.4	278	43.8%	5.2%	44.3%	6.6%
7.3	311	53.9%	2.9%	33.4%	6.5%	24.7	277	45.2%	6.1%	42.5%	6.4%
7.6	153	56.3%	1.5%	33.5%	12.9%	25.3	296	45.3%	5.4%	43.5%	5.7%
7.8	278	50.9%	2.1%	38.3%	6.9%	25.6	314	42.8%	3.3%	49.0%	5.1%
8.4	296	33.7%	2.5%	57.2%	6.4%	25.9	366	40.2%	3.5%	51.1%	4.2%
8.7	282	34.1%	3.6%	55.1%	6.6%	26.1	241	34.1%	5.7%	55.3%	6.3%
9.0	214	44.4%	3.1%	45.0%	8.5%	26.4	338	34.5%	9.2%	50.8%	4.5%
9.6	238	54.0%	2.9%	34.8%	7.2%	26.7	268	30.7%	9.6%	54.7%	5.6%
10.2	177	53.2%	1.8%	37.6%	9.1%	27.0	317	40.7%	6.7%	47.6%	4.7%
10.5	254	44.1%	1.8%	47.7%	5.9%	27.6	315	49.0%	3.4%	42.9%	4.7%
10.7	327	46.6%	3.6%	43.3%	4.3%	27.9	317	62.3%	1.0%	31.9%	4.7%
11.3	138	44.7%	4.2%	45.1%	9.4%	28.2	286	62.3%	1.0%	32.1%	5.1%
11.6	271	51.9%	5.2%	36.4%	4.4%	28.5	362	60.6%	0.9%	33.9%	4.1%
11.9	188	46.8%	3.4%	44.8%	5.8%	28.8	354	55.2%	0.8%	39.7%	4.2%
12.5	242	53.9%	3.1%	37.7%	4.7%	29.0	324	56.8%	0.8%	37.6%	4.7%
12.8	233	66.8%	3.0%	24.3%	5.1%	29.3	276	54.5%	0.7%	40.1%	5.5%
13.1	152	67.9%	2.7%	23.2%	8.0%	29.6	368	61.0%	0.7%	33.5%	3.8%
13.7	225	62.3%	3.9%	27.1%	5.6%	29.9	246	60.0%	0.7%	35.2%	5.2%
14.2	214	45.9%	4.1%	44.2%	6.1%	30.2	338	61.6%	0.7%	34.0%	3.4%
14.8	235	43.6%	4.9%	45.5%	5.7%	30.5	388	58.7%	1.3%	36.6%	2.6%
15.1	218	55.9%	4.7%	32.3%	6.3%	30.8	285	57.3%	2.4%	36.9%	3.9%
15.4	145	58.2%	4.3%	30.6%	9.6%	31.1	329	54.0%	3.2%	39.1%	3.7%
16.0	295	72.0%	4.7%	15.6%	4.8%	31.4	370	45.2%	3.5%	47.6%	3.5%
16.3	164	67.8%	4.0%	21.6%	8.7%	31.7	348	38.2%	2.7%	55.4%	4.0%
16.6	234	62.4%	3.9%	27.2%	6.2%	31.9	432	32.7%	1.8%	62.1%	3.5%
16.8	315	40.8%	3.5%	49.8%	4.7%	32.2	534	34.3%	1.1%	61.0%	2.9%
17.1	222	31.8%	3.8%	57.9%	6.8%	32.5	357	42.7%	1.5%	51.7%	4.4%
17.4	188	30.7%	4.0%	58.8%	7.8%	32.8	318	47.1%	2.0%	46.2%	5.0%
17.7	292	38.6%	3.8%	51.1%	4.9%	33.0	374	41.5%	2.0%	52.1%	4.4%
18.0	205	45.9%	2.7%	45.1%	6.8%	33.2	399	28.8%	1.4%	65.7%	4.0%
18.3	193	53.8%	2.7%	36.9%	7.0%	33.4	397	22.0%	1.1%	72.7%	4.0%
18.6	229	51.3%	2.9%	40.2%	5.8%	33.6	342	18.5%	0.9%	76.1%	4.5%
18.9	309	56.6%	3.2%	34.8%	4.1%	33.8	306	16.5%	0.9%	77.8%	5.0%
19.5	198	62.2%	3.2%	29.3%	6.3%	34.0	306	14.5%	0.8%	80.0%	4.9%
19.8	214	69.7%	3.2%	21.5%	5.7%	34.3	343	12.9%	0.6%	82.3%	4.3%
20.0	234	60.0%	2.9%	32.3%	5.0%	34.6	398	12.7%	0.4%	82.8%	3.6%
20.3	319	53.4%	2.3%	40.1%	3.6%	34.8	350	12.9%	0.4%	82.3%	4.1%

more data of this table on the next page

Table A8b: Procentual iron speciation, page 2 (Fig. 3.1)

Depth is in cm, Fe(tot) in $\mu\text{mol/g}$

Depth	Fe(tot)	AVS	CRS	Fe(II)	Fe(III)	depth	Fe(tot)	AVS	CRS	Fe(II)	Fe(III)
35.0	305	12.7%	0.5%	81.7%	5.4%	67.2	380	2.4%	0.0%	66.9%	43.0%
35.1	323	12.6%	0.5%	81.2%	5.7%	68.3	526	1.2%	0.0%	67.5%	25.8%
35.4	348	11.9%	0.4%	82.1%	5.9%	69.3	610	0.9%	0.0%	74.3%	25.2%
35.7	441	14.6%	0.4%	79.2%	5.1%	69.3	610	0.9%	0.0%	74.0%	23.3%
36.0	390	19.6%	0.4%	73.7%	6.4%	70.4	563	0.9%	0.0%	72.7%	26.6%
36.3	375	24.7%	0.5%	67.3%	7.2%	71.4	521	1.8%	0.0%	71.8%	29.3%
36.9	320	24.1%	0.5%	67.3%	9.1%	72.5	537	3.2%	0.0%	71.4%	23.2%
37.2	399	20.9%	0.6%	69.6%	7.8%	73.5	538	3.3%	0.0%	72.3%	23.7%
37.5	334	17.4%	0.5%	73.3%	10.0%	74.6	599	2.6%	0.0%	72.5%	26.4%
38.0	411	17.7%	0.5%	71.1%	8.8%	74.6	599	1.2%	0.0%	71.3%	24.7%
38.3	287	16.1%	0.3%	72.1%	13.5%	75.6	625	1.0%	0.0%	68.9%	31.4%
38.6	335	11.1%	0.3%	75.6%	12.3%	76.6	688	0.8%	0.0%	66.1%	34.2%
39.2	337	5.2%	0.3%	81.6%	13.0%	77.7	613	1.3%	0.0%	61.4%	33.6%
39.5	339	1.3%	0.2%	84.9%	13.6%	78.7	592	1.7%	0.0%	62.9%	44.2%
39.8	341	1.3%	0.2%	84.2%	14.3%	79.8	611	1.9%	0.0%	64.1%	28.4%
40.4	344	1.2%	0.2%	84.3%	14.9%	79.8	611	1.7%	0.0%	68.9%	29.4%
40.7	346	1.0%	0.3%	85.2%	13.5%	80.8	544	1.8%	0.0%	64.6%	30.3%
41.0	348	0.8%	0.2%	86.8%	12.1%	81.9	561	3.7%	0.0%	61.4%	41.1%
41.5	350	0.9%	0.2%	88.2%	10.7%	82.9	524	4.3%	0.0%	53.0%	33.3%
41.8	352	1.4%	0.2%	89.1%	9.3%	84.0	435	4.9%	0.0%	48.7%	53.8%
42.1	354	3.5%	0.1%	85.0%	8.0%	85.0	438	3.7%	0.0%	38.5%	52.4%
43.2	341	5.1%	0.0%	79.6%	17.0%	85.0	438	3.6%	0.0%	44.5%	67.1%
44.2	353	7.0%	0.0%	74.7%	20.9%	86.1	446	3.9%	0.0%	47.6%	36.3%
45.2	364	7.0%	0.0%	72.9%	17.2%	87.1	472	5.0%	0.0%	53.1%	41.9%
46.3	381	8.1%	0.0%	74.4%	22.4%	88.2	486	7.6%	0.0%	-7.6%	0.0%
47.3	392	6.8%	0.0%	72.6%	12.9%	89.2	523	9.4%	0.0%	-9.4%	0.0%
48.4	374	5.6%	0.0%	70.2%	26.5%	90.3	576	10.5%	0.0%	-10.5%	0.0%
49.4	356	3.4%	0.0%	65.0%	33.4%	90.3	576	7.2%	0.0%	-7.2%	0.0%
49.4	356	3.6%	0.0%	63.7%	35.1%	91.3	647	5.7%	0.0%	-5.7%	0.0%
50.5	389	3.6%	0.0%	63.3%	29.7%	92.3	655	4.3%	0.0%	-4.3%	0.0%
51.5	396	3.7%	0.0%	67.1%	34.6%	93.4	715	4.4%	0.0%	-4.4%	0.0%
52.6	403	3.7%	0.0%	68.8%	23.3%	94.4	691	3.5%	0.0%	-3.5%	0.0%
53.6	404	4.2%	0.0%	72.6%	24.6%	94.4	691	1.8%	0.0%	-1.8%	0.0%
53.6	406	4.9%	0.0%	73.9%	21.7%	95.5	662	2.1%	0.0%	-2.1%	0.0%
54.7	408	5.3%	0.0%	76.3%	17.5%	96.5	605	1.7%	0.0%	-1.7%	0.0%
55.7	407	4.6%	0.0%	75.2%	15.8%	97.6	533	1.7%	0.0%	-1.7%	0.0%
56.8	405	3.3%	0.0%	71.5%	27.4%	98.6	612	1.1%	0.0%	-1.1%	0.0%
57.8	410	2.1%	0.0%	70.0%	32.6%	99.7	601	1.4%	0.0%	-1.4%	0.0%
58.9	434	2.1%	0.0%	71.7%	23.6%	100.7	570	1.7%	0.0%	-1.7%	0.0%
59.9	462	2.6%	0.0%	74.6%	22.3%	100.7	570	1.9%	0.0%	-1.9%	0.0%
59.9	462	2.8%	0.0%	75.2%	22.3%	101.8	493	1.4%	0.0%	-1.4%	0.0%
60.9	466	3.6%	0.0%	75.5%	21.5%	102.8	555	1.0%	0.0%	-1.0%	0.0%
62.0	518	3.4%	0.0%	74.6%	19.0%	103.9	557	0.9%	0.0%	-0.9%	0.0%
63.0	460	2.8%	0.0%	74.3%	25.4%	104.9	560	0.7%	0.0%	-0.7%	0.0%
64.1	473	1.7%	0.0%	71.4%	24.2%	106.0	562	0.6%	0.0%	-0.6%	0.0%
64.1	473	1.6%	0.0%	70.5%	31.2%	106.0	562	0.6%	0.0%	-0.6%	0.0%
65.1	454	2.7%	0.0%	69.7%	28.3%	107.0	565	0.8%	0.0%	-0.8%	0.0%
66.2	463	2.8%	0.0%	65.7%	23.1%						

Table A9a: Correlation of BA97-6 and BA97-4, page 1 (Fig. 4.3)

Values are the absolute depths of BA97-4 in cm. Example: The sediment material in BA97-6 in the 2nd section from 7-8 cm was correlated with BA97-4 at a (cumulated) depth of 140 cm

cm in BA97-6	BA97-6/1A	BA97-6/1B	BA97-6/2	BA97-6/3	BA97-6/4	BA97-6/5	BA97-6/6	BA97-6/7	BA97-6/8
0-1		72	130	228	325	405	499	592	691
1-2		72	134	230	326	407	502	595	696
2-3		73	135	231	328	408	503	597	697
3-4		74	136	233	329	410	505	598	698
4-5		75	137	234	330	411	506	599	699
5-6		76	138	235	331	412	507	601	700
6-7		77	139	236	332	413	508	602	701
7-8	11	78	140	237	333	414	509	603	702
8-9	12	79	141	238	334	415	510	604	704
9-10	13	80	142	239	334	416	511	605	705
10-11	14	81	143	240	335	417	512	606	706
11-12	15	82	144	241	336	418	513	607	707
12-13	16	83	145	243	337	419	514	608	708
13-14	17	84	146	244	338	420	515	609	709
14-15	17	85	146	245	339	421	516	610	710
15-16	18	86	147	246	340	422	517	611	711
16-17	19	87	148	248	341	423	518	612	712
17-18	21	87	149	249	342	424	519	613	714
18-19	22	88	150	250	343	425	521	614	715
19-20	23	89	151	251	344	426	522	615	716
20-21	24	90	152	253	345	427	523	616	717
21-22	25	91	152	254	345	428	524	617	718
22-23	26	92	153	255	346	429	525	618	719
23-24	27	93	154	256	347	430	526	619	720
24-25	28	94	155	258	348	431	527	620	721
25-26	29	95	156	259	348	432	528	621	722
26-27	30	96	157	260	349	433	528	622	723
27-28	31	96	158	261	350	434	529	623	724
28-29	31	97	159	262	350	436	530	624	725
29-30	32	98	159	263	351	437	531	626	726
30-31	33	99	160	264	352	438	532	627	726
31-32	34	100	161	265	352	439	533	628	727
32-33	36	101	162	267	353	440	534	629	728
33-34	37	102	163	268	354	441	535	630	729
34-35	38	103	164	269	354	442	536	631	730
35-36	39	104	165	270	355	443	537	633	731
36-37	40	105	166	271	356	444	538	634	732
37-38	41	105	167	272	356	445	539	635	732
38-39	42	106	168	273	357	446	540	636	733
39-40	43	107	169	274	358	447	541	637	734
40-41	44	108	170	275	358	448	542	638	735
41-42	45	109	171	276	359	449	543	639	736
42-43	46	110	171	277	360	450	544	640	737
43-44	47	112	172	278	360	451	545	641	738
44-45	49	113	173	279	361	451	546	642	739
45-46	50	114	174	280	362	452	547	643	740
46-47	52	115	175	281	363	453	548	643	741
47-48	53	116	177	282	364	454	549	644	742
48-49	54	117	178	283	365	455	550	645	743
49-50	56	118	179	284	365	456	551	646	744

more data of this table on the next page

Table A9b: Correlation of BA97-6 and BA97-4, page 2 (Fig. 4.3)

cm in BA97-6	BA97-6/1A	BA97-6/1B	BA97-6/2	BA97-6/3	BA97-6/4	BA97-6/5	BA97-6/6	BA97-6/7	BA97-6/8
50-51	57	119	180	285	366	457	552	647	745
51-52	58	120	181	286	367	458	553	648	745
52-53	59	121	182	287	368	459	554	649	746
53-54	60	122	184	288	369	460	555	650	747
54-55	61	123	185	290	370	461	556	651	748
55-56	62	124	186	291	371	462	557	652	749
56-57	63	125	188	292	372	463	558	653	750
57-58	64		189	294	373	464	559	654	750
58-59	65		190	295	374	465	560	655	751
59-60	65		191	296	375	466	561	656	
60-61	66		193	297	376	467	562	657	
61-62	67		194	298	377	468	563	658	
62-63	68		195	299	378	469	564	658	
63-64	69		196	299	379	470	564	659	
64-65	70		197	300	379	471	565	660	
65-66	70		198	301	380	472	566	661	
66-67	71		199	302	381	473	567	661	
67-68			200	303	382	474	568	662	
68-69			201	304	383	475	568	663	
69-70			203	305	384	476	569	663	
70-71			204	306	384	477	570	664	
71-72			205	307	385	478	571	665	
72-73			206	307	386	479	572	665	
73-74			207	308	387	480	573	666	
74-75			208	309	388	481	573	667	
75-76			209	310	388	482	574	669	
76-77			210	311	389	483	576	670	
77-78			212	312	390	484	577	671	
78-79			213	313	391	485	578	672	
79-80			214	314	392	486	579	673	
80-81			215	315	393	487	580	674	
81-82			216	316	393	487	581	675	
82-83			217	317	394	488	582	676	
83-84			218	318	395	489	583	677	
84-85			219	319	396	490	584	679	
85-86			221	320	397	491	584	680	
86-87			222	321	398	492	585	681	
87-88			223	322	398	493	586	682	
88-89			224	323	399	494	587	683	
89-90			225	324	400	495	588	684	
90-91			226		401		589	685	
91-92					402				
92-93					403				
93-94					403				

Table A10: AVS concentrations in BA97-4 in $\mu\text{mol/g}$ (Fig. 4.4)

cm from	cm to	AVS	cm from	cm to	AVS	cm from	cm to	AVS	cm from	cm to	AVS
0	8	129.7	180	182.5	7.2	315	317	11.6	535	536	45
8	9	82.9	182.5	185	4.3	317	321	12.3	536	537	40
9	10	39.8	185	190	4	321	323	28.1	537	538	55
10	11.5	88.1	190	192.5	4.6	323	333	35.7	538	539	60.5
11.5	14	3.2	192.5	195	5	333	343	3.1	539	540	55.8
14	15	25.9	195	197	5.2	343	353	3.2	540	541	33.7
15	17	36.5	197	198	10.2	353	363	2.1	541	542	20.4
17	19.5	10.1	198	199	11.7	363	373	2	542	543	26.4
19.5	21	15	199	200	19.6	373	381	4.6	543	544	43.9
21	22	25.1	200	201	10.6	381	389	3.4	544	545	54.3
22	26.5	5.2	201	203	9.5	389	393	8.7	545	546	40.8
26.5	28	24.7	203	205	11.9	393	394	20.6	546	547	50.6
28	29.5	9.9	205	208	10.8	394	399	7.7	547	548	38.6
29.5	30.5	7.3	208	210	15.7	399	409	5.8	548	549	48.6
30.5	31.5	21.7	210	212	20.6	409	419	7.4	549	550	40.9
31.5	33	7.1	212	214	12.8	419	421	3.9	550	551	41.2
33	34	3.6	214	216	6.9	421	423	9	551	561	4.6
34	37.5	2.4	216	218	5.7	423	424	22.1	561	572	0
37.5	39.5	26	218	220	11.2	424	425	36.4	572	578	7
39.5	45.5	5.2	220	222	11.1	425	426	32.3	578	580	5.9
45.5	51.5	8.4	222	223	28.3	426	428	28.3	580	584	7.5
51.5	52.5	14.2	223	224	25.5	428	429	29.4	584	586	14.2
52.5	53.5	36.6	224	227	12.6	429	430	36.8	586	590	5.8
53.5	55	16.2	227	228	4.5	430	431	52	590	592	18.9
55	56	21.5	228	230	4.2	431	432	58	592	594	22
56	58.5	8.7	230	233	6.8	432	433	41.4	594	596	3.3
58.5	59.5	14.7	233	235	9	433	434	25.4	596	599	4
59.5	60.5	11.1	235	238	5.9	434	439	8.5	599	604	9.2
60.5	61.5	22.8	238	242	5	439	449	8.1	604	612	4.3
61.5	62.5	33.6	242	244	10.2	449	459	5.7	612	619	4.5
62.5	63.5	57.6	244	246	13.9	459	469	6.3	619	626	2.8
63.5	64.5	59.4	246	248	12.2	469	475	3.1	626	628	2.3
64.5	65.5	10.5	248	250	17.5	475	481	4.3	628	630	1.8
65.5	66.5	41.5	250	252	15.6	481	491	4.4	630	640	4.1
66.5	76.5	10.6	252	254	11.3	491	496	4	640	650	4
76.5	77.5	10.4	254	256	7.6	496	499	6.4	650	656	2.1
77.5	78.5	10.2	256	258	5.7	499	501	3.5	656	663	17.5
78.5	79.5	13.4	258	262	4.6	501	503	16.8	663	669	6.9
79.5	80.5	22.9	262	264	7.4	503	504	19.1	669	671.5	4.2
80.5	87.5	4.8	264	266	11	504	505	14.3	671.5	681.5	5.7
87.5	92.5	4.1	266	268	8.9	505	508	9.5	681.5	690	5
92.5	97.5	8.2	268	270	9.9	508	509	27.7	690	698	7.3
97.5	102.5	8.7	270	275	6.3	509	510	47.5	698	700	4.8
102.5	107.5	10.4	275	280	5.8	510	511	21	700	706.5	5.4
107.5	112.5	8.4	280	282	5.3	511	512	28.7	706.5	708.5	6.7
112.5	117.5	11.9	282	283	13.6	512	513	24	708.5	712.3	4.1
117.5	122.5	13.1	283	284	21.7	513	516	12.1	712.3	713.8	4.6
122.5	128.5	6.8	284	285	25.4	516	519	25.2	713.8	724	5.1
128.5	130.5		285	286	21.3	519	523	15.5	724	731	4.8
130.5	134	4	286	287	21.8	523	524	42.7	731	734	4.4
134	138.5	2.6	287	288	26.3	524	525	45.5	734	736	5.5
138.5	140	3.6	288	290	9.2	525	526	53.8	736	738	3.8
140	145	3.6	290	292	6.1	526	527	35.6	738	739	2.4
145	150	4.3	292	294	5.3	527	528	33.2	739	747	3
150	155	4.2	294	296	6.8	528	529	29.6	747	748	2.3
155	160	5.4	296	297	22.4	529	530	32.1	748	749	0
160	165	6.5	297	298	38.6	530	532	55.8	749	751	5.1
165	170	3.8	298	299	37.5	532	533	50.2			
170	175	3.1	299	309	9.1	533	534	19.7			
175	180	3.4	309	315	10.8	534	535	33.1			

Table A11a: Dry weight of BA97-6 [g/g], page 1 (Fig. 4.5), sections have romain labels.

Depth [cm]	prefall	I A	I B	II	III	IV	V	VI	VII	VIII
0-1	0.380	0.288	0.456	0.451	0.475	0.433	0.491	0.473	0.437	0.511
1-2	0.345	0.254	0.441	0.455	0.491	0.425	0.484	0.421	0.441	0.518
2-3	0.342	0.253	0.456	0.460	0.473	0.453	0.467	0.399	0.454	0.519
3-4	0.344	0.252	0.457	0.461	0.479	0.447	0.459	0.430	0.461	0.526
4-5	0.312	0.271	0.454	0.467	0.432	0.477	0.459	0.418	0.515	0.522
5-6	0.272	0.297	0.428	0.486	0.447	0.485	0.454	0.429	0.537	0.532
6-7	0.325	0.342	0.526	0.505	0.469	0.472	0.469	0.398	0.514	0.527
7-8	0.281	0.356	0.534	0.512	0.473	0.495	0.469	0.399	0.424	0.526
8-9	0.269	0.350	0.474	0.532	0.451	0.541	0.484	0.387	0.426	0.529
9-10	-0.783	0.375	0.419	0.487	0.444	0.559	0.451	0.400	0.441	0.526
10-11	0.306	0.402	0.447	0.452	0.434	0.536	0.481	0.354	0.437	0.530
11-12	0.281	0.403	0.462	0.443	0.424	0.485	0.449	0.396	0.449	0.528
12-13	0.278	0.380	0.477	0.439	0.423	0.463	0.421	0.414	0.457	0.573
13-14	0.281	0.408	0.533	0.440	0.423	0.470	0.413	0.394	0.452	0.617
14-15	0.317	0.397	0.538	0.457	0.428	0.489	0.413	0.436	0.448	0.571
15-16	0.388	0.426	0.488	0.476	0.442	0.566	0.428	0.402	0.445	0.529
16-17	0.308	0.426	0.464	0.492	0.407	0.548	0.461	0.415	0.452	0.531
17-18	0.285	0.424	0.471	0.473	0.389	0.509	0.401	0.367	0.457	0.558
18-19	0.268	0.411	0.469	0.454	0.383	0.485	0.381	0.411	0.459	0.600
19-20	0.287	0.401	0.481	0.458	0.424	0.483	0.403	0.403	0.458	0.548
20-21	0.281	0.427	0.471	0.450	0.431	0.494	0.384	0.402	0.451	0.528
21-22	0.313	0.506	0.452	0.440	0.422	0.506	0.370	0.418	0.445	0.521
22-23	0.310	0.476	0.446	0.432	0.429	0.493	0.378	0.371	0.457	0.522
23-24	0.312	0.445	0.441	0.444	0.447	0.501	0.356	0.387	0.471	0.526
24-25	-0.781	0.434	0.438	0.503	0.478	0.511	0.361	0.367	0.465	0.544
25-26	0.265	0.474	0.440	0.528	0.482	0.552	0.390	0.382	0.473	0.541
26-27	0.279	0.528	0.447	0.517	0.538	0.579	0.363	0.345	0.471	0.551
27-28	0.289	0.479	0.453	0.484	0.506	0.594	0.410	0.397	0.464	0.553
28-29	0.314	0.463	0.464	0.489	0.470	0.599	0.452	0.355	0.469	0.545
29-30	0.335	0.467	0.485	0.511	0.467	0.599	0.403	0.355	0.485	0.526
30-31	0.364	0.500	0.501	0.533	0.442	0.607	0.395	0.350	0.497	0.518
31-32	0.415	0.497	0.510	0.479	0.428	0.514	0.405	0.344	0.475	0.524
32-33	0.423	0.469	0.478	0.456	0.418	0.486	0.408	0.407	0.479	0.522
33-34	0.426	0.458	0.455	0.469	0.429	0.486	0.403	0.382	0.477	0.527
34-35	0.401	0.449	0.439	0.490	0.426	0.490	0.443	0.362	0.471	0.520
35-36	0.423	0.430	0.433	0.497	0.434	0.525	0.426	0.346	0.472	0.514
36-37	0.464	0.434	0.437	0.497	0.503	0.531	0.468	0.371	0.476	0.521
37-38	0.461	0.449	0.437	0.459	0.450	0.555	0.415	0.365	0.480	0.522
38-39	0.459	0.465	0.431	0.476	0.422	0.540	0.423	0.370	0.506	0.556
39-40	0.464	0.465	0.456	0.503	0.422	0.545	0.426	0.395	0.471	0.587
40-41	0.459	0.493	0.481	0.527	0.421	0.554	0.440	0.418	0.463	0.550
41-42	0.446	0.503	0.477	0.592	0.409	0.565	0.510	0.410	0.467	0.535
42-43	0.445	0.442	0.442	0.585	0.401	0.563	0.438	0.452	0.461	0.531
43-44	0.458	0.444	0.425	0.562	0.436	0.562	0.444	0.426	0.476	0.532
44-45	0.418	0.428	0.423	0.561	0.439	0.512	0.457	0.402	0.457	0.534
45-46	0.447	0.424	0.443	0.549	0.417	0.515	0.540	0.402	0.457	0.543
46-47	0.462	0.444	0.456	0.472	0.396	0.483	0.487	0.410	0.488	0.579
47-48	0.446	0.436	0.437	0.448	0.386	0.493	0.446	0.401	0.515	0.531
48-49	0.452	0.439	0.419	0.452	0.367	0.495	0.445	0.384	0.477	0.533
49-50	0.432	0.432	0.422	0.460	0.359	0.526	0.449	0.451	0.502	0.527

More data of this table on the next page

Table A11b: Dry weight of BA97-6 [g/g], page 2 (Fig. 4.5)

depth [cm]	prefall	I A	I B	II	III	IV	V	VI	VII	VIII
50-51	0.418	0.465	0.417	0.521	0.354	0.488	0.440	0.472	0.483	0.531
51-52	0.419	0.486	0.415	0.523	0.347	0.469	0.444	0.476	0.490	0.528
52-53	0.471	0.457	0.420	0.445	0.335	0.450	0.450	0.425	0.486	0.533
53-54	0.553	0.468	0.435	0.441	0.358	0.439	0.439	0.454	0.484	0.546
54-55	0.465	0.473	0.458	0.476	0.400	0.448	0.457	0.456	0.485	0.569
55-56	0.446	0.419	0.447	0.474	0.389	0.438	0.468	0.453	0.485	0.595
56-57	0.445	0.405	0.446	0.487	0.385	0.449	0.475	0.457	0.490	0.623
57-58	0.480	0.416		0.521	0.405	0.461	0.466	0.475	0.502	0.549
58-59	0.599	0.473		0.562	0.459	0.457	0.478	0.457	0.515	0.561
59-60	0.467	0.552		0.573	0.504	0.470	0.483	0.456	0.526	0.537
60-61	0.472	0.519		0.495	0.378	0.460	0.473	0.463	0.502	0.455
61-62	0.489	0.431		0.456	0.357	0.455	0.481	0.441	0.491	0.493
62-63	0.531	0.425		0.500	0.337	0.448	0.501	0.449	0.491	0.532
63-64	0.475	0.435		0.537	0.339	0.450	0.481	0.494	0.490	0.535
64-65	0.460	0.435		0.518	0.369	0.468	0.473	0.457	0.500	0.588
65-66	0.069	0.440		0.478	0.381	0.459	0.468	0.448	0.490	0.566
66-67	0.441	0.457		0.486	0.385	0.446	0.463	0.405	0.465	0.531
67-68	0.463			0.440	0.454	0.452	0.472	0.449	0.471	0.550
68-69	0.476			0.397	0.489	0.442	0.469	0.456	0.475	0.623
69-70	0.506			0.434	0.450	0.425	0.475	0.475	0.478	0.557
70-71	0.479			0.455	0.480	0.416	0.485	0.494	0.495	0.656
71-72	0.446			0.446	0.482	0.415	0.473	0.493	0.466	0.564
72-73	0.446			0.439	0.405	0.421	0.480	0.456	0.485	0.624
73-74	0.435			0.449	0.389	0.409	0.473	0.450	0.495	0.635
74-75	0.449			0.444	0.365	0.421	0.482	0.455	0.489	0.609
75-76	0.502			0.471	0.375	0.424	0.484	0.425	0.499	0.561
76-77				0.486	0.383	0.437	0.486	0.472	0.514	0.569
77-78				0.480	0.381	0.411	0.480	0.512	0.552	0.590
78-79				0.459	0.436	0.405	0.475	0.499	0.520	0.561
79-80				0.437	0.448	0.393	0.479	0.514	0.496	0.552
80-81				0.438	0.409	0.391	0.478	0.501	0.498	0.637
81-82				0.463	0.361	0.432	0.484	0.536	0.499	0.671
82-83				0.476	0.362	0.387	0.474	0.533	0.498	0.684
83-84				0.524	0.363	0.388	0.484	0.480	0.497	0.706
84-85				0.514	0.371	0.398	0.472	0.488	0.501	0.676
85-86				0.436	0.365	0.450	0.484	0.474	0.498	0.701
86-87				0.447	0.377	0.440	0.472	0.460	0.504	0.567
87-88				0.477	0.375	0.460	0.467	0.453	0.511	
88-89				0.466	0.374	0.459	0.464	0.473	0.511	
89-90				0.474	0.419	0.449	0.451	0.461	0.509	
90-91				0.438		0.444		0.449	0.521	
91-92						0.466				
92-93						0.462				
93-94						0.463				

Table A12: Concentration of iron species in $\mu\text{mol/g}$ (Fig. 4.6)

depth	AVS	CRS	depth	AVS	CRS	depth	AVS	CRS
0.3	27	2.4	27	102	26.3	63	10	0
0.9	31	1.5	27.6	173	2.9	64.1	7	0
1.5	39	1.1	28.2	206	3.1	65.1	9	0
2	47	2.8	28.8	194	3.1	66.2	22	0
2.6	68	1.2	29.3	166	2.2	67.2	7	0
3.2	84	4	29.9	185	1.8	68.3	4	0
3.8	87	3.6	30.5	203	2.8	69.3	6	0
4.4	89	3.7	31.1	175	12.3	70.4	4	0
4.9	22	2.6	31.7	140	11.9	71.4	5	0
5.5	24	2	32.2	138	1.6	72.5	20	0
6.1	62	4.2	32.8	182	8.8	73.5	26	0
6.7	71	11.7	33.4	76	3.6	74.6	8	0
7.3	137	2.4	34	41	2.5	75.6	5	0
7.8	117	4.2	34.6	49	1.3	76.6	5	0
8.4	82	8.1	35.1	38	1.8	77.7	6	0
9	93	10.5	35.7	50	1.3	78.7	13	0
9.6	140	2.8	36.3	104	2.2	79.8	11	0
10.2	106	4.7	36.9	85	1.5	80.8	10	0
10.7	103	3.4	37.5	60	2.4	81.9	12	0
11.3	93	11.1	38	66	1.2	82.9	37	0
11.9	99	7.7	38.6	44	1.1	84	16	0
12.5	126	6.5	39.2	4	0.7	85	17	0
13.1	138	5.7	39.8	4	0.7	86.1	15	0
13.7	125	3.8	40.4	5	0.7	87.1	23	0
14.2	86	13.7	41	2	1	88.2	32	0
14.8	99	9.7	41.5	3	0.6	89.2	59	0
15.4	112	8.4	42.1	8	0.5	90.3	58	0
16	145	9	43.2	24	0	91.3	9	0
16.6	151	8.6	44.2	21	0	92.3	37	0
17.1	56	8.7	45.2	29	0	93.4	42	0
17.7	86	9.6	46.3	27	0	94.4	19	0
18.3	115	3.5	47.3	37	0	95.5	7	0
18.9	128	11.1	48.4	15	0	96.5	15	0
19.5	150	5.5	49.4	11	0	97.6	8	0
20	149	8.4	50.5	18	0	98.6	7	0
20.6	147	4.3	51.5	13	0	99.7	5	0
21.2	148	5.8	52.6	13	0	100.7	12	0
21.8	182	5.9	53.6	19	0	101.8	6	0
22.4	182	5	54.7	21	0	102.8	5	0
22.9	166	6.4	55.7	25	0	103.9	6	0
23.5	152	11.2	56.8	10	0	104.9	4	0
24.1	126	9.5	57.8	5	0	106	3	0
24.7	114	18.9	58.9	12	0	107	5	0
25.3	151	18.5	59.9	12	0			
25.9	123	1.3	60.9	15	0			
26.4	86	32.5	62	25	0			

depth	Fe(III)	depth	Fe(III)
28.8	-1	66.2	107
29.3	-5	67.2	163
29.9	-6	68.3	135
30.5	-7	69.3	142
31.1	-2	70.4	150
31.7	3	71.4	153
32.2	-2	72.5	125
32.8	-6	73.5	127
33.4	-5	74.6	158
34	-4	75.6	197
34.6	39	76.6	236
35.1	56	77.7	206
35.7	73	78.7	262
36.3	43	79.8	173
36.9	14	80.8	165
37.5	24	81.9	231
38	33	82.9	174
38.6	47	84	234
39.2	61	85	229
39.8	103	86.1	162
40.4	102	87.1	198
41	100		
41.5	102		
42.1	104		
43.2	58		
44.2	74		
45.2	63		
46.3	85		
47.3	51		
48.4	99		
49.4	119		
50.5	115		
51.5	137		
52.6	94		
53.6	88		
54.7	71		
55.7	64		
56.8	111		
57.8	134		
58.9	102		
59.9	103		
60.9	100		
62	99		
63	117		
64.1	115		
65.1	128		